ENTRY PERFORMANCE OF THE MERCURY SPACECRAFT HEAT SHIELD

by

R. Bryan Erb and Stephen Jacobs

NASA Manned Spacecraft Center
Houston, Texas

Presented to
The Heat Protection Session of
the American Institute of Aeronautics
and Astronautics Entry Technology Conference

Williamsburg - Hampton, Virginia

October 12 - 14, 1964

ENTRY PERFORMANCE OF THE MERCURY SPACECRAFT HEAT SHIELD

R. Bryan Erb
Chief, Thermo-Structures Branch
NASA Manned Spacecraft Center

Stephen Jacobs
Aerospace Technologist, Fluid and Flight Mechanics
NASA Manned Spacecraft Center

Summary 15350

The flight performance of the Mercury Spacecraft ablative heat shield is summarized with respect to its conceptual development, thermal design and performance, and manufacturing and testing.

A full-scale Research and Development (R and D) shield was flight tested to provide a qualification of the ablative approach in general and the shingle-layup glass-reinforced phenolic system employed in particular. Thermal performance parameters were derived from this test which formed a basis for subsequent analysis and predictions.

Flight-test results from the seven production shields flown, including the six that entered from orbit, are presented. Ground-test results and theoretical performance predictions were compared with the flight results and good correlation was found.

The Mercury spacecraft heat shield performed consistently well during the project. While ablative in the general sense, very little mass loss occurred and no change in shield thickness was noted. The most dominant mechanism of heat rejection was found to be radiation from the char. The engineering approach to the shield design and performance analysis was quite satisfactory and this type of shielding system was considered well suited to satellite entry conditions such as those experienced by the Mercury manned spacecraft.

Introduction Author

It is the objective of this paper to describe the development and flight performance of the heat shield used for entry thermal protection of the Mercury spacecraft. This paper considers only the ablative protection utilized on the forebody of the spacecraft.

The Mercury spacecraft and its mission have been described in references [1] and [2]. Basically, the spacecraft was a blunt ballistic vehicle sized for a single pilot and for launch by an Atlas launch vehicle. The launch-escape configuration for the spacecraft is shown in figure 1.

The heat shield was protected from the boost environment because of its position in the spacecraft-launch vehicle adapter. During the orbital mission, the heat shield faced forward in the direction of flight and was exposed to the near-earth vacuum environment and to temperature excursions ranging from 60° to 90° F. Entry was achieved by atmospheric braking along a shallow flight path which resulted in deceleration levels of about 10g, and maximum heating rates of approximately 50 Btu/ft^2-sec. A cold-wall heat pulse of about 8,000 Btu/ft^2 was experienced in the 5-minute entry time for which significant heating occurred.

For reasons to be described an ablative shield was chosen for the spacecraft. A full-scale Research and Development (R and D) shield of conservative design was built and flown to demonstrate the concept of ablation as a means of thermal protection for satellite vehicles. Design, ground test, analysis, and flight qualification of the prototype shield followed and excellent performance of the shield was obtained. A total of six orbital entries, four of them manned, were carried out successfully during Project Mercury. The thermal performance of the heat shield and the approach to its design, fabrication, and qualification form the substance of this paper. Practically no thermostructural analysis was performed on the Mercury shield.

The structural consideration of most concern was that for landing impact. Loading and strength analyses and extensive tests were performed for this condition. The discussion of this aspect of the heat shield is not, however within the scope of this paper.

Exhaustive thermal analysis was not performed on the Mercury heat shield, but fairly complete data on recovered shields were obtained and are included in this paper.

Symbols

A	area, ft^2
C_D	coefficient of drag
c	specific heat, Btu/lb-°R
g	acceleration loading
H	enthalpy, Btu/lb
k	conductivity, Btu/ft-sec-°F
m	mass of vapor produced in ablation process, lb
N_{PR}	Prandtl number
Q	total heat, Btu/ft^2
q	heating rate, Btu/ft^2-sec
R_N	body nose radius, ft
T	temperature, °F
t	time, sec
V	flight velocity
V_c	reference satellite velocity, 26,000 ft/sec
W	weight of spacecraft, lb
x	distance from front face, in.
α	parameter described by equation (2), appendix B
δ	thickness of element, ft
ϵ	emissivity
ρ	density, lb/ft^3

σ Stefan-Boltzman constant, $0.1714 \times 10^{-8} \frac{\text{Btu}}{\text{hr-ft}^2\text{-}°\text{R}^4}$

Subscripts:

a	at ablation condition
Aero	aerodynamic
am	ambient
BL	blockage
e	edge of boundary layer
N	surface element
n	typical internal element
p	at constant pressure
SL	sea level
w	wall
Z	stagnation
2	conditions behind shock

NOTE: Barred quantities denote mean properties in the boundary layer.

History of the Mercury Heat Shield

Configuration

The Mercury spacecraft configuration was primarily determined by heating considerations and the final configuration shown in figure 1 evolved from an extensive study of shapes which would minimize the entry heating problem as well as satisfy numerous stability requirements. A blunt vehicle was selected very early in the project to provide a low value of the ballistic parameter W/C_DA. An afterbody over which the flow would be separated was also chosen by considerations of both heating and stability for the entry portion of flight. A compromise between stability and the requirement of uniform heating on the shield resulted in the 80-inch radius of curvature assigned to the blunt face. The design of the spacecraft structure required a pressure vessel over which a heat protection shell was fitted. The configuration was such that the optimum heat shield was a segment of the surface of a sphere, supported continuously around the edge.

The Heat-Sink Approach

The first approach considered for the heat shield was a beryllium heat sink. The total heat load to be expected, approximately 6,000 Btu/ft^2 for the early predictions, could be handled reasonably well by a beryllium heat sink 1-inch thick with a unit weight of approximately 10 lb/ft^2. Such a heat sink would have experienced an increment in temperature of about 1,200° F. Considerations of toxicity and fire hazard from the shield in the event of a land impact eventually ruled out this approach for the orbital entries. However, by the time this decision had been made, a number of heat sinks had been fabricated. These heat sinks were forged shield of QMV beryllium, a form of the material that is produced by sintering beryllium powder.

Since these shields were available early in the program, they were employed on the ballistic flights by Astronauts Alan B. Shepard and Virgil I. Grissom, May 5 and July 21, 1961, respectively.

The Ablative-Shield Approach

Ablation technology was advancing rapidly at this time, and it was apparent that a shield of the type then used on missile nose cones could provide protection without the disadvantages of the heat sink and with a possible saving in weight. This approach was adopted for the heat shield qualification flight and was continued for the remainder of the program. At an early stage in the design of the Mercury spacecraft, the fall of 1958, a Jupiter missile nose cone was successfully recovered. This nose cone involved a composite shingle-type construction which provided structural strength while still permitting the large volumes of gas generated by the heat to flow between the ablative laminates without forcing the laminates to separate.

Since no directly applicable satellite entry flight experience had been gained with a heat shield of this design, it was considered essential that a conservatively designed prototype shield be flown on a trajectory that would simulate the conditions for entry from orbit. It was also considered absolutely necessary to recover the heat shield for postflight examination, and, accordingly, a ballistic trajectory was selected for this qualification flight. This preliminary flight qualification test is described in the following section of this paper. This qualification flight demonstrated the suitability of the shingle-laminated phenolic glass heat shield for the Mercury entry heat protection, and operational shields were constructed in a similar manner.

The shield construction and dimensions, including a photograph, are shown in figure 2.

The general performance of the ablative shield was highly satisfactory, and the six shields that entered from orbit all performed their function perfectly.

Preliminary Flight Qualification Test (Big Joe)

Introduction

A flight-test program utilizing a full-scale spacecraft was considered essential for early verification of design concepts under actual flight conditions because no ground-test facility existed at that time with the capability of simulating the entry environment. The first Atlas-boosted flight used a boilerplate vehicle named "Big Joe", and was conceived to investigate some of the many problems associated with entry from orbit as well as to provide an early check on the basic approach to the heat protection being employed in the Mercury design. This flight test was planned to simulate as nearly as possible the conditions of atmospheric entry from a shallow earth orbit of a full-scale spacecraft. This spacecraft was equipped with an ablation heat shield made of a phenolic fiber-glass resin material of the type planned for the Mercury heat shield and was so instrumented that its thermal performance could be determined. This was one of the primary objectives of the flight test.

The spacecraft flight test was conducted on September 9, 1959, from the Air Force Missile Test Center, Cape Canaveral, Florida.[1] This section presents only the results of the ablation-heat-shield performance during this test.

Spacecraft Description

The boilerplate spacecraft had essentially the same external dimensions as the Mercury spacecraft with the exception that it was not fitted with an escape tower. Structural details of the boilerplate spacecraft were not typical of the Mercury spacecraft, as it was designed to meet only the requirements of this flight test. A sketch showing the general dimensions of the boilerplate spacecraft is given in figure 3. It consisted of the following four major assemblies: the heat shield, pressurized instrumentation compartment, conical and cylindrical afterbody, and aft canister. A photograph of the assembled boilerplate spacecraft is shown in figure 4.

The heat shield was an ablative type made of phenolic resin and fiber glass and the afterbody was made of inconel sheet. The spacecraft instrumentation was contained in a pressurized compartment, and the parachute system and recovery aids were contained in the afterbody and aft canister sections.

Heat Shield Description

The heat shield used on Big Joe was geometrically a 74.5-inch diameter spherical segment with a radius of curvature of 80 inches. A sketch of the heat shield is shown in figure 5. The heat shield consisted of two laminates: an outer ablation laminate, 1.075 inches thick and an inner structural laminate, 0.350 inch thick. The ablation laminate was made of concentric layers of fiber-glass cloth orientated so that the layers were at a 20° angle with the local heat-shield surface. The structural laminate was made of fiber-glass cloth orientated with the individual layers parallel to the outer surface. Both the ablation and structural laminates were made from a special finish fiber-glass cloth with a 9410 phenolic resin. Resin content, by weight, of the ablation and structural laminates was 40 percent and 30 percent, respectively. A circular ring (fig. 5) 3 inches high, made of fiber glass and resin, was attached to the back of the heat shield and served to bolt the heat shield to the pressurized compartment of the spacecraft.

Heat Shield Instrumentation

The heat shield was instrumented to obtain temperature and char-penetration time histories during flight. Unique sensors were specifically developed and the heat shield was instrumented with 13 of these sensors located at the positions indicated in table 1. Each of the sensors consisted of 2 distinct types of measurements; first, 6 thermocouples spaced in depth as shown in table 1 and second, the char sensor circuits which consisted of 20 pairs of wires spaced in depth. The individual pairs of wires utilized the property of the resin becoming an electrical conductor when charred to complete the electrical circuit between adjacent wires. A description of the sensor work is given in appendix A.

[1] Hereinafter referred to as Cape Kennedy

Flight Description

The launch vehicle used for this flight test was the Atlas 10D missile. The boilerplate spacecraft was attached to the adapter by means of a special ring-type clamp.

The vehicle was launched on September 9, 1959, from the Air Force Missile Test Center, Cape Kennedy, Florida. A malfunction occurred during the launch phase because the booster engine did not separate from the Atlas sustainer stage after burnout. This added weight caused the entry conditions to be different than programed and an entry angle somewhat steeper than that planned for the simulated orbital entry resulted. This malfunction also led to a delay in the separation of the spacecraft from the Atlas. After separation, the spacecraft attained a general heat-shield forward attitude which it maintained throughout entry.

The spacecraft coordinates in space near apogee were obtained from radar data and used in conjunction with data from accelerometers to calculate the entry trajectory. The accuracy of the trajectory determined by this technique is affected by uncertainties in various parameters in the calculations, such as drag coefficient and air density. By varying these parameters over a range, it was possible to obtain a trajectory for which calculated load factors closely approximated those measured on board. The actual achieved trajectory thus calculated is shown in figure 6.

The spacecraft was equipped with an automatic reaction control system to control its motion during entry. However, because of the delay in spacecraft-launch vehicle separation, the control-system fuel supply was expended in an attempt to control the motion of the spacecraft-launch vehicle combination. Attitude data obtained during entry indicated an oscillatory motion about the trim angle. This trim angle, caused by the spacecraft's center of gravity being offset from its longitudinal axis was approximately 4°. The average amplitude of the oscillation about the trim angle over the time interval of interest in the analysis of the heat-shield performance was approximately 12° to 15°.

The spacecraft's parachute larding system operated successfully, resulting in a safe water landing. The recovery aids enabled prompt location and the spacecraft was recovered in excellent condition 7 hours after launch.

Results and Discussion

The desired insertion conditions for this flight test were intended to simulate closely the atmospheric entry from a shallow earth orbit. However, because of the failure of the launch vehicle's engine to separate from the Atlas, the heating environment of the heat shield was not as severe as would have occurred had the desired trajectory been obtained. A comparison of the heating estimated for the actual entry with that estimated for the planned flight was made with a widely used theory (ref. 3). This comparison of values (fig. 7) based on a zero value for wall enthalpy, showed the peak heating rate obtained during the flight to be approximately 77 percent of the target value and the total cold-wall heat load obtained to be approximately 42 percent of the taget value of 7,100 Btu/ft^2.

An evaluation of the heat-shield performance involved analysis of the test results with regard to: general condition of the recovered heat shield, heat-shield temperatures and char characteristics, and heat-shield heating rate and mechanisms of ablation. A detailed discussion of each of these items follows:

Description of recovered heat shield.- The ablative heat shield withstood both the entry and recovery phases of the flight test with only superficial damage.

Figure 8 shows the photograph of the recovered heat shield. The pie-shaped discolored region in quadrant II was caused by a dye-marker recovery aid and was not caused by any effects of heating. The random dark marks are scuff marks made during the recovery operation. Small droplets of fused glass were observed over the entire heat-shield surface. A stagnation point offset of approximately 6 inches caused by the trim angle was evident from the streamlined glass droplets. Small circumferential hairline cracks which follow the fiber-glass laminations were also observed. The only significant damage to the heat shield was a 3-inch delamination which occurred in quadrant III near the stagnation point. A crack was observed at the edge of the large center plug and a separation around the smaller center plug. It was found by sectioning the heat shield at appropriate locations that these cracks and delaminations in the heat shield did not extend in depth beyond the visible charred portion and did not affect the structural integrity of the heat shield.

Measurements were made of the heat-shield profile and thickness after recovery to determine if there was a change as a result of the flight test. The results indicated that any profile change which might have occurred was within the accuracy of the measurements (±0.01 inch). The heat shield was weighed after recovery and the results indicated a weight loss of 6 pounds. An independent evaluation of the weight loss will be discussed later.

Heat shield temperatures and char characteristics.- The Big Joe heat shield faired temperature-time histories at a typical sensor location are shown in figure 9, and a typical thermocouple plot is shown in figure 10. A comparison of temperatures from the different sensors showed that there was no significant effect of radial location on the heat-shield temperatures, an indication that the heat shield essentially experienced a uniform heating over its surface. Core samples were taken from the recovered heat shield at various locations on its surface to obtain evidence on its physical condition. It was found by measurements of these samples that a visibly charred region penetrated to a depth of approximately 0.20 inch or some 12 percent of the total thickness. A discolored region extended to a total depth of approximately 0.35 inch or about 20 percent of the total thickness.

As a means of obtaining a better understanding of the extent of the char rather than arbitrarily defining char visually, specimens of the Big Joe heat shield were tested to obtain its electrical resistance and specific-gravity properties. The electrical resistance of a typical core sample cut from the heat shield was measured at regular intervals from its front face. There is a definite transition at a depth of about 0.12 inch with the outer portion being electrically conductive while the interior retains its original property as a dielectric (fig. 11). Specific-gravity measurements were made from sections cut from one of the heat-shield core samples (no. 13). Sections representative of the electrically conductive portion, the remainder of the visual char, the discolored region, and virgin material were used to obtain the variation of specific gravity with depth (fig. 12). By integrating this specific gravity variation, a shield weight loss of 6.5 pounds was obtained. It was assumed that the specific gravity of the electrically conductive region was a constant value of 1.55. This region, extending to a depth of approximately 0.11 inch, lost approximately 25 percent of its original resin content. The results of the specific-gravity tests agree approximately with the char depths of 0.12 inch indicated from electrical-resistance measurements. These tests also indicated three distinct regions which reflect the results of the entry heating and are defined as follows along with the general range in depth in the heat shield at which they exist:

Region of sample	Depth, x, in.
Change of electrical resistance	0 to 0.12
Visible char	0.12 to 0.20
Discolored region	0.20 to 0.35

During this flight test the heating rates were low enough so that the ablation process was confined to charring the resin portions of the heat shield with no surface recession. The char sensors were calibrated to indicate the progression of the char front. This calibration was obtained from ground tests conducted by the heat-shield contractor using sensor-instrumented models. The results obtained from the sensor readings during this flight test were satisfactory in a qualitative sense but indicated excessive char depths ranging from 0.275 inch to 0.365 inch as compared to the value for change of electrical resistance of about 0.12 inch. This disagreement is attributed to difficulties associated with a proper simulation for the calibration.

A sample cut from the extreme edge of the heat shield showed the visible char penetration level to be essentially the same as noted at other points over the heat shield. The uniformity of the visible char depths over the heat shield, like the uniform temperature distribution, lends credence to the fact that the heat shield had essentially undergone a uniform heating.

Summary of Results

The Big Joe flight test yielded the following results:

(1) Although the trajectory flown by the test vehicle was different from that anticipated for a typical Mercury entry, the test proved that the ablation heat shield was an efficient and reliable heat protective device. Not only did the heat shield demonstrate its ability to withstand the heating during entry with only minor surface effects, but it also showed no effects caused by landing loads.

(2) Measured heat-shield temperatures and char depths indicated that the heat shield essentially experienced a uniform heating over its

surface. Specific-gravity measurements of the recovered heat shield (fig. 12) indicated that in the charring process only 25 percent of the available resin content was lost.

(3) The heat shield could, at the heating rates experienced, function as a char-forming reradiative shield with no surface recession and only a very little mass loss caused by the advance of the char interface through the resin system.

(4) The peak temperatures reached were just in the range of glass melting temperatures; thus, the glass forms a reasonable reinforcement for such conditions.

This test provided both an encouraging demonstration of the soundness of the ablative approach in general and of this type of construction in particular. Further, it provided, early in the program, a source of data on which an analytical model could be based. This model was constructed and used as a tool to describe the probable performance of the operational shields based on the observed performance of the Big Joe shield.

Thermal Performance Analysis

Trajectory Considerations

The thermal performance of an ablative heat shield will depend not only on the properties of the shield material but also on the external flow conditions in the region of interest. Only the stagnation point was considered for the analysis; however, because of the uniform flow conditions, the results were assumed valid for the entire shield.

The required external flow conditions are temperature and enthalpy as functions of time. These conditions were derived from an analysis of the normal shock at a number of points along the entry trajectory (ref. 4). Since conditions at the edge of the boundary layer were closely approximated by conditions immediately behind the shock, these latter were used. Also derived from the trajectory was a time variation of the stagnation point convective heating-rate (ref. 4), as expressed by:

$$q_{Aero} = \frac{17,600}{\sqrt{R_N}} \sqrt{\frac{\rho_{am}}{\rho_{SL}}} \left(\frac{V}{V_c}\right)^{3.15} \left(\frac{H_2 - H_w}{H_2 - 120}\right) \qquad (1)$$

An extension of the analysis could have been made to include shock layer radiation heating, but, as this source of heat is less than 1 percent of the convective heating for a typical Mercury entry, it has not been included. Further discussion of the ablation model and numerical analysis is given in appendix B.

Determination of Ablation Parameters from Analysis of the Big Joe Flight

In addition to the thermal properties of the uncharred ablation material, which were presumed known and treated as functions of temperature only, it was necessary to obtain certain ablation parameters.

In the ablation process, the resin undergoes decomposition of a complicated nature which depends partly upon the temperature and the reinforcing material. A portion of the resin decomposes completely to a gas, the remainder decomposing only partially. Near the surface, prolonged exposure to higher temperatures causes more complete pyrolysis, thus the surface layers of the char show a more complete decomposition than the inner layers. This behavior is shown in figure 12 where specific gravity is plotted against the distance from the surface measured for the Big Joe heat shield. Accordingly, conductivity could be expected to vary considerably across the char layer. Further, in each element of the ablator, decomposition will occur progressively as the temperature increases.

The development of an analysis for this very complex process required some simplifying assumptions which are as follows:

(1) Ablation occurs at one specified temperature.

(2) The char layer is homogeneous and its conductivity and specific heat are functions of temperature only.

(3) A known fraction of the resin is pyrolysed.

(4) Further decompostion of the products of pyrolysis neither requires nor produces heat.

From the Big Joe heat-shield test results a char specific gravity of 1.55 was selected corresponding to the measured surface value. The change in specific gravity of 0.18 corresponded to a loss of 26 percent of the resin. The resin originally comprised 40 percent of the weight of the composite.

A value of 1,000 Btu/lb for heat of vaporization of that fraction of charred resin is commonly quoted and was used in the analysis. Surface emissivity was taken as 0.9 and the blockage coefficient, $\alpha\epsilon_p$, taken as 0.15, corresponding to a Prandtl number of 0.74 and a mean specific heat of 0.25 Btu/lb-° F.

More difficult to define were the ablation temperature and effective char conductivity, parameters of prime importance. To obtain these, an empirical approach was taken. The set of values which best matched the Big Joe flight data was sought, and these values were used for subsequent analysis of the various Mercury entries. A range of char conductivities was obtained for study by interpolating curves between data for fully charred and uncharred material as shown in figure 13.

A number of cases were run by using different values of ablation temperature and char conductivity as the two independent variables and two criteria were selected to determine when Big Joe results had been matched. These were total mass loss and temperature distribution in the shield after the ablation was complete. A comparison of temperature distribution was based on the definition of a single number ΔT, which is the difference between an average Big Joe shield temperature at depths of 0.19, 0.29, and 0.39 inch from the surface and the average of analytical temperatures at the same depths. Plots of unit mass loss and ΔT against ablation temperature and char conductivity are shown in figures 14 and 15, and the "match point" determined the effective values of ablation temperature and char conductivity which had to be used in the analysis to give a mass loss of 0.2 lb/ft^2

and a $\Delta T = 0$, that is, to give results which agreed with those observed in the Big Joe shield.

The effects on unit mass loss of variations in the values used for heat of vaporization and blockage coefficient are shown in figures 16 and 17. These figures show that there was only a weak dependence of shield performance on these parameters. The effect of variations in the fraction of resin vaporized upon unit mass loss is shown in figure 18.

Finally, results from the analysis of the Big Joe case using the parameters selected as indicated previously were compared with flight data. In figure 19, this comparison is made of the temperature distribution at particular times during the flight.

Interpretation of Char Depth

It is observed that the depth of char is somewhat arbitrary. Change of electrical resistance, visual charring, and a less pronounced discoloration occur at three different depths. In the present analysis, another definition of char has been introduced; that is, the depth over which density must change from the uncharred to the charred value to account for the total mass loss. For the Big Joe shield, these four char depths were related as follows: (1) change of electrical resistance, 0.12 inch; (2) visual char, 0.20 inch; (3) discolored region, 0.35 inch; and (4) mass-loss depth, 0.21 inch. From this relationship a simple scaling to other cases can be performed by taking a ratio of the char depths which can be physically observed to the "mass-loss" depth which results from the analysis as follows: (1) change of electrical properties, 57 percent of mass-loss depth; (2) visual char, 95 percent of mass-loss depth; and (3) discolored region, 170 percent of mass-loss depth.

The results of this analysis demonstrated that a reasonable engineering model of a simplified nature could be contrived to reconcile the observed flight results. The accuracy with which the data were fitted gave assurance that at least the major mechanisms involved were being treated correctly. An important deduction from this and from the result that the ablation surface operated at essentially radiation equilibrium temperature is that for this type of material and environment the dominant mode of heat rejection is radiation. The Mercury heat shield is in essence a thermal protection system which operates primarily by the spontaneous formation of a high temperature radiative surface and the utility of which is only slightly improved by internal kinetics and convective blockage.

Design and Fabrication of Production Shield

Selection of Design Trajectories

The Mercury spacecraft entry was typical of satellite entry at low flight path angles dictated by permissible g limits for the human occupant and minimal retrograde decrement of velocity. A concern over the possible failure of a retrograde rocket led to the selection, for design purposes, of the case of one retrorocket failing to function. The range of heating rate and pulse experienced by the shield along with trajectory parameters is shown in figure 20 for such a case. This design case yields a heat pulse of approximately 8,910 Btu/ft^2 for a spacecraft weight of 2,439 pounds.

Design Criteria

The environment experienced by the spacecraft is extremely severe. Temperatures in the shock layer immediately ahead of the blunt drag-body surface are in excess of 10,000° F, beyond the melting point of all materials. The Mercury heat shield was designed to protect the spacecraft for all design entries and control entry temperatures to specified limits. In order to provide adequate protection for the astronaut, whose back lies only a few inches away from the inner surface of the heat shield, a criterion on the temperature of the inner surface of the shield was set at 150° F. Considerations of the double layer makeup of the shield and the bonding state-of-the-art led to a further criterion on bondline temperatures being set at 600° F. The heat shield must also have the capability to withstand the dynamic pressures involved while sustaining a very hot condition and sustain the high water-impact forces before the structure has cooled appreciably. The heat shield should have the capability to withstand the acoustic and vibration environments imposed during launch and the hard-vacuum and low-temperature conditions of the space environment.

Thermal Performance Criteria

The thermal performance of the heat shield of the Mercury spacecraft required the following:

(1) Contain the extent of ablation within the region of the inclined laminates.

(2) Maintain the specified bondline temperature to preclude delamination.

(3) Maintain the specified backface temperature to minimize heat rejection to the interior.

These conditions were to be fulfilled for any abort situations and for any entries from orbit in which two or more retrograde rockets functioned.

Fabrication of Production Shields

To utilize the experience gained in the construction of the prototype shield flown on Big Joe, the prime contractor for the Mercury spacecraft was directed to produce heat shields for the Mercury program similar to the basic design proven in the Big Joe flight.

The operational shields were made as shown previously in figure 2. An inclined ablation laminate, with shingles at 20° to the local tangent as for the R and D shield, 0.65 inch thick formed the outer element. The structural (parallel) laminate was 0.30 inch thick.

Appendix C describes in some detail the fabrication technique employed for the shield.

Of the several fabrication problems encountered the most significant was that of maintaining the correct orientation of the inclined ablation laminates.

There was concern whether 20° inclination of the laminates was actually being attained and consequently several shields were bored near the outer diameter so that the actual angle of inclination could be observed. The results of this inspection

indicated that the angles, in general, were being produced. These holes which measured about 1 inch in diameter were plugged with representative shingle material, and the plugs were retained in the shield by the parallel backup structure. Only in the center of the shield did the circumferential orientation become a problem. Observations made at the exposed surface showed that the innermost shingle laminates were wrinkling and buckling in groups. By cross-sectioning a test shield near the center the contractor found that the angle of inclination deviated appreciably from the desired 20° angle. In some examples, the fibers close to the parallel liminate were perpendicular to the face and then bent over and either were directed parallel to the face or in some cases even at a negative angle before returning toward the outer face. This poor orientation indicated that a section of the center of the shield could be lost as a result of delamination and improperly attached fibers. A decision was therefore made to machine out the center of the shield and replace it with a high-pressure molded plug of 15-inch maximum diameter (fig. 2). A large block of properly orientated material was produced by stacking developed cones of the proper included angle. A segment was then cut from this block to form a plug. The plug was secured in the heat shield by 12 inclined dowel pins, 4 located on an inner circle and 8 located at a larger diameter. To provide additional strength behind the central plug, a larger diameter patch pad composed of additional parallel laminates was added to the inside or concave side of the shield after the dowel pins were cemented in place. This pad was a maximum of two-tenths of an inch thick. Additional structural details are given in appendix C.

The bond between the inclined laminate and the parallel laminate was provided by a high-temperature aluminized epoxy bonding agent.

Ground Testing

Establishment of the Heating Environment

Numerous wind-tunnel studies were conducted to investigate the heating, aerodynamic stability and loads experienced by the spacecraft in the Mach number range from 0 to 20. Models ranging from as small as 1 percent of full scale to full scale were used in these investigations. Further, full-size spacecraft components were employed for studying detailed heating effects. These tests played an invaluable part in defining the aerodynamic heating of the Mercury spacecraft. Reference [1] further outlines the Mercury wind-tunnel program.

Early Thermal Performance Tests

Thermal tests included plasma-arc, radiant-lamp, and oxyhydrogen blowtorch tests. Radiant-lamp tests were performed on a 2-inch diameter specimen representative of the heat shield material to attempt to simulate the heating encountered during reentry conditions. During these tests, the specimen severly delaminated. Radiant-lamp tests were also performed on a one-third scale model and resulted in specimen failure. This was due to the monitoring thermocouple being located 0.1 inch below the surface. Since the thermocouple did not respond, the lamps were driven at full power, twice overload, to try to achieve the programed thermocouple response. Oxyhydrogen blowtorch tests were performed on specimens from a production shield. In general, however, the simulation was poor because of different chemistry and the low temperature and enthalpy of the stream. No really useful data resulted from these early thermal performance tests.

Arc-Jet Tests

Introduction.- The failure of previous heat shield ablation tests and other thermal tests to duplicate the severe reentry conditions properly made it necessary to evaluate further the performance of the Mercury heat shield. This was done in a series of ablation tests, conducted at the NASA Langley Research Center Structures Division arc-jet facility using air as the working medium.

These tests were planned to simulate as nearly as possible, with a model designed to limit edge failure, the heat fluxes which would be encountered by the Mercury spacecraft heat shield during atmospheric entry.

Description of Model and Instrumentation.- Test specimens were obtained from a production Mercury heat shield (no. 13), which had been rejected because of structural defects apparent during ultrasonic examination. The defective area, which contained voids, delaminations, or other flaws or imperfections, was confined to a ring about 6 inches wide located approximately 2 feet from the center of the shield. Five specimens were obtained from sound areas of the shield, while two specimens were obtained from defective areas.

The model design shown in figure 21 was used for the original five sound specimens (tests 1 to 5) and one of the defective specimens (test 7). Care was taken to protect the specimen edges from heating by use of a phenolic asbestos collar which was bonded to the specimen with a room temperature vulcanizing rubber. Fiber-glass disks and thermoflex insulation were incorporated to protect the back surface of the specimen from heating. For model 6, a change in the design of the model was made. In this design the fiber-glass disk that was originally bonded to the heat shield specimen was displaced $\frac{1}{8}$ inch from the specimen and located by three $\frac{1}{8}$ inch dowels inserted 120° apart through the phenolic asbestos collar. These dowels were employed to provide a three-point specimen support to determine if the continuous peripheral constraint in the other models prevented bondline or parallel layup delaminations. A photograph of a typical model before testing is shown in figure 22.

Each specimen was instrumented with six chromel-alumel thermocouples; two at the back surface, one on the bondline between the shingle and parallel laminate structure, and three others at various depths as shown in figure 23.

Description of Tests.- The ablation heat shield tests were conducted in arc facility no. 20 of the structures division of the NASA Langley Research Center. A complete description of this facility is given in reference [5].

A multiple calorimeter probe, geometrically similar to the specimens, was used to determine the cold-wall heating rate obtained from the arc-jet stream. The power of the jet and the distance of the model from the jet nozzle were varied until the

desired heating rate, approximately 67 Btu/ft^2-sec, was obtained. Probe measurements showed little variation of the heating rate across the diameter of the specimen surface. The stream enthalpy was not measured but was estimated from previous experience to be approximately 4,000 Btu/lb. A summary of test conditions is given in table 2.

The tests were conducted in the following manner. The jet flow was initiated and after 40 seconds the calorimeter probe was inserted into the stream. The probe was removed after a few seconds and the heat-shield model, which was mounted on a water-cooled sting, was immediately swung into the stream. As soon as the model was removed, the heating-rate probe was again swung into the stream for an additional check on the heating rate. After testing, each specimen was photographed and cross-sectioned for further examination. The heating time for each model is given in table 2.

Results.- Temperature-time histories from thermocouple readings and surface temperature measurements observed by optical pyrometry were taken for each test. Figure 24 shows the measured time history for a typical (test 1) arc-jet test specimen.

Thermocouple 6, located closest to the front surface of the model, had a very rapid temperature rise and reached its peak temperature shortly after the cessation of heating for all tests. After the removal of the model from the arc stream, the temperature indicated by thermocouple 6 dropped very rapidly and when the recording of temperatures ceased (600 to 850 seconds), the temperature of thermocouple 6 was comparable with the remaining interior temperatures. Thermocouples located at the bondline and the backface of the model, as well as other interior points, peaked at later times and at lower temperatures. Figure 25 shows a typical (test 5) surface temperature plot obtained from optical pyrometry.

Application of Analysis to Arc-jet Tests

To assess these tests in detail and to establish the validity of the analytical model derived from the Big Joe flight, predictions were made of model performance in the arc-jet environment. This was done using a step heat input and the same material properties found to match best the Big Joe flight results.

Experimental results were compared with these predictions and the results are shown in figure 26 correlated on the basis of the total cold-wall heat pulse experienced by the model.

Part a of figure 26 depicts the visual char depth plotted as a function of total heat flux to the specimen. The visual char depths at these heat pulses closely matched the char depths obtained by the analysis using step heat inputs. Because of this good agreement, it was presumed that char depths could be accurately predicted for the Mercury heat shield in flight.

Part b of figure 26 compares the maximum experimental and predicted bondline temperatures for the tests. Experimental bondline temperatures were consistently higher than those calculated; the difference ranged from 40° F at low heat pulses to 150° F at high heat pulses. This difference is due mainly to the value of char conductivity used in the calculations. The value used provided good agreement with test results for the shorter heating periods, up to the 150 seconds experienced on the Big Joe flight. However, relatively small errors in conductivity would be amplified during the longer heating periods of the high-pulse ground tests, up to 300 seconds.

Figure 27 shows a curve of the maximum temperature of each arc-jet specimen at various depths from the front surface as given by thermocouple measurement. Also shown is visual char depth for each specimen. This determined the temperature at which visual char is complete and is defined as the effective ablation temperature. This parameter increased from 600° F at low heat pulses, the value found to match best the Big Joe results, to almost 900° F at high heat pulses. Since calculations were based on a fixed effective temperature of ablation of 600° F, this further explains why agreement between experimented and calculated bondline temperature is better at low heat pulses than at high heat pulses.

Flight Performance

Flight Descriptions

The background provided by the Big Joe flight and the arc-jet simulations gave confidence that the operational shield would perform satisfactorily. Predictions were made for a wide range of entry heat-pulse conditions from early abort to near decay, including typical entries such as that for MA 8 shown in figure 28. Following is a brief description of the Mercury flights covered in this report:

MA-2.- This was a suborbital flight launched on February 21, 1961, and designed to subject the spacecraft to maximum "g" and to produce maximum afterbody heating. Consequently, the total heat load on the shield was less than during an orbital entry. The heat shield was recovered in excellent condition.

MA-4.- This was the first orbital flight for the Mercury heat shield and was launched September 13, 1961. After traversing a single orbit in the unmanned condition, the spacecraft experienced normal entry heating conditions and was recovered. The center plug section of the shield had cracked free at the outer diameter and resulted in a gap at the parting line of about three-sixteenths inch. The plug was still tightly retained by the inclined dowel pins and was forcibly separated from the heat shield by breaking two of the dowel pins and tearing the holes around the other dowels. Examination of the parts showed that the previously curved center plug had flattened considerably during the cooling-off phase of the flight period. Also, the bonded surface showed the bondline thickness to be excessive, 0.047 inch thick as opposed to the specified 0.010 inch thick maximum thickness and further showed large air bubbles covering about 30 percent of the bond surface.

MA-5.- This was a two-orbit primate flight launched on November 29, 1961. The heat shield from this flight showed a similar char depth as the previous flight; however, the center plug was completely missing from the shield upon recovery. Again the glue line was excessively thick, 0.030 inch, but the

loss of the center plug was attributed primarily to an error in the drilling of the holes for the inclined dowel pins. The holes were two-tenths of an inch too shallow which resulted in essentially a complete loss of grip by the dowel pins upon the center plug section. A thermocouple protruding into the center plug area and still functioning upon water impact provided continuous flight data that indicated that the plug was in place up to the instant of water impact and separated from the shield upon impact. As a result of this separation and the separation during the preceding flight, an X-ray technique was developed that distinctly showed the air pockets in the bondline between the shield and center plug. The sharpness of definition of the air bubbles also indicated to some extent the height of the air bubbles or the thickness of the glue joint. Several experimental fabrication techniques were explored in an effort to eliminate the air pockets and to reduce the thickness of the glue joint. All shields that had been fabricated were X-rayed and the percentage of void in the glue joints was measured. All shields that exhibited greater than 20 percent void were returned to the manufacturer where the center plug was machined away and a new plug was installed, reinspected, and evaluated. In some cases, three and four new central plugs had to be installed before the percentage of voids was reduced to an acceptable level.

MA-6.- This was the first manned orbital flight of a Mercury spacecraft and was successfully made on February 20, 1962. The flight was planned for three orbits and was a culmination of the program to develop the Mercury spacecraft and to use it for manned orbital flight. In general, the spacecraft functioned well during the mission. Because of a false indication of heat-shield detachment it was decided to perform the entry with the retropackage on the heat shield. The external surface of the shield was charred in the normal pattern. The center plug of the shield had separated as in the previous orbital missions. The same area contained several radial marks approximately 4 inches in length. It is possible that a large piece of the retropackage slipped off in this direction.

MA-7.- This was the second manned orbital flight and was conducted on May 24, 1962. The flight was planned for three orbits and was a continuation of a program to acquire operational experience and information for manned orbital space flight. The performance of the MA-7 heat protection system was as expected and was quite satisfactory. The maximum recorded values of temperature on the ablative shield were compared with previously obtained orbital reentry values. The magnitudes of these temperatures, as well as the ablation shield weight loss during reentry, were comparable with previous flights. The external surface of the heat shield had the normal, evenly charred, glass-streaked appearance and some circumferential separation of the edge laminations were evident. The ablation shield center plug was found to be missing, with evidence that the plug remained intact throughout the reentry heat pulse, as in the MA-5 mission. A number of cracks similar to those experienced in some previous missions were found in the ablation shield exterior; however, these cracks did not compromise mission safety. Considerable recovery-handling dents and cuts were noted. The weight loss of the heat shield during the reentry phase amounted to approximately 13 pounds. The supporting structure behind the ablation shield was found to be in excellent condition following the flight.

MA-8.- The third manned orbital space flight was conducted on Obtober 3, 1962. The flight was planned for six orbital passes or less and was a continuation of a program to acquire new knowledge while extending the operational experience in manned orbital space flight. All objectives were accomplished. The performance of the heat protection system was satisfactory. The materials and construction of the heat shield were the same as for heat shields used on previous orbital missions, with the exception that the center plug was bolted to the structural laminate to prevent its loss after reentry. The center plug was found to be firmly attached to the heat shield during postflight examination. During entry the heat shield provided satisfactory thermal protection as on previous orbital missions. As expected, the stagnation point appeared to have been very near the center of the shield and the usual glass droplet streaks extended out from the center of the shield. Minor and major cracks in the ablation laminate and separation at the bondline were evident in postflight inspection. The separation at the bondline, where the ablation laminate is glued to the structural laminate, was found to be extensive over the center portion of the shield and extended approximately one-half the radius of the shield. The unbonded surfaces were smooth. The cracks in the ablation laminate apparently occurred after reentry heating, as evidenced by a uniform char depth in the cracked and uncracked portions of the ablation laminate. When the bondline separation was found in the shield used for the MA-8 mission, a section was cut from the MA-7 shield and it was found that substantial bondline separation was evident without major cracks showing at the exterior of the ablation laminate. The heating appeared to be uniform over the shield as indicated by 12 core samples taken at various locations in the shield. Char depth measurements were normal, varying from 0.33 to 0.40 inch as in previous missions. The measured weight loss, 17.43 pounds, was more than that experience during previous missions. The MA-7 heat shield lost 13.1 pounds and the calculated loss was approximately 11 pounds. The measured weight loss for previous missions has been as low as 6.1 pounds. However, the heat-shield drying procedure used after flight to remove water has not been the same for all flights, thus leading to some uncertainty as to the significance of the apparent differences in weight loss.

MA-9.- The fourth and last manned orbital space flight was performed on May 14, 1963, and was highly successful. The materials and construction of the heat shield were the same as those for heat shields used on previous orbital missions with the exception that six steel bolts were installed in a circle having a radius of 14 inches from the center of the heat shield to aid in retaining the shingle portion of the shield at landing in case of bondline separation. Postflight examination revealed only minor cracks in the ablation laminate. A section through the center of the shield indicated that the bondline had separated, but that it had been held together by the bolts. The separated area was not nearly as extensive as that evident on the MA-8 heat shield, and the surfaces of the separation region were smooth. No large cracks were observed to emanate from the separated bondline area, as had occurred in the previous two flights. During reentry, the heat shield provided

satisfactory thermal protection, as on all previous orbital missions. The extended time of exposure of the heat shield to the space environment did not result in any noticeable effects regarding the heat-shield performance. As expected, the stagnation point appeared to have been close to the center of the shield, as evidenced by the usual glass droplet streaks that extended out from this point. The reentry heating appeared to be uniform over the shield, as indicated by 10 core samples taken at various locations. Char depth measurements of these samples indicated normal heating, and these values varied from 0.34 to 0.38 inch similar to previous missions. The measured weight loss of the heat shield was 15.34 pounds. The spacecraft heat protection system performed satisfactorily as in previous missions.

Heat Shield Instrumentation

Each Mercury flight had a unique set of heat-shield instrumentation. This instrumentation consisted of thermocouples located at various depths and radial locations. These locations are given for each shield in table 3. The following section gives the data from these thermocouple and sensor locations.

Observed Temperatures

Figure 29 shows the Mercury-Atlas heat-shield temperatures for all sensors for each flight. Maximum bondline temperatures experienced a range of from 300° to 450° F, values meeting the 600° F bondline criteria. These maximum temperatures occurred at water impact. Temperatures in excess of 300° F were observed on the shield backface in some cases. Such temperatures, however, did not apparently affect equipment or the structural integrity of the shield.

Postflight Measurements

Postflight measurements of visual and electrical char depths and specific gravity were taken of specimens from the heat shield of each Mercury spacecraft. Additional postflight measurements of glass content, water absorption, and weight loss under vacuum conditions were taken of specimens from the MA-9 orbital heat shield and specimens from virgin Mercury heat-shield material. These measurements are reported on in appendix D.

Analysis of Spacecraft Entries

A variety of Mercury spacecraft entries was studied by using the prediction analysis which has been previously described. Entries from nominal missions and from a wide range of abort and emergency conditions were analyzed to determine char depth and temperature distribution of the heat shield. The results of these studies are compared with the data obtained in flight in figure 30 correlated on the basis of total heat pulse.

Figure 31 shows a variation of maximum Mercury-Atlas heat shield temperatures with depth from the front surface for all sensors flown on orbital entries. Fairly good correlation of all temperature sensors can be shown on a plot of this type. Additionally, appearance of a flight heat shield plug can be correlated as to temperatures corresponding to the visual char depths shown. It can be inferred that the regions described in the section entitled "Interpretation of Char Depth" can be correlated with maximum temperatures in the tabulation which follows:

Conditions	Temperature, °F
Completely charred	> 1,000 to 1,200
Partially charred	> 600 to 800
Discolored	> 400 to 500
No visible heating effects	< 400

In summary, it is considered that an adequate engineering analysis was developed to predict the performance of the Mercury spacecraft heat shield. The results of the Big Joe heat-shield flight test were used to aid in the selection of parameters for the analysis which has been applied to a variety of Mercury entries. Good agreement between the analytical and observed test results is noted for all the flights.

Linear variations of char depth and backface temperatures with total heat pulse are found to exist over a wide range of entries from early abort to near decay.

This analysis is based on the assumption that the parameters determined from the Big Joe heat-shield test apply to the larger heat pulses of orbital entries. Support of this assumption is indicated from the results of arc-jet tests on specimens of the Mercury shield at heat pulses from 7,400 to 20,700 Btu/ft^2. A second iteration on the properties to be used in the analysis could have been made by using ground-test data. Further refinements in the analysis are also obvious. However, these refinements were never made during the lifetime of the project and will probably never be important because of the change in direction of entry ablative technology.

Conclusions

The Mercury spacecraft heat shield was shown to be well suited and reliable for the entry conditions encountered. The dominant mechanism of heat rejection is radiation from the surface which does not recede during entry. A straightforward one-dimensional analysis was developed to reconcile the results of flight and ground testing. Manufacturing difficulties were experienced but overcome and consistently good performance was obtained from the seven shields that were flown.

Appendix A.- Ablation Sensors

Three types of ablation sensors were developed for NASA (types 1, 2, and 3).

The type 1 ablation sensor was a slightly truncated cone with a tip end exposed at the front face and measuring $\frac{1}{8}$-inch in diameter. The operating principle was that the material remaining after charring was carbonaceous in nature and formed an electrical conductor. Fine wires were brought within various distances of the front face and electrical power was passed through the wires. When the char reached a certain depth, an electrical circuit was thus completed between a pair of the fine wires. This sensor was tested by a contractor and found to be satisfactory.

The type 2 ablation sensor consisted of a $\frac{1}{2}$-inch-diameter plug with a double twelve-pitch thread cut into the outer surface. The plug was heavily copperplated and then carefully ground so that a pair of interwound helical copper wires remained at the base of the threads. The dual wires formed a condenser, the total capacitance of which decreased as the char layer progressively advanced into the shield and caused a short circuit in part of the wire lengths. Prototype samples of this sensor were tested by NASA but did not perform satisfactorily and the concept was discarded.

The type 3 sensors operated on the same principle as the type 1 sensor. However, three were tested by NASA and did not function properly.

Appendix B.- Program for Ablation Analysis

The ablation model assumed is one-dimensional and considers the overall thickness to be constant while a char front advances through the material. A finite difference analysis is used in which the material is divided into thin elements. An element is treated as ablating when it reaches a specified "ablation" temperature. When the heat necessary to vaporize a specified fraction of the resin has been absorbed, the element becomes "charred." A heat blockage term is included based on the rate of ablation and conditions outside the boundary layer (ref. 6).

$$q_{BL} = \alpha \bar{c}_p (T_e - T_a) \frac{dm}{dt} \tag{2}$$

in which

$$\alpha = 1 - \frac{1}{3} (N_{PR,e})^{-.6}$$

Because of the assumption of unchanged overall thickness, the analysis cannot be applied to cases in which the heating rates are high enough to cause the removal of appreciable amounts of the charred material, rates on the order of 100 Btu/ft^2-sec, nor to cases in which mechanical removal of the char caused by high shear forces occurs. Neither of these situations occurred for the Mercury heat shield.

The numerical analysis is based on a conventional finite difference solution of the conduction between adjacent one-dimensional elements described in reference 7.

The difference equation for a typical internal element n is written as:

$$\Delta T_n = \frac{2\Delta t}{\rho_n \delta_n c_p} \left[\frac{(T_{n+1} - T_n) k_{n+1} k_n}{\delta_n k_{n+1} + \delta_{n+1} k_n} - \frac{(T_n - T_{n-1}) k_n k_{n-1}}{\delta_n k_{n-1} + \delta_{n-1} k_n} \right] \tag{3}$$

and

$$T_n' = T_n + \Delta T_n$$

The time increment ΔT is assumed small so that properties k_n and c_n can be evaluated at the temperature T_n prevailing at the beginning of the step.

For the surface element N the difference equation is written

$$T_n' = T_n + \frac{\Delta t}{\rho_n \delta_n c_n} \left[q_{Aero} - q_{BL} - \sigma T_n^4 - \frac{2(T_n - T_{n-1}) k_n k_{n-1}}{\delta_n k_{n-1} + \delta_{n-1} k_n} \right] \tag{4}$$

The inner surface was considered to be adiabatic.

This analysis was programed for machine computation on an IBM 704 digital computer.

Appendix C.- Ablation Shield Fabrication and Manufacturing Problems

Fabrication Technique

The fabrication procedure which was eventually employed involved first the buildup of the ablation shingle laminate and the subsequent addition of the ring and the parallel laminate. The shingle laminate was fabricated by laying the resin-impregnated fiber-glass cloth tape obliquely on a mandrel and building in to the center in a single continuous process. This component was then cured at a pressure of 65 psi for approximately 12 hours at temperatures up to 300° F. This was followed by a 72-hour post cure at 250° F. The edge ring and parallel layup were subsequently applied over an aluminized epoxy bond. The entire assembly was post cured for 21 days, 7 days each, at temperatures of 250°, 300°, and 350° F.

The molded center plug measured 15.5 inches in diameter and was 0.65 inch thick with a 0.23 inch high 1-inch-diameter nubbin in the center. The taper angle was $14\frac{1}{2}° \pm \frac{1}{4}°$. The plug was held by 12 0.202-inch-diameter dowels in 0.219-inch holes, 8 at a $5\frac{3}{4}$-inch radius and 4 at a 2-inch radius (at concave surface) inclined at a 45° angle inward. The depth of the dowel measured 1.15 inches on the dowel axis, or 0.813-inch through shield thickness. The shield was 1.15-inches thick at the center (0.95-inch + 0.2-inch backup). Thus, dowels are set 0.313-inch into the plug.

The backup plate measured 33 inches in diameter (maximum) and was feathered to a diameter of 29 inches. The plate was 0.20-inch thick in the center, 0.177-inch thick at the outer edge (29 inches diameter), and 0.020-inch at 33 inches diameter.

Manufacturing Problems

Shingle Delamination.- Early in the program, the manufacturer of the spacecraft prepared two of the heat shields for static-load tests. The first shield was ruined by placing the entire shield in a large oven for the purpose of curing some bonded load pads for the ground-test program. The rapid

uniform heating of the entire shield resulted in delamination of areas in the parallel laminated backup structure as a result of volatile gases being generated between the parallel laminates where there was no venting. Large blisters, measuring 6 to 10 inches in diameter, occurred at several locations in the backup structure. A second shield was also ruined in an attempt to bond loading pads to the shield when the oven temperature regulator went out of control. This shield was first quartered and then cut up into many small test specimens. Upon sectioning the shield, areas were visible where the shingle section of the shield was extensively delaminated. It was theorized that these delaminations between plies were opened to the surface and the long post cure cycle of heating the shield at 250°, 300°, and 350° F for 7 days each resulted in oxidizing the resin in those areas where porosity existed. These porous or delaminated areas were not detectible by X-ray. The heat shield contractor, however, experimented with various inspection methods to detect porous areas in the final product without destructive testing of the shield. By using ultrasonic transmission through the thickness of the shield, the contractor could detect even very small areas of porosity. Specimens from the second damaged shield were used to calibrate the degree of porosity. Small confined local areas of porosity were not considered detrimental to the integrity of the shield; however, the large areas were considered unacceptable. Each shield thereafter was completely ultrasonically surveyed in various phases of its construction. Small areas of porosity were observed to increase in size as the shields were exposed to additional heat cure and post cure cycles. Shields that showed areas of porosity too large to be acceptable for flight were generally salvaged by completely machining all the shingle laminates away from finished shields and rebuilding the shingle laminate thus salvaging the parallel laminates and the outer rings. In some cases where shingle buildup was examined prior to the addition of the parallel or ring sections, the complete shingle layer was scrapped when found to be excessively porous. All shields produced showed some small areas of porosity as a result of the sensitive ultrasonic inspection methods; however, upon postflight examination, none of these areas ever showed an indication of affecting the performance of the shield.

Ring Separation. - During the pressure and heat-curing cycle of some of the shields during fabrication, cracks developed between the outer composite ring assemblies and the parallel or shingle laminates. These cracks sometimes covered a circumferential angle of greater than 120°. The cracks were always repaired by filling the cracks with raw laminate material and resins and by adding dowel pins between the parallel and ring assemblies. Some 218 helical inserts that were later used to attach the landing bag to the heat shield also gave confidence that these cracks would never pose a structural problem. Repaired cracks were never found to reopen as a result of ground-test loads or flight conditions.

Appendix D. - Postflight Measurements

Visual and Electrical Char Depths

Postflight measurements of visual and electrical char depths were taken of the heat shield of each Mercury spacecraft. These measurements are shown in table 4. In order to obtain specimens for postflight examination, cylindrical cores measuring 2 inches in diameter were taken from each shield. A sketch of typical core locations (MA-7) is shown in figure 32. Visual char depths were measured after one edge of each specimen was polished flat to obtain a clean smooth surface. Visual char depth measurements averaged between 0.30 inch and 0.40 inch for all flights, tending to be slightly higher on the average for the later flights. The increasing spacecraft weight for the later flights, as shown in table 5, which contributes to the greater heating is a factor in increasing char depth. Electrical char depth measurements were made by successively removing thin (0.030 in.) layers of char material and taking resistance measurements across the surface of the specimen. After changes in resistance started to occur, cuts of 0.005 inch to 0.010 inch were made before each measurement. This change in resistance determined the "electrical" char depth. A direct correlation was established between electrical and visual char depths as determined from postflight measurements. Electrical char depth is generally about 57 percent of visual char depth.

Specific Gravity Measurements

Postflight measurements of specific gravity of the heat-shield specimens are shown in table 6. Two specimens measuring $\frac{1}{2}$ inch by $\frac{1}{2}$ inch in cross section and extending the full depth of the shield were cut from every core of each heat shield. Specific gravity measurements for specimens from the MA-9 shield are approximately 15 percent higher than for other shields because of differences in measuring techniques. It is believed that prime reliance should be placed on the data from shields MA-2 through MA-8.

Figure 33 shows a typical variation of specific gravity with depth through the heat-shield specimen (MA-7). The figure shows that char formed during entry is less dense than the virgin material and the density starts becoming uniform after approximately 0.40 inch.

Water Absorption Measurements

A unidirectional water-absorption study of MA-9 preflight and postflight heat-shield material was performed. Samples consisted of preflight-virgin and postflight-charred material. Six right circular cylindrical samples were supplied; three of these samples were virgin material with a diameter of 1.59 centimeters and a height of 2.42 centimeters, and three were charred samples of similar dimensions.

In an effort to determine an upper limit to water absorption, void volumes for the virgin and charred samples were determined. A specially prepared pycnometer, which could be inserted in an evacuated desiccator, was used to made void volume measurements. The pycnometer was evacuated to insure that entrapped air was removed from the samples.

Unidirectional water-absorption measurements were made by sealing all but one end of the sample with tape and paraffin, immersing the samples in water, and removing and weighing them at appropriate time intervals.

Figure 34 shows unidirectional water absorption for virgin samples as a function of time. Since the same surface area was exposed to water for each sample, the variations of water-absorption rates for the three samples probably were caused by variations in the reproducibility of the method. Good sealing around the sample was not easily maintained. Approximately 12 percent of the total surface area was exposed to water for each sample. A limiting value for water absorption is represented in the average void volume for the virgin samples which was previously given.

Figure 35 indicates the water-absorption history for the charred samples. The average void volume of the charred samples represents the average limiting value of water absorption for the same samples. As shown in figure 34, the variations in water-absorption rates were probably caused by variations in the reproducibility of the method.

Weight Loss

A study of weight loss in the vacuum of the MA-9 heat-shield material at 75°F and at 375° F was performed. The samples supplied consisted of preflight-virgin, and postflight-charred material. Six samples were supplied; three plate samples of virgin material with dimensions of 2.5 by 2.5 by 0.3 centimeters and three plate samples, charred, of similar dimensions.

Experimental equipment.- All weight loss and pressure measurements were obtained and recorded by using a recording balance with vacuum system.

Heating of the sample was accomplished by using three reflector-mounted infrared heat lamps. The lamp-sample distance was adjusted to provide the desired sample temperature.

Experimental procedure.- Prior to the weight-loss determinations, the samples were weighed and then desiccated for approximately 48 hours. The system was pumped down to approximately 1×10^{-6} millimeters of mercury. After the system reached equilibrium at room temperature, the temperature was raised to 375° F. An equilibrium weight-loss rate was attained at 375° F and the experiment was terminated. The same procedure was used for both charred and uncharred samples.

Results.- The observed results are shown in the following tabulation:

Sample	Initial sample weight, g	Equilibrium weight-loss rate		Total weight loss after $2\frac{1}{4}$ hours at 375° F (Initial), mg
		Room temperature, mg/hr	375° F, mg/hr	
Uncharred	2.9389	0.24	0.56	19.7
Charred	2.5895	.15	.22	19.2

The tabulation shows that the weight-loss rates are very small for both charred and virgin heat-shield material and are quite insensitive to temperature. This weight loss probably represents the loss of absorbed contaminants.

Chemical analysis of MA-9 Heat Shield for Glass Content and Combustible Volatiles

A chemical analysis of the Mercury heat shield for glass content was performed. Samples consisted of preflight virgin, and postflight charred heat shield material. Both kinds of samples were taken from the ring region of MA-9. A sample of each material was analysed to determine in each the fraction by weight of combustible volatiles, the fraction by weight of fiberglass, and, in the case of the charred heat-shield sample, the fraction of unbound silica remaining in the char region.

The procedure used in making the chemical analysis was as follows: A sample, weighing approximately 2 to 3 grams, was cut from the uncharred, virgin specimen and one from the charred specimen. Both samples were ignited in air at 1,400° F in platinum crucibles until the contents maintained a constant weight. It was found that the combustible volatiles were 30.06 percent[1] for the virgin heat shield, and 24.42 percent for the charred heat-shield material.

The silica content of the specimens was next determined. The residues from the combustible volatiles measurement, still in the platinum crucibles, were treated with a 50-50 mixture of concentrated nitric and hydrofluoric acid solution. The moistened residues were dried on a hot plate and heated with a burner. The process was repeated until constant weights were obtained. The silica was determined to be 39.23 percent for the virgin material and 43.15 percent for the charred MA-9 material.

A summary of results and comparison with the manufacturer's specifications for virgin MA-9 heat shield material is given in the table which follows:

Sample materials	Manufacturer's spacification, %	MA-9 virgin heat shield, %	Charred MA-9 heat shield, %
Combustible volatiles	--	30.06	24.42
Resin content	31.8	32.6	26.5
Total incrganics	--	69.94	75.58
Total silica	36.15	39.23	43.15
Portion of silica in fiberglass	34.98	35.68	29.01
Fiber-glass content	68.2	67.33	54.79
Unbound (free) silica	--	--	12.02

[1] All percentage measurements are by weight.

Good correlation existed between the virgin heat-shield analysis and the manufacturer's specifications. The analysis of the charred heat shield showed the loss of volatile carbonaceous materials, the corresponding increase in concentration of inorganics, and the fall in concentration of undisturbed fiberglass in the overall composition. The total silica concentration increased in the charred material and existed as unbound, free silica, probably concentrated totally in the charred regions of the heat shield.

References

1. Bond, Aleck C. and Kehlet, Alan B.: Review, Scope, and Recent Results of Project Mercury Research and Development Program. Presented at the Twenty-Eighth Annual Meeting of the Institute of Aeronautical Sciences, New York, N.Y., Jan. 25-27, 1960, Paper 60-35.

2. Staff of NASA Manned Spacecraft Center: Mercury Project Summary Including Results of the Fourth Manned Orbital Flight, May 15 and 16, 1963. NASA SP-45, Supt. Doc., U.S. Government Printing Office (Washington, D.C.).

3. Detra, R. W., Kemp, N. H., and Riddell, F. R.: Addendum to Heat Transfer to Satellite Vehicles Reentering the Atmosphere. Jet Propulsion, Vol. 27, No. 12, Dec. 1957, pp. 1256-1257.

4. Moekel, W. E.: Oblique-Shock Relations at Hypersonic Speeds for Air in Chemical Equilibrium. NASA TN 3895, 1957.

5. Peters, R. W. and Rasnick, T. A.: Investigation of Oxidation Resistant Coatings on Graphite and Molybdenum in Two Arc-Powered Facilities. NASA TN D-838, 1961.

6. Roberts, L.: An Approximate Analysis of Unsteady Vaporization Near the Stagnation Point of Blunt Bodies. NASA TN D-41, 1959.

7. Jakob, M.: Heat Transfer. Vol. 1. John Wiley and Sons, Inc., 1949.

TABLE I.- BIG JOE HEAT SHIELD INSTRUMENTATION

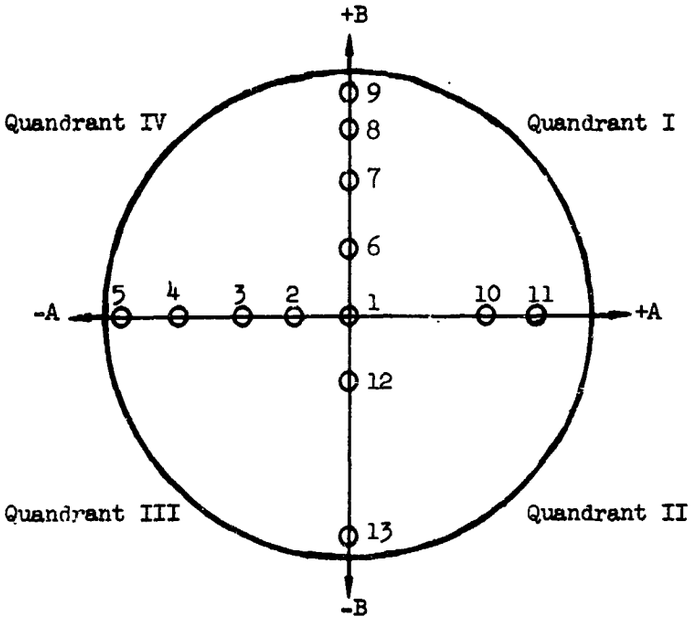

Sensor	Location		Thermocouple	Depth from surface, in.
	A, in.	B, in.	(a)	(b)
1	0	0	1	0.067
			2	.187
			3	.347
			4	.677
			5	1.067
			6	1.607
2	-7.4	0	34	0.071
			35	.191
			36	.351
			37	.681
			38	1.071
			39	1.611
3	-14.8	0	7	0.085
			8	.365
			9	1.085

[a]All thermocouples were chromel-alumel.

[b]The accuracy of depth measurement is ±0.001 inch.

TABLE I.- BIG JOE HEAT-SHIELD INSTRUMENTATION - Concluded

Sensor	Location		Thermocouple	Depth from surface, in.
	A, in.	B, in.	(a)	(b)
4	-26.6	0	40	0.092
			41	.372
			42	1.092
5	-35.8	0	43	0.096
			44	.216
			45	.376
			46	.706
			47	1.096
			48	1.636
6	0	11.2	10	0.099
			11	.379
			12	1.099
7	0	21.6	49	0.086
			50	.206
			51	.366
			52	.696
			53	1.086
			54	1.626
8	0	29.2	13	0.080
			14	.360
			15	1.080
9	0	35.8	16	0.098
			17	.378
			18	1.098
			55	1.098
10	21.6	0	19	0.092
			20	.372
			21	1.092
11	29.2	0	22	0.099
			23	.379
			24	1.099
12	0	-11.2	28	0.095
			29	.375
			30	1.095
13	0	-35.8	31	0.103
			32	.383
			33	1.103

[a]All thermocouples were chromel-alumel.

[b]The accuracy of depth measurement is ±0.001 inch.

TABLE II. - ARC-JET TEST SUMMARY

Test	Cold-wall heating rate, Btu/ft^2-sec	Heating time, sec	Total heat, Btu/ft^2	Distance from jet, in.	Flow rate, lb/sec	Stream enthalpy, Btu/lb
1	68	109	7,400	4	0.06	4,000
2	67	119	8,100	4	.06	4,000
3	67	142	9,500	4	.06	4,000
4	[a]58	180	10,400	4	.06	4,000
5	67	240	16,000	4	.06	4,000
6	69	300	20,700	4	.06	4,000
7	100	164	16,400	2	.08	>4,000

[a]Heating rate decreased from an initial value of 66 Btu/ft^2-sec to 51 Btu/ft^2-sec at the end of heating.

BLANK PAGE

TABLE III.- MERCURY FLIGHT HEAT-SHIELD TEMPERATURE INSTRUMENTATION

Flight	Segment	Sensor depth, in.	Location	Type of thermocouple[1]	Range, °F
MA-2	24	0.95	RX33, TY1	1	-20 to 500
	25	.95	X0, TY2	1	-20 to 500
	47	.80	LX1, TY2	2	-20 to 800
	48	.80	RX33, TY3	2	-20 to 800
	49	.65	RX1, TY2	2	-20 to 800
	50	.65	RX33, TY2	2	-20 to 800
MA-4	19a	.65	RX1, BY1.73	2	-40 to 1,050
	19b	.65	LX1.37, TY1.37	2	-60 to 1,000
	20	.40	LX2, BY1.5	2	-50 to 1,050
MA-5	25	1.15	LX1, Y0	1	-20 to 500
	48	0.95	RX33, TY3	2	-20 to 800
	49	1.15	LX1, TY1	2	-20 to 800
	79	.18	LX2.4, BY1.5	2	0 to 2,500
MA-6	76	.18	LX2, BY1.5	2	0 to 2,500
MA-7	19a	.65	RX33, Y0	2	-60 to 1,000
	19b	.65	X0, Y0	2	-60 to 1,000
MA-8	19a	.65	RX33, Y0	2	-60 to 1,000
MA-9	75	.65	X0, Y0	2	0 to 1,800

[1]Type 1 thermocouple; chromel-constantan

Type 2 thermocouple; chromel-alumel

TABLE IV.- P STFLIGHT MEASUREMENTS OF VISUAL AND ELECTRICAL CHAR DEPTHS

Flight	Specimen	Visual char depth, in.	Electrical char depth, in.	Flight	Specimen	Visual char depth, in.	Electrical char depth, in.
MA-2	1	0.15	-	MA-8	1	.33	.21
					2	.35	.21
MA-4	1	.35	0.20		3	.36	.21
	2	.34	.22		4	.35	.21
	3	.31	.215		7	.35	.22
					9	.40	.22
-5	4	.35	.232		10	.36	.23
	6	.36	.240				
				MA-9	1	.35	.30
6	1	.30	.24		2	.34	.28
	8	.30	.26		3	.35	.31
	10	.35	.25		4	.38	.31
	11	.35	.26		5	.37	.29
	12	.33	.24		6	.36	.29
					7	.37	.29
MA-7	1	.40	.23		8	.38	.31
	5	.37	.23		9	.35	.30
	6	.36	.25		10	.36	.29
	7	.35	.22				
	8	.37	.25				
	10	.40	.23				

TABLE V.- SPACECRAFT ENTRY WEIGHT HISTORY

AND AVERAGE VISUAL CHAR DEPTH

Spacecraft	Entry weight, lb	Average visual char depth, in.
MA-2	2,439.46	0.35
MA-4	2,432	.33
MA-5	2,645.12	.35
MA-6	2,698.12 (without retropackage)	.33
MA-6	2,815.95 (plus retropackage; rockets fired)	
MA-7	2,663.36	.36
MA-8	2,732.50	.36
MA-9	2,681.45	.36

BLANK PAGE

TABLE VI.- PO[illegible] FLIGHT MEASUREMENTS OF SPECIFIC GRAVITY

Flight	Specimen	Distance of wafer center from front surface, in.	Specific gravity	Flight	Specimen	Distance of wafer center from front surface, in.	Specific gravity
MA-2	1	-	1.74	MA-5	4	-	1.71
	1a	0.06	1.29		4a	0.08	1.50
	1b	.18	1.48		4b	.24	1.56
	1c	.30	1.71		4c	.40	1.65
	1d	.42	1.78		4d	.56	1.73
	1e	.54	1.79		4e	.72	1.78
	1f	.66	1.80		4f	.88	1.71
	1g	.78	1.80				
	1h	.90	1.85		6	-	1.72
MA-4	1	-	1.75		6a	0.08	1.62
					6b	.24	1.66
	1a	0.12	1.51		6c	.40	1.58
	1b	.36	1.74		6d	.56	1.73
	1c	.60	1.85		6e	.72	1.74
	1d	.84	1.92		6f	.88	1.69
	2	-	1.62	MA-6	1	-	1.54
	2a	0.08	1.55		1a	0.08	1.64
	2b	.24	1.63		1b	.24	1.69
	2c	.40	1.67		1c	.40	1.76
	2d	.56	1.74		1d	.56	1.71
	2e	.72	1.79		1e	.72	1.65
	2f	.88	1.76		1f	.88	1.74
	3	-	1.61		8	-	1.60
	3a	0.08	1.61				
	3b	.24	1.58		8a	0.07	1.40
	3c	.40	1.67		8b	.21	1.47
	3d	.56	1.76		8c	.35	1.70
	3e	.72	1.79		8d	.49	1.83
	3f	.88	1.74		8e	.63	1.65
					8f	.77	1.69
					8g	.91	1.66

TABLE VI.- POSTFLIGHT MEASUREMENTS OF SPECIFIC GRAVITY - Continued

Flight	Specimen	Distance of wafer center from front surface, in.	Specific gravity
MA-6	10	-	1.62
	10a	0.08	1.56
	10b	.24	1.56
	10c	.40	1.67
	10d	.56	1.74
	10e	.72	1.71
	10f	.88	1.74
	11	-	1.63
	11a	0.08	1.58
	11b	.24	1.58
	11c	.40	1.58
	11d	.56	1.72
	11e	.72	1.72
	11f	.88	1.73
	12	-	1.58
	12a	0.095	1.54
	12b	.285	1.52
	12c	.475	1.67
	12d	.665	1.75
	12e	.855	1.76
MA-7	1	-	1.66
	1a	0.095	1.60
	1b	.285	1.65
	1c	.475	1.77
	1d	.665	1.82
	1e	.885	1.89
MA-7	5	-	1.63
	5a	0.095	1.59
	5b	.285	1.61
	5c	.475	1.65
	5d	.665	1.78
	5e	.855	1.82
	6	-	1.64
	6a	0.07	1.36
	6b	.21	1.76
	6c	.35	1.69
	6d	.49	1.77
	6e	.63	1.81
	6f	.77	1.84
	6g	.91	1.74
	7	-	1.64
	7a	0.095	1.59
	7b	.288	1.61
	7c	.475	1.68
	7d	.665	1.78
	7e	.855	1.80
	8	-	1.64
	8a	0.095	1.58
	8b	.285	1.59
	8c	.475	1.68
	8d	.665	1.78
	8e	.855	1.81

TABLE VI.- POSTFLIGHT MEASUREMENTS OF SPECIFIC GRAVITY - Continued

Flight	Specimen	Distance of wafer center from front surface, in.	Specific gravity	Flight	Specimen	Distance of wafer center from front surface, in.	Specimen
MA-7	10	-	1.71	MA-8	4	-	1.59
	10a	0.08	1.60		4a	0.12	1.57
	10b	.24	1.69		4b	.36	1.62
	10c	.40	1.69		4c	.60	1.64
	10d	.56	1.77		4d	.84	1.69
	10e	.72	1.81				
	10f	.88	1.81		7	-	1.58
MA-8	1	-	1.62		7a	0.12	1.58
					7b	.36	1.61
	1a	0.08	1.59		7c	.60	1.62
	1b	.24	1.59		7d	.84	1.68
	1c	.40	1.65				
	1d	.56	1.71		9	-	1.47
	1e	.72	1.73				
	1f	.88	1.69		9a	0.095	1.31
					9b	.285	1.44
	2	-	1.56		9c	.475	1.54
					9d	.665	1.61
	2a	0.07	1.57		9e	.855	1.66
	2b	.21	1.65				
	2c	.35	1.60		10	-	1.66
	2d	.49	1.64				
	2e	.63	1.76		10a	0.08	1.63
	2f	.77	1.85		10b	.24	1.65
	2g	.91	1.84		10c	.40	1.67
					10d	.56	1.72
	3	-	1.55		10e	.72	1.86
					10f	.88	1.84
	3a	0.12	1.43				
	3b	.36	1.53				
	3c	.60	1.51				
	3d	.84	1.70				

TABLE VI.- POSTFLIGHT MEASUREMENTS OF SPECIFIC GRAVITY - Continued

Flight	Specimen	Distance of wafer center from front surface, in.	Specific gravity	Flight	Specimen	Distance of wafer center from front surface, in.	Specific gravity
MA-9	1	-	1.92	MA-9	5	-	1.90
	1a	0.07	1.88		5a	0.07	1.89
	1b	.21	1.86		5b	.21	1.83
	1c	.35	1.88		5c	.35	1.82
	1d	.49	2.25		5d	.49	1.92
	1e	.63	1.95		5e	.63	2.18
	1f	.77	2.00		5f	.77	1.95
	1g	.91	1.98		5g	.91	1.81
	2	-	1.92		6	-	1.95
	2a	0.08	1.90		6a	0.08	1.93
	2b	.24	2.00		6b	.24	.95
	2c	.40	1.88		6c	.40	1.83
	2d	.56	1.81		6d	.56	1.98
	2e	.72	1.81		6e	.72	1.83
	2f	.88	2.21		6f	.88	1.99
	3	-	1.90		7	-	1.93
	3a	0.00	1.86		7a	0.08	1.99
	3b	.24	1.91		7b	.24	1.79
	3c	.40	1.90		7c	.40	1.94
	3d	.56	1.81		7d	.56	1.88
	3e	.72	2.27		7e	.72	1.91
	3f	.88	1.98		7f	.88	2.20
	4	-	1.79		8	-	1.86
	4a	0.07	1.81		8a	0.07	1.81
	4b	.21	2.19		8b	.21	1.69
	4c	.35	1.92		8c	.35	1.79
	4d	.49	1.84		8d	.49	1.82
	4e	.63	1.88		8e	.63	1.82
	4f	.77	1.85		8f	.77	1.77
	4g	.91	2.00		8g	.91	1.8-

TABLE VI.- POSTFLIGHT MEASUREMENTS OF SPECIFIC GRAVITY - Concluded

Flight	Specimen	Distance of wafer center from front surface, in.	Specific gravity	Flight	Specimen	Distance of wafer center from front surface, in.	Specific gravity
MA-9	9	-	1.88				
	9a	0.07	2.08				
	9b	.21	2.12				
	9c	.35	1.85				
	9d	.49	1.88				
	9e	.63	1.81				
	9f	.77	1.82				
	9g	.91	1.95				
	10	-	1.91				
	10a	0.06	2.17				
	10b	.18	2.01				
	10c	.30	1.93				
	10d	.42	1.97				
	10e	.54	1.98				
	10f	.66	1.86				
	10g	.78	1.84				
	10h	.90	1.83				

BLANK PAGE

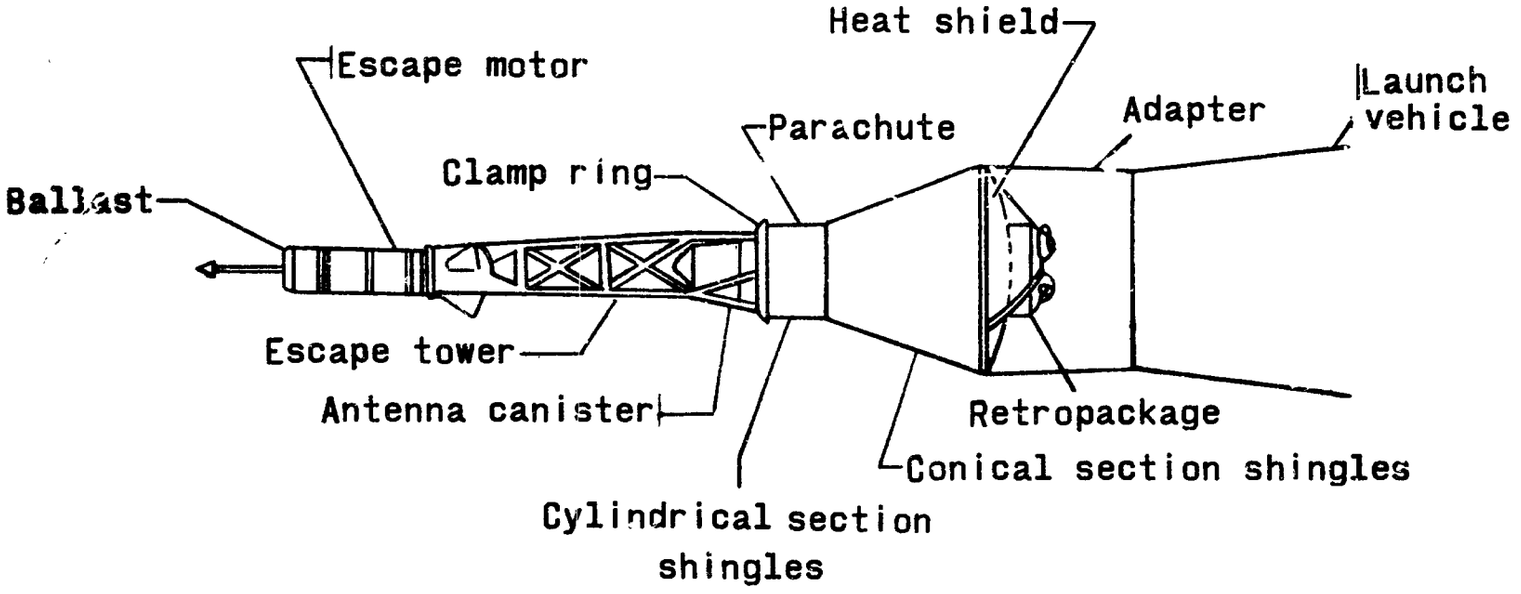

Figure 1.- Mercury spacecraft configuration.

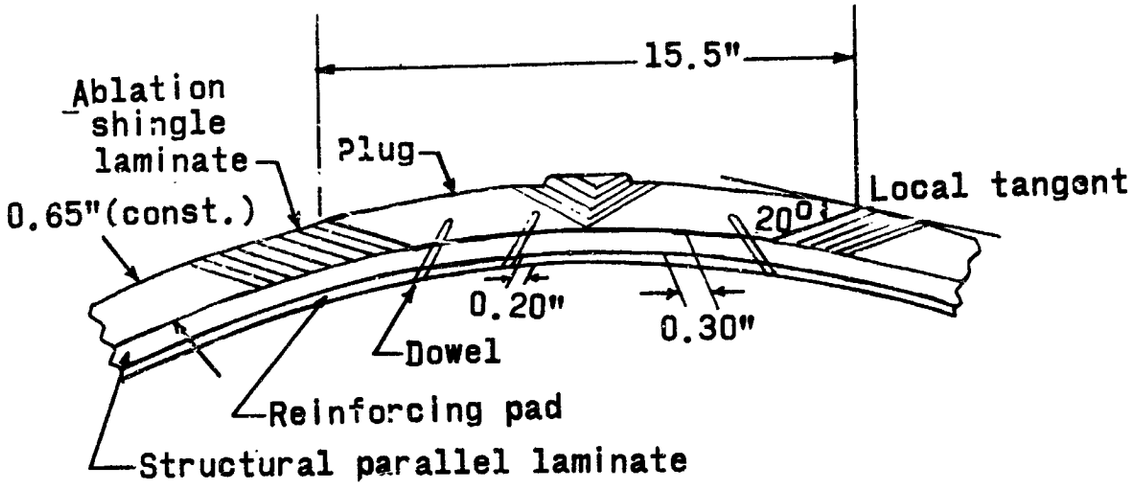

Section A-A

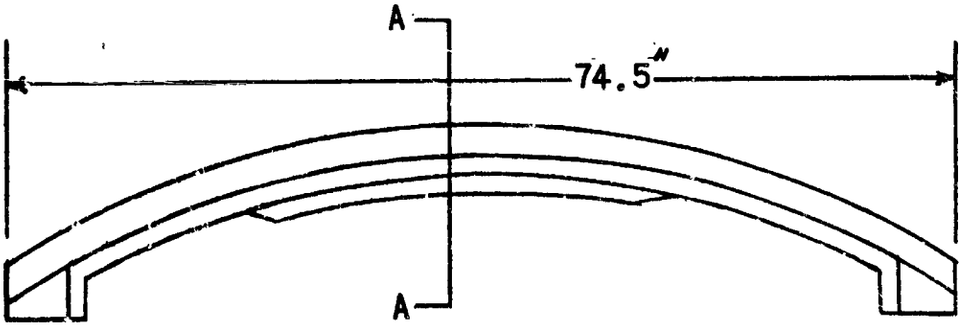

(a) Cross-section sketch of shield.

Figure 2.- Mercury heat shield.

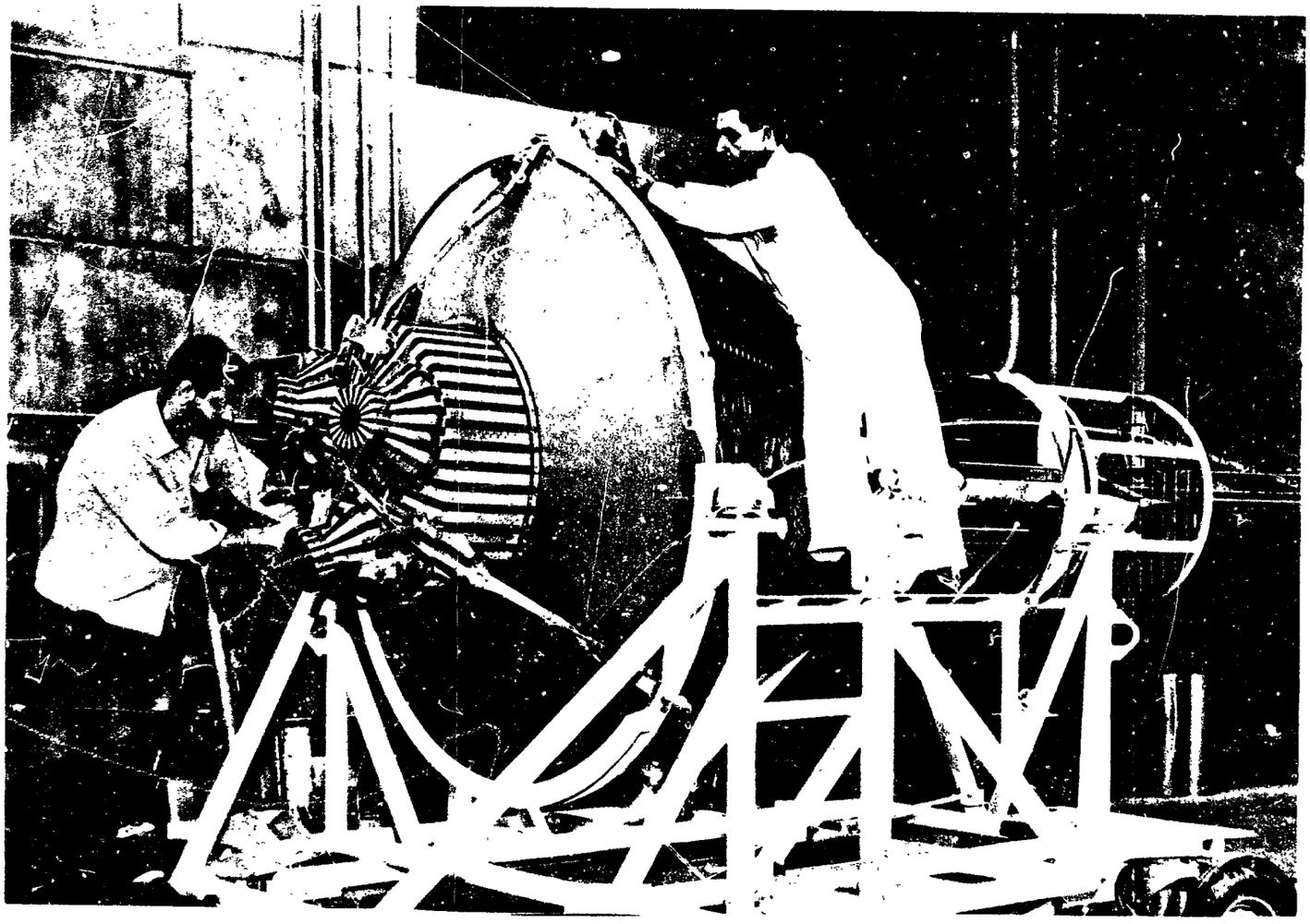

(b) Photograph of spacecratt showing part of the heat shield.

Figure 2.- Concluded.

BLANK PAGE

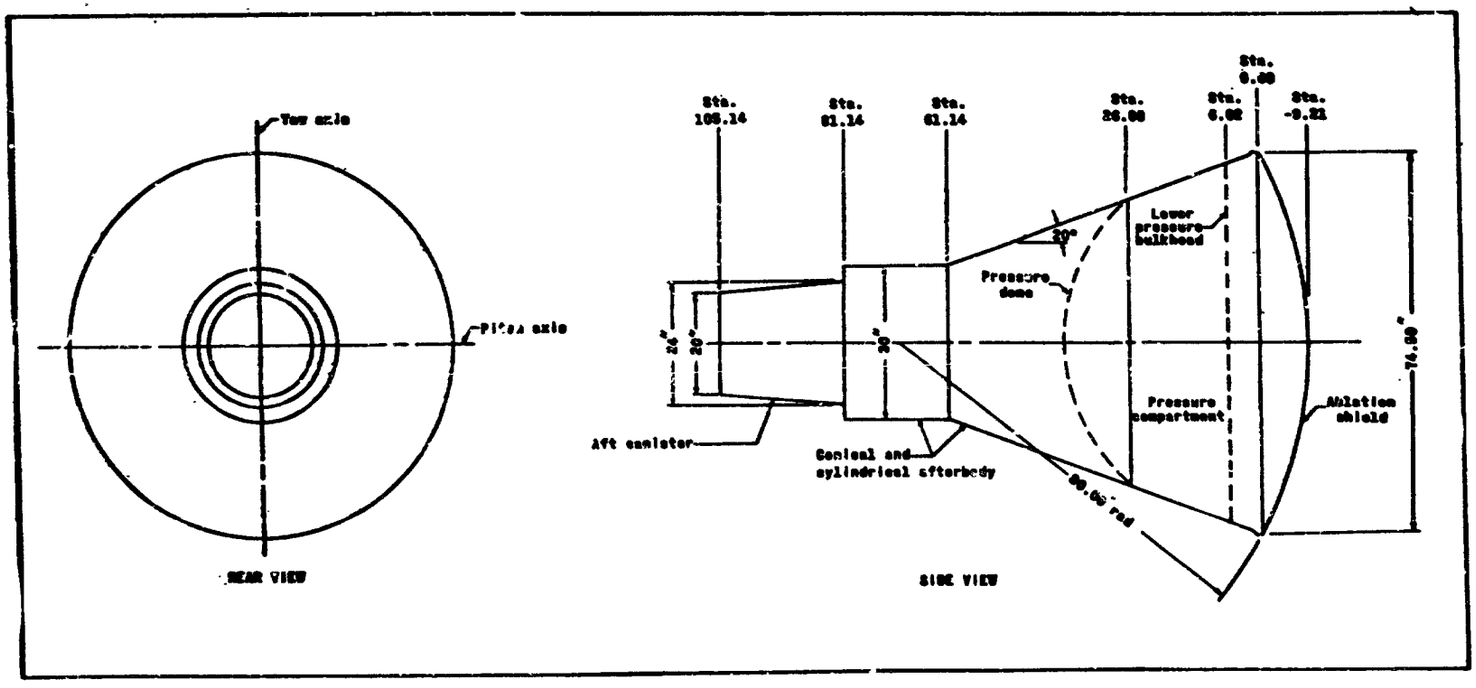

Figure 3.- Sketch of Big Joe boilerplate spacecraft.

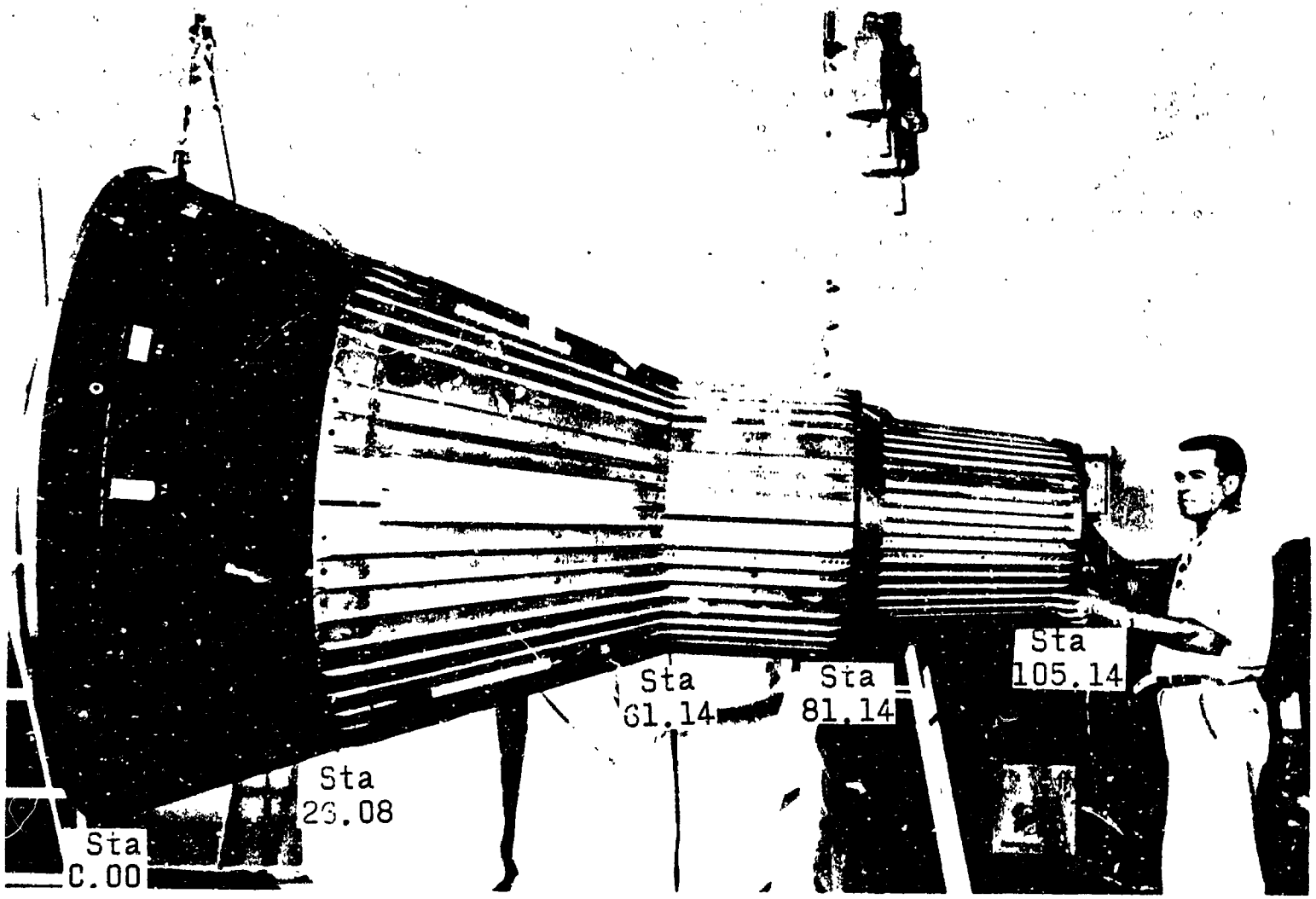

Figure 4.- Photograph of assembled Big Joe boilerplate spacecraft.

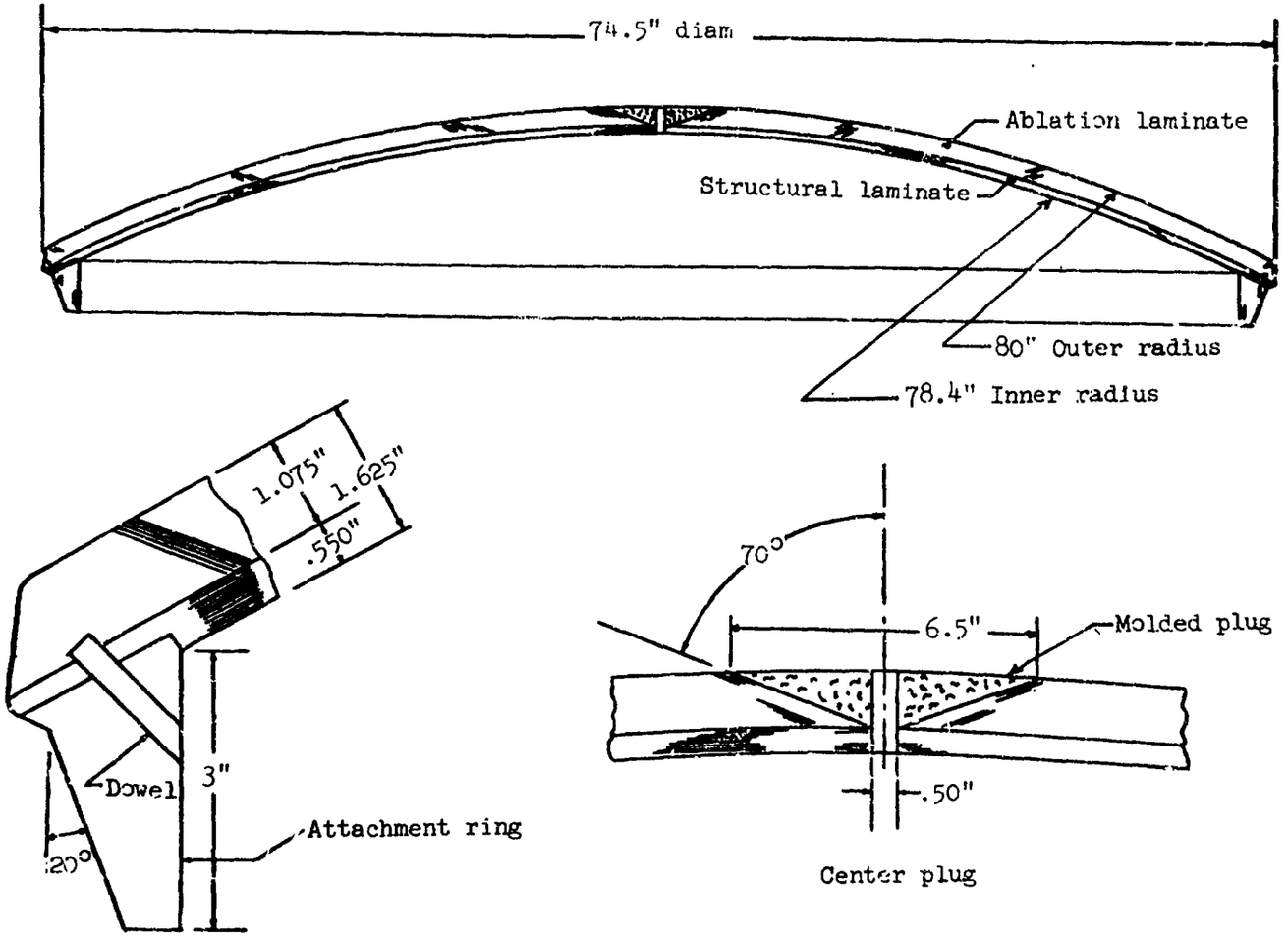

Figure 5.- Schematic drawing of Big Joe heat shield.

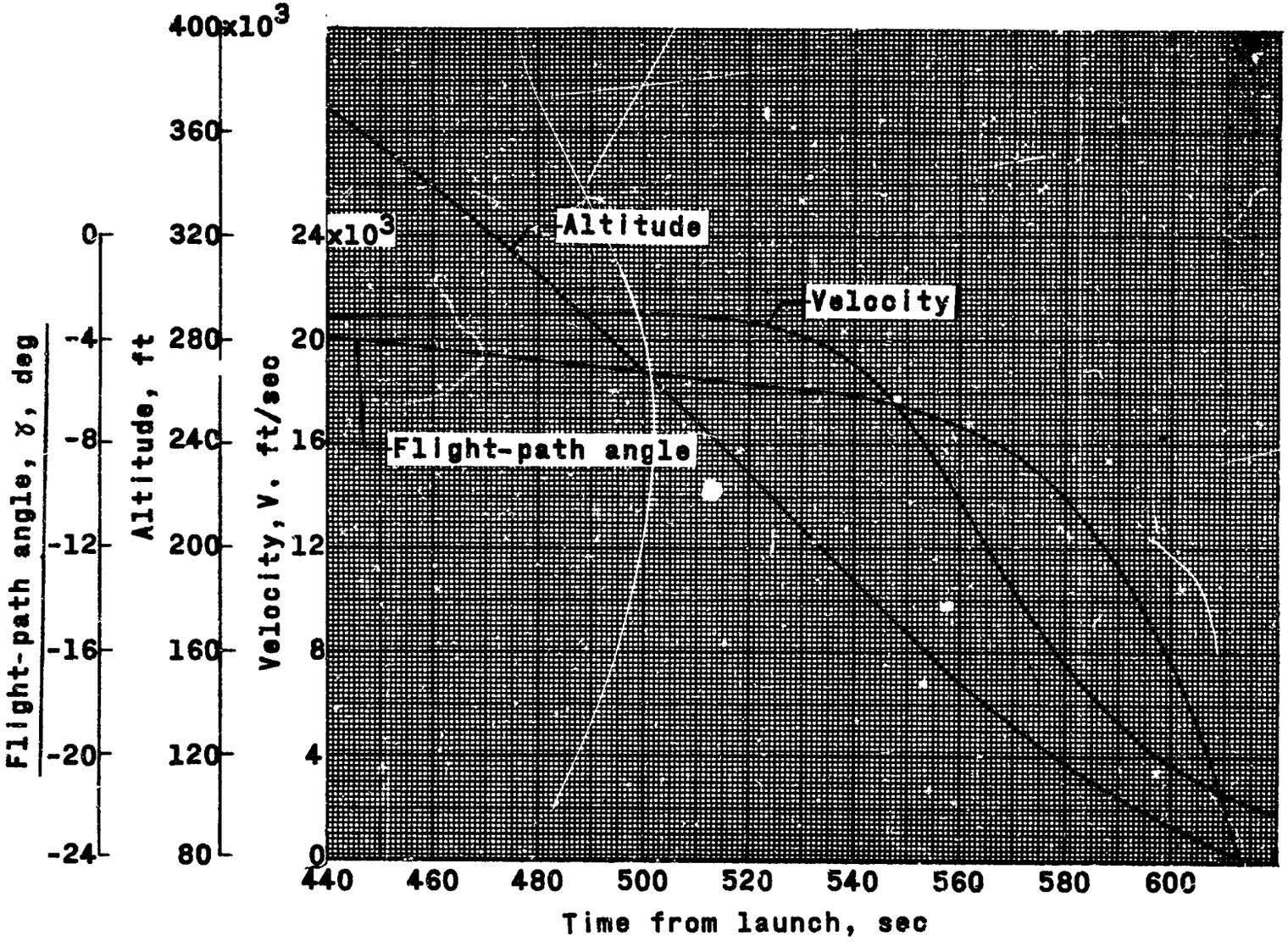

Figure 6.- Big Joe actual entry trajectory.

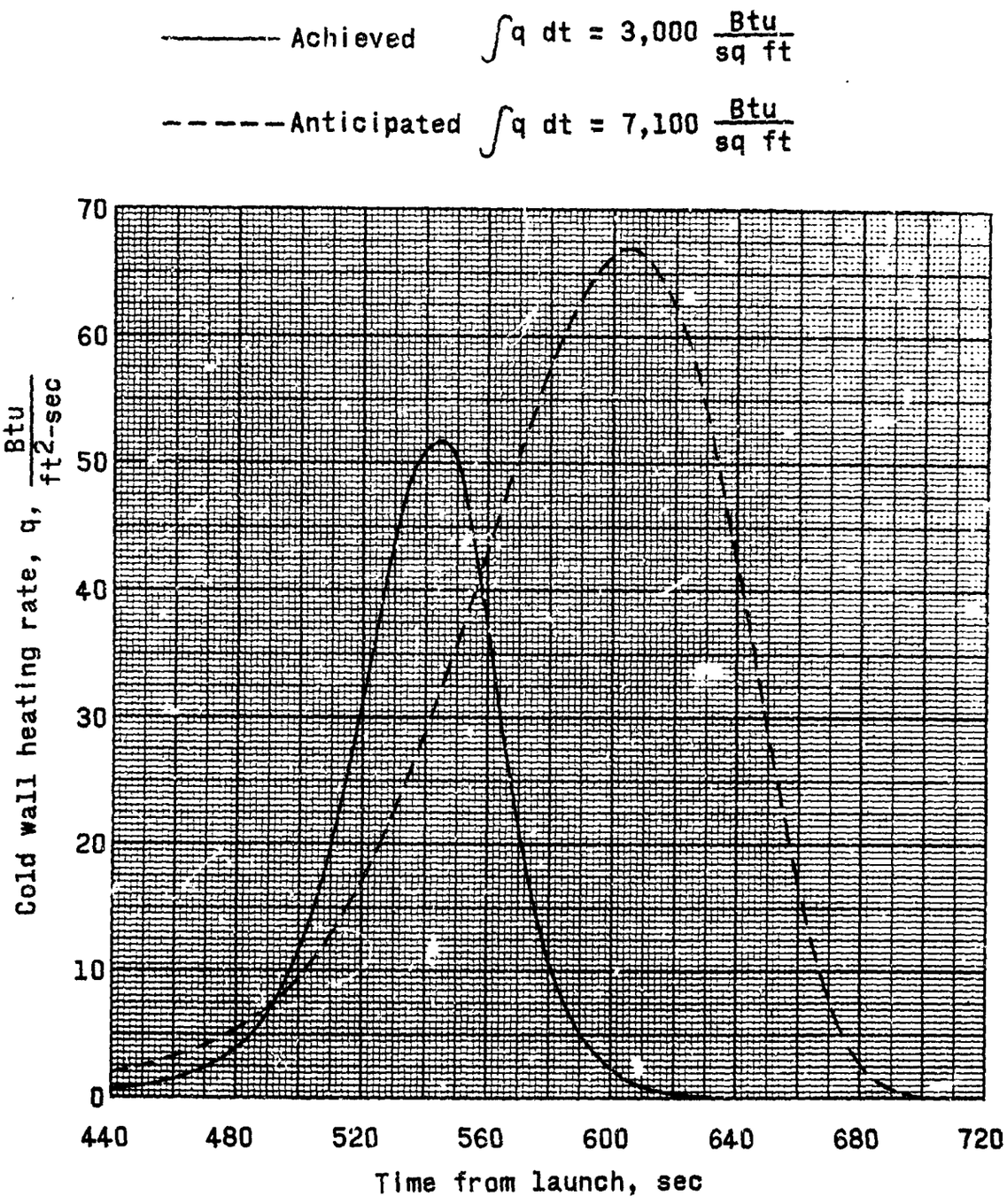

Figure 7.- Comparison of stagnation point heating rates for achieved and anticipated flight trajectories.

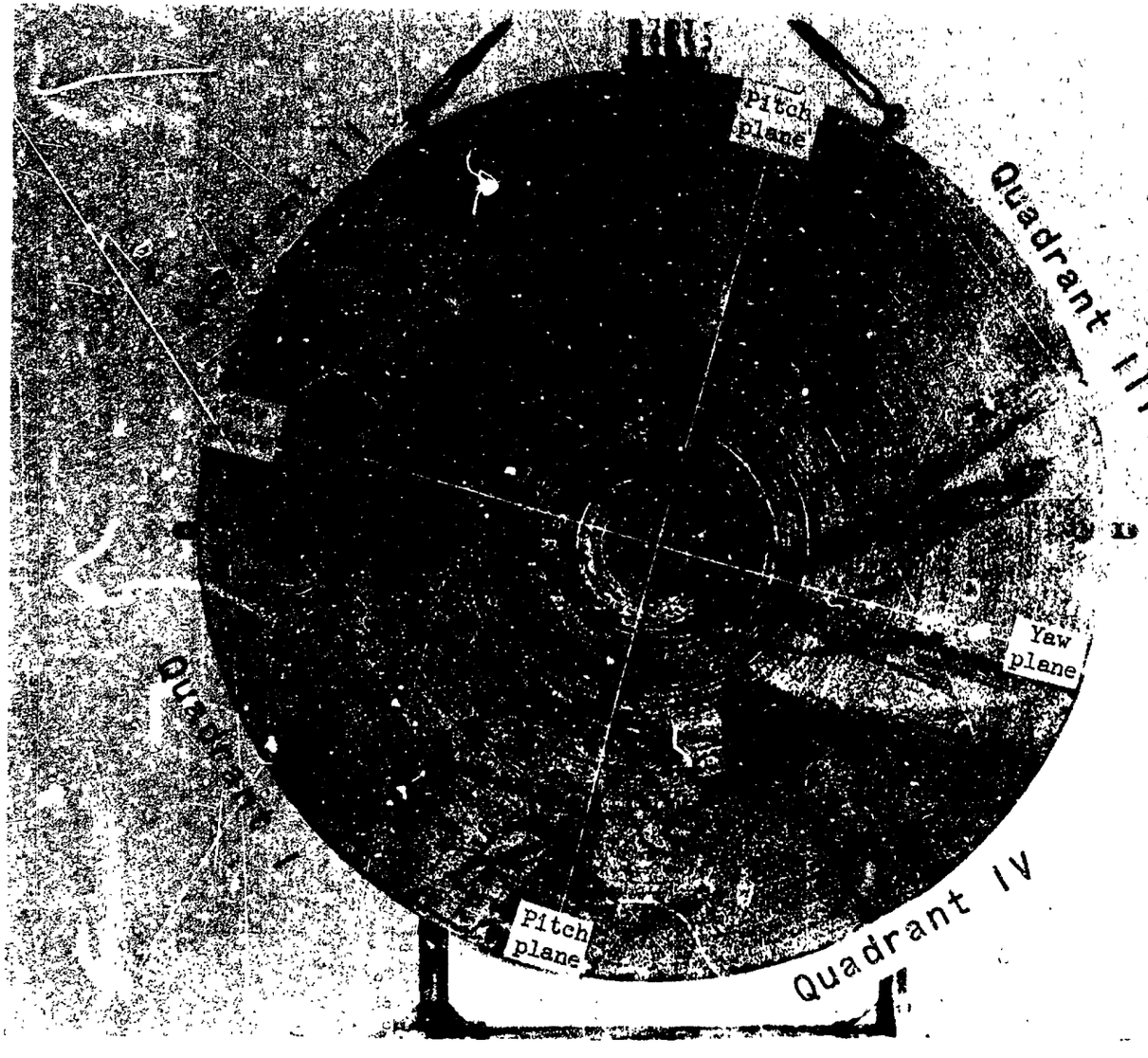

Figure 8.- Photograph of recovered Big Joe heat shield.

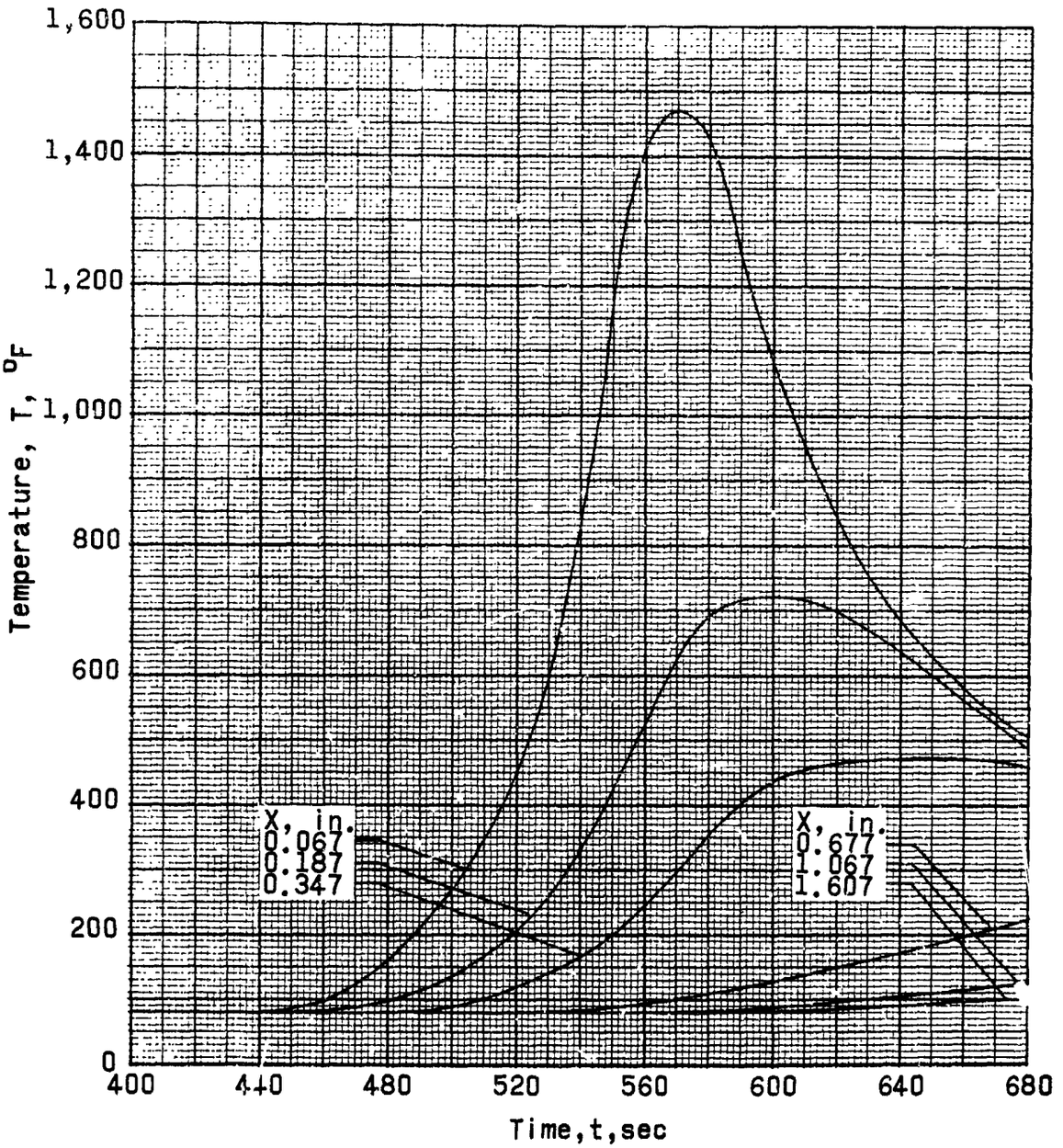

Figure 9.- Big Joe heat-shield faired temperature-time histories from a typical sensor, No. 1.

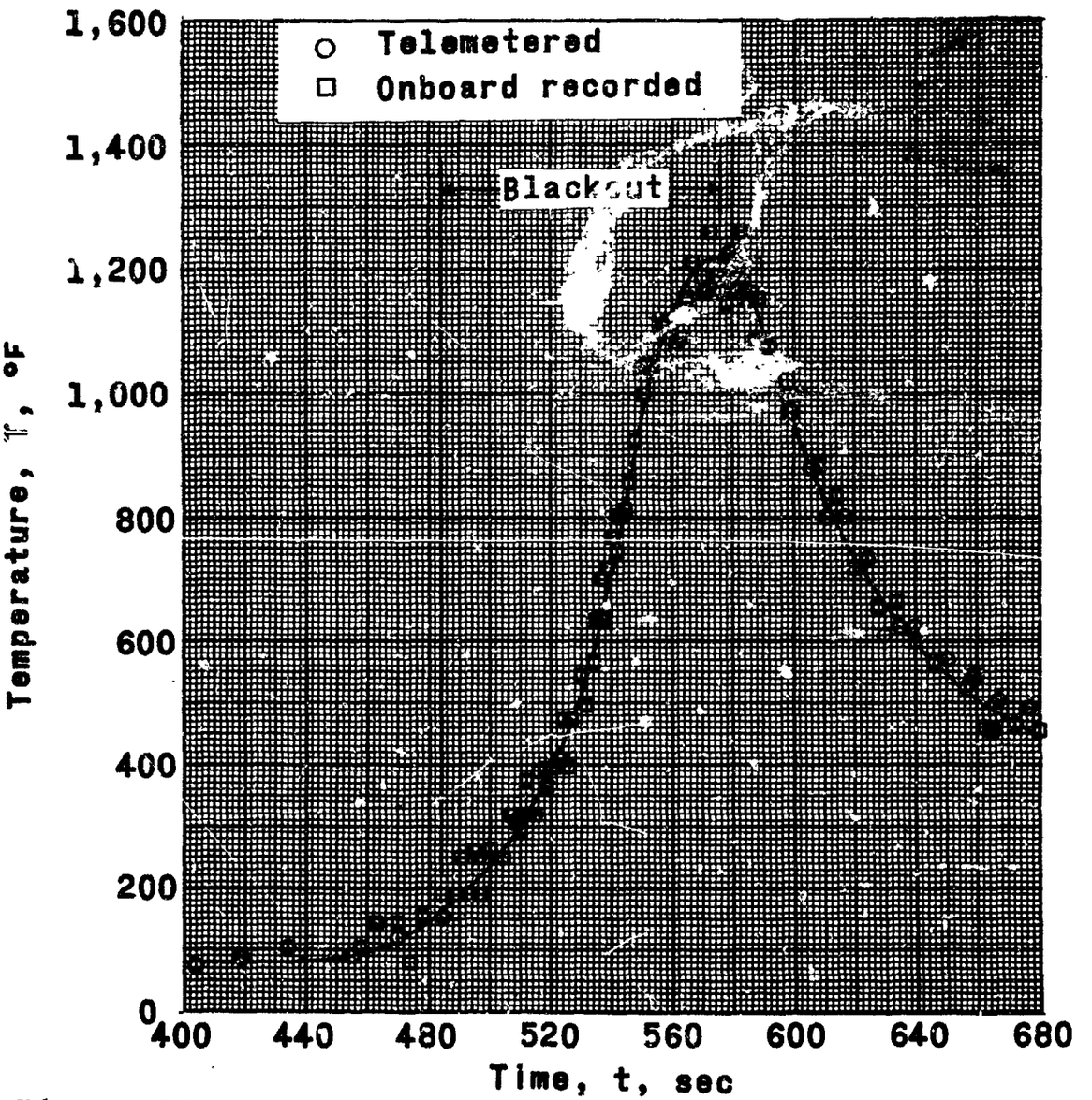

Figure 10.- Measured Big Joe heat-shield temperatures at a typical thermocouple, No. 10.

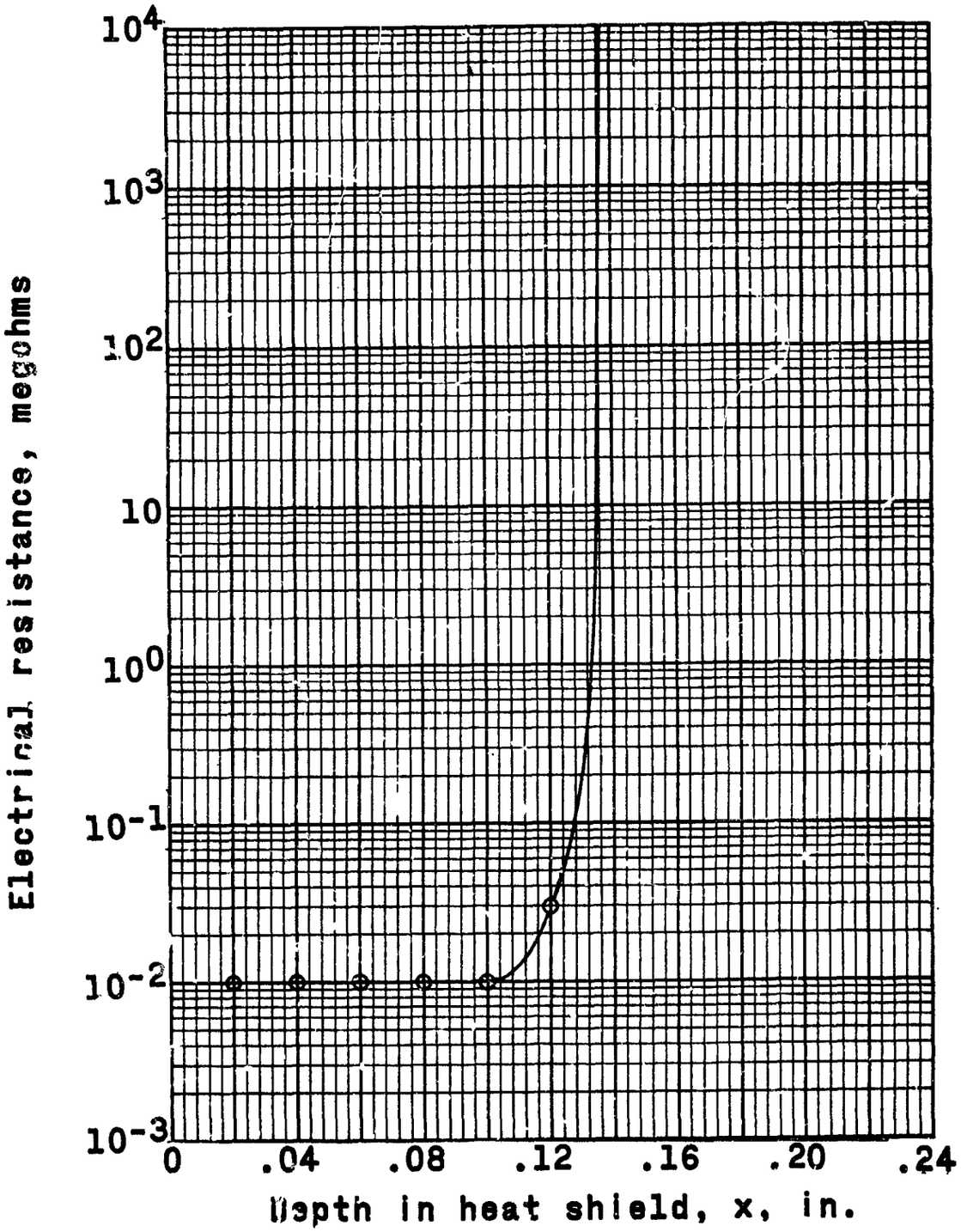

Figure 11.- Measured dielectric properties of a Big Joe heat-shield specimen.

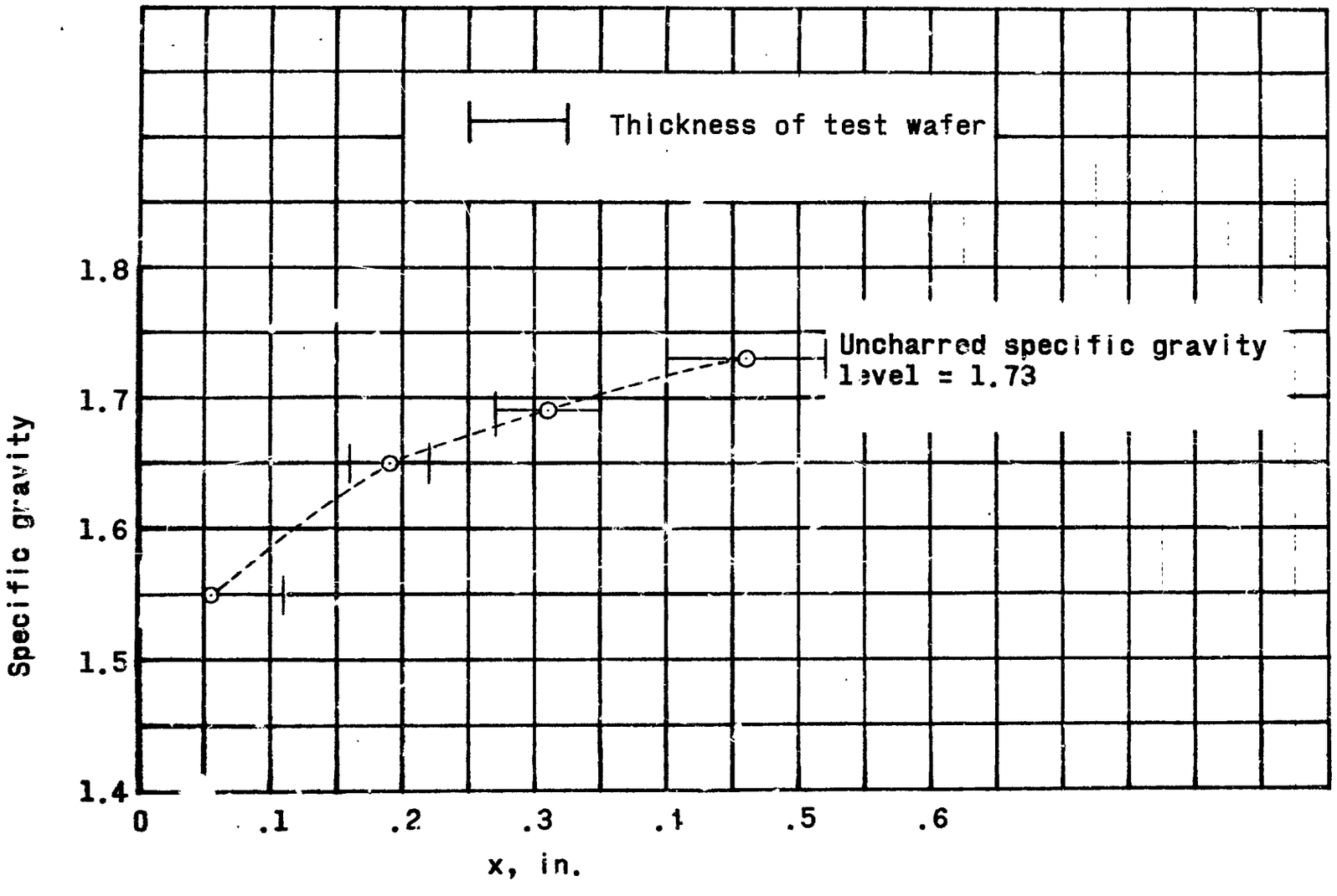

Figure 12.- Specific-gravity measurements of Big Joe heat shield.

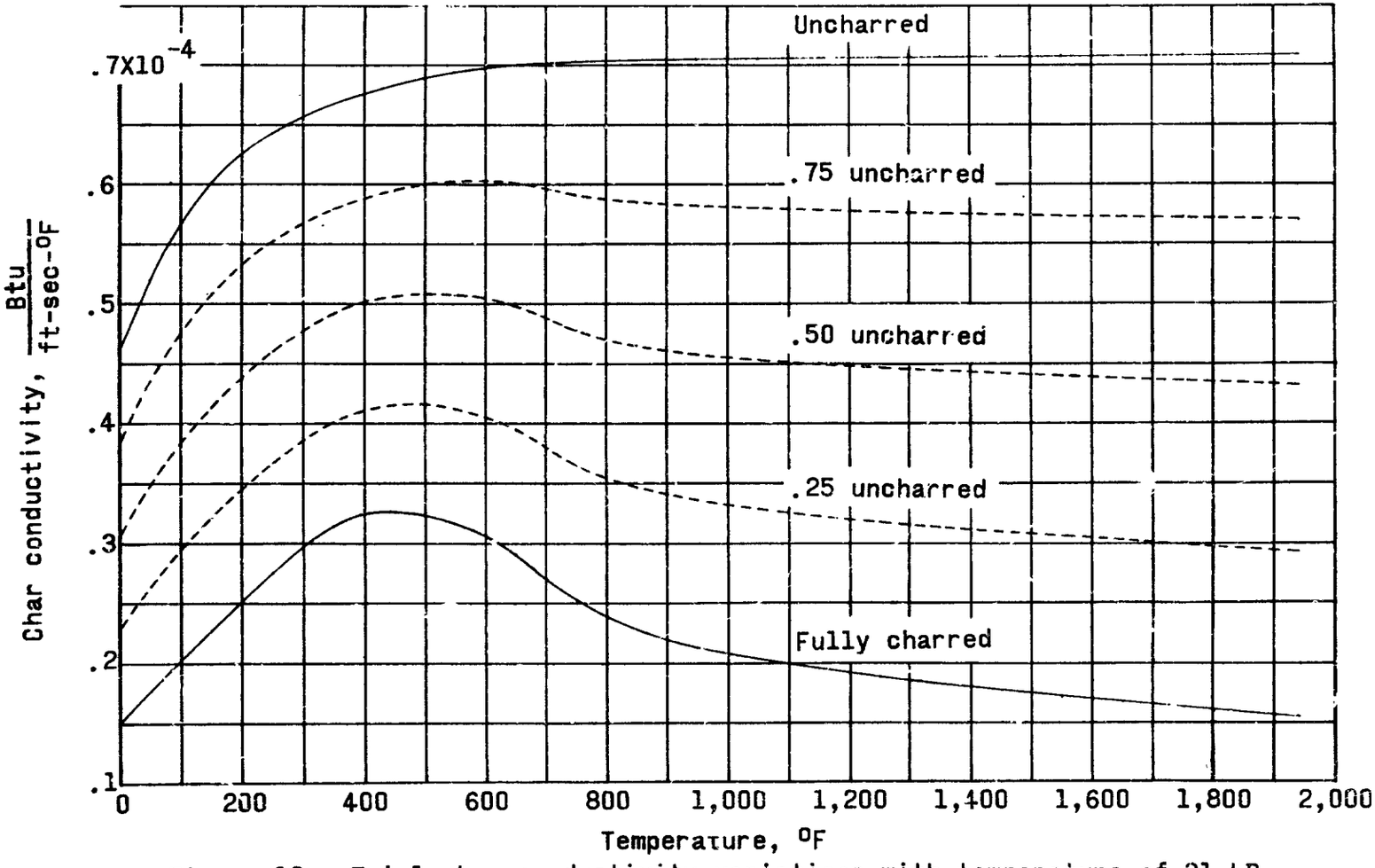

Figure 13.- Trial char conductivity variations with temperature of 91 LD phenolic fiberglass with interpolated values between data for fully charred and uncharred material.

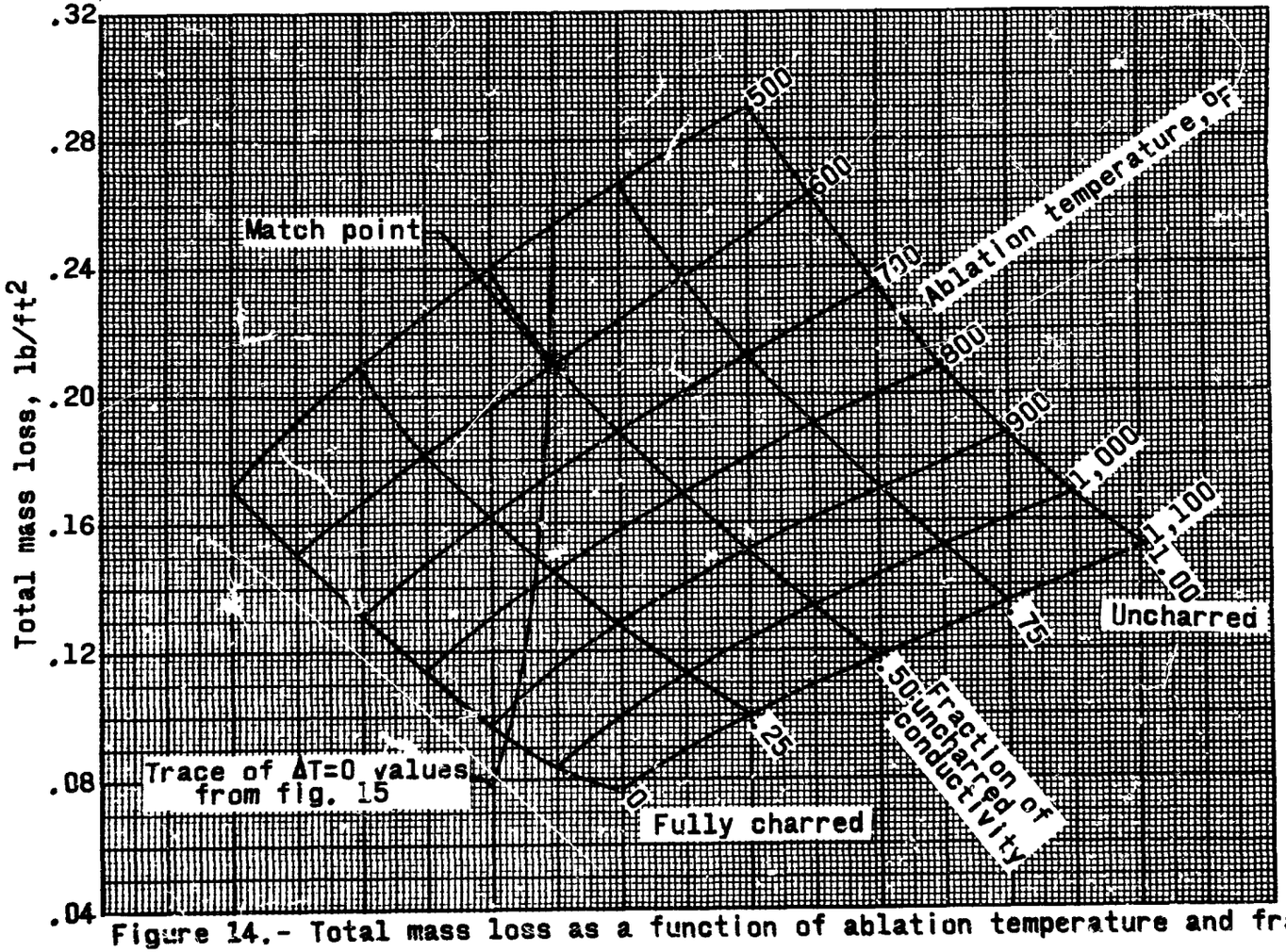

Figure 14.- Total mass loss as a function of ablation temperature and fraction of uncharred conductivity for the Big Joe entry.

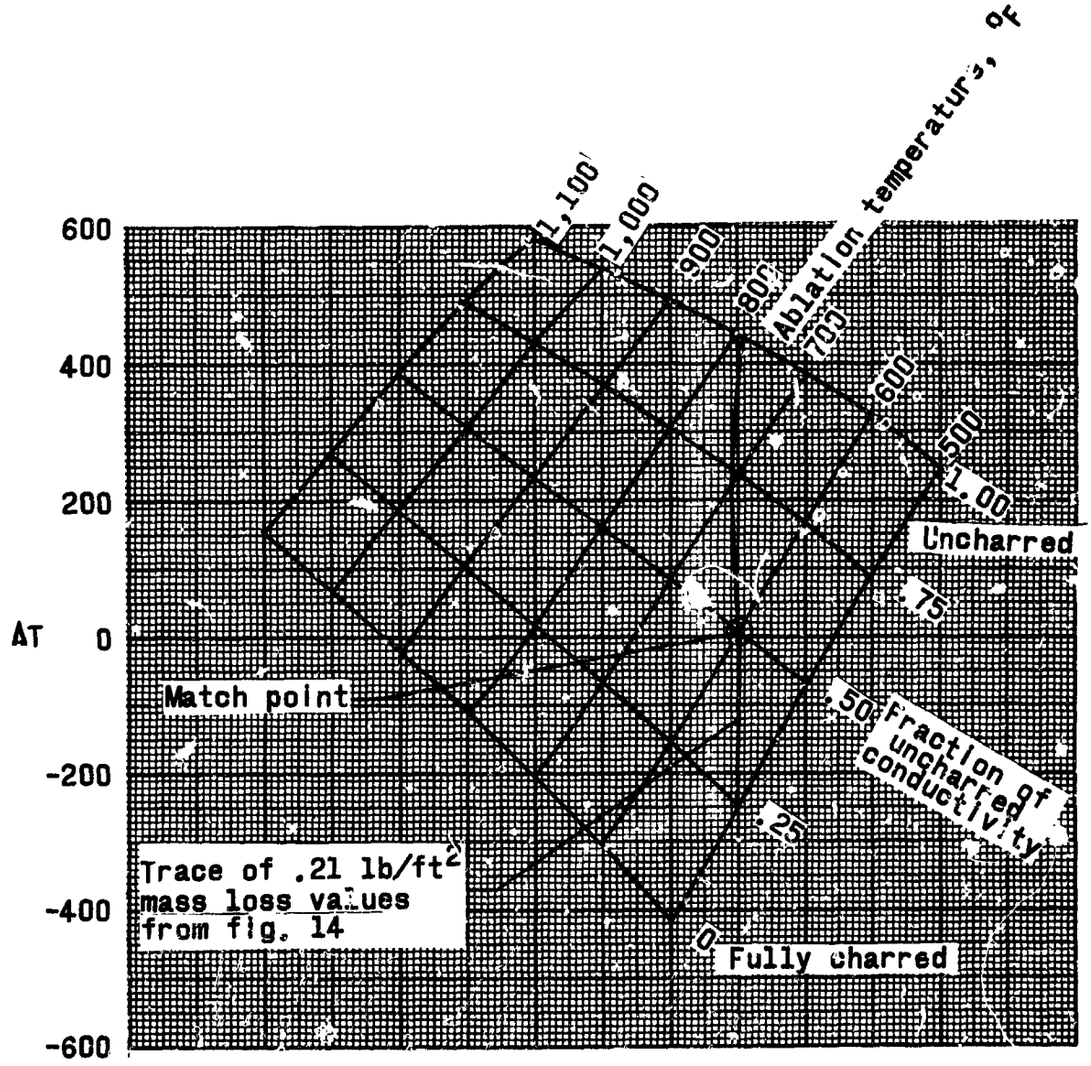

Figure 15.- Difference between measured and analytical temperatures as a function of ablation temperature and fraction of uncharred conductivity for the Big Joe entry.

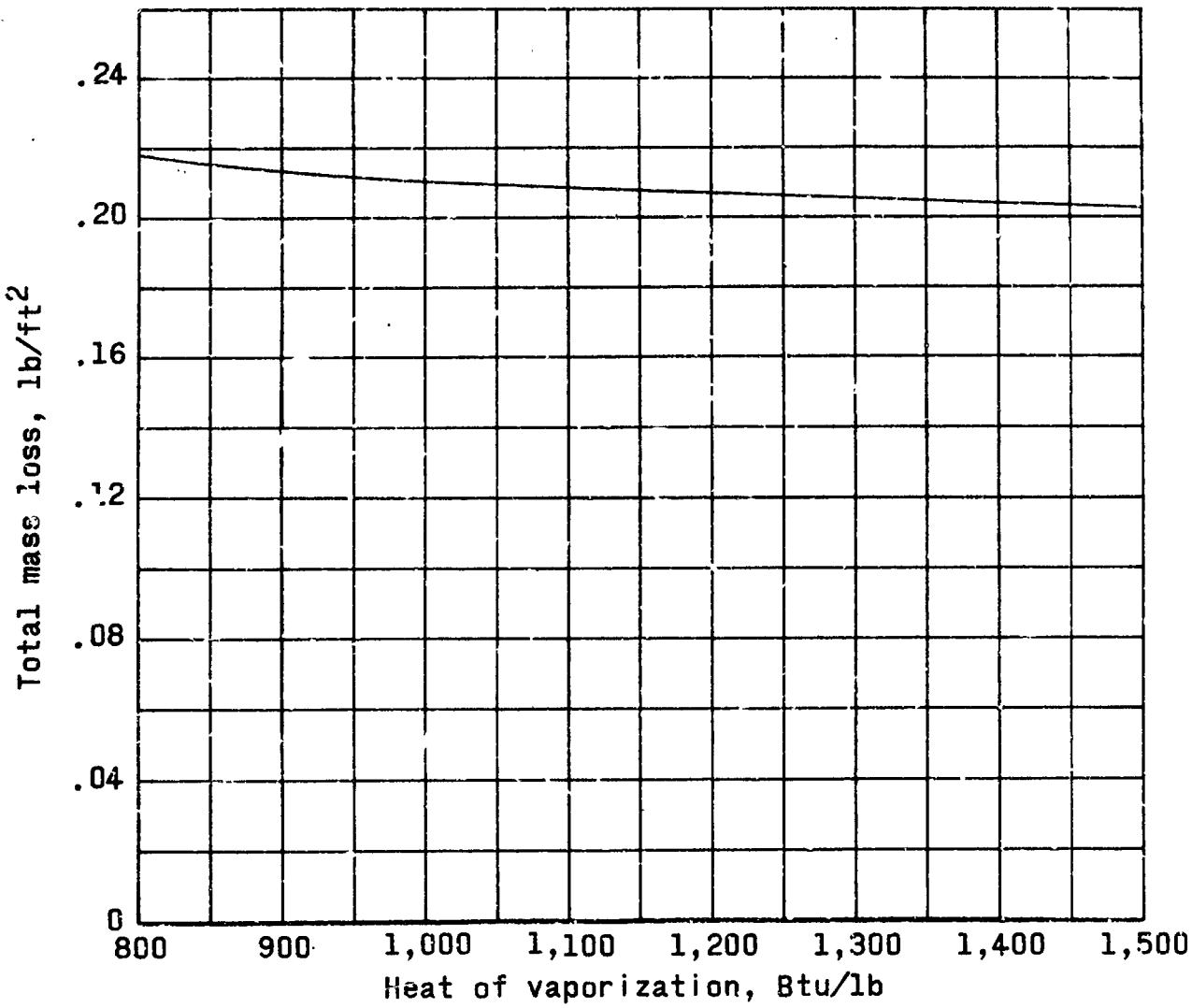

Figure 16.- The effect of heat of vaporization on total mass loss.

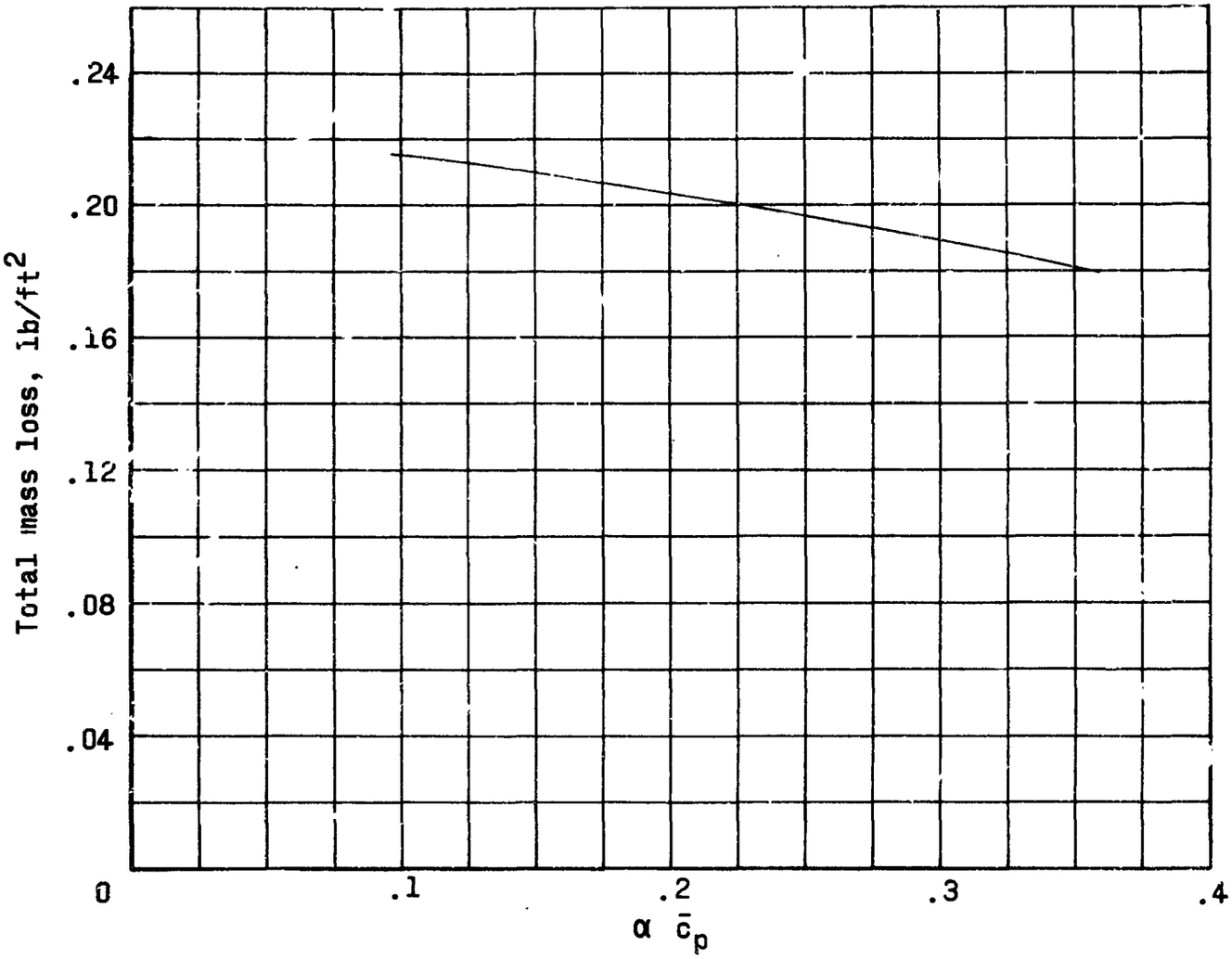

Figure 17.- The effect of the blockage parameter, $\alpha\bar{c}_p$, on total mass loss.

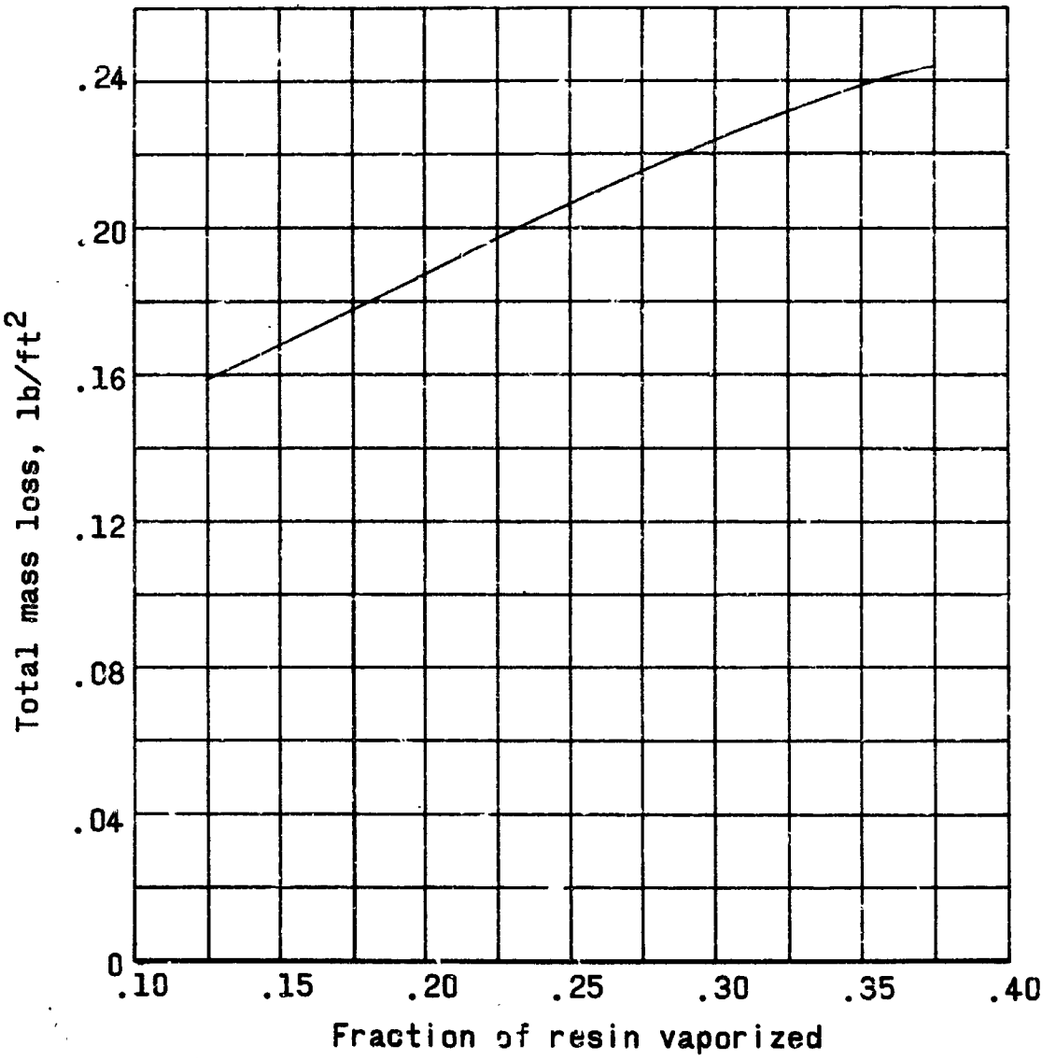

Figure 18.- The effect of fraction of resin vaporized on total mass loss.

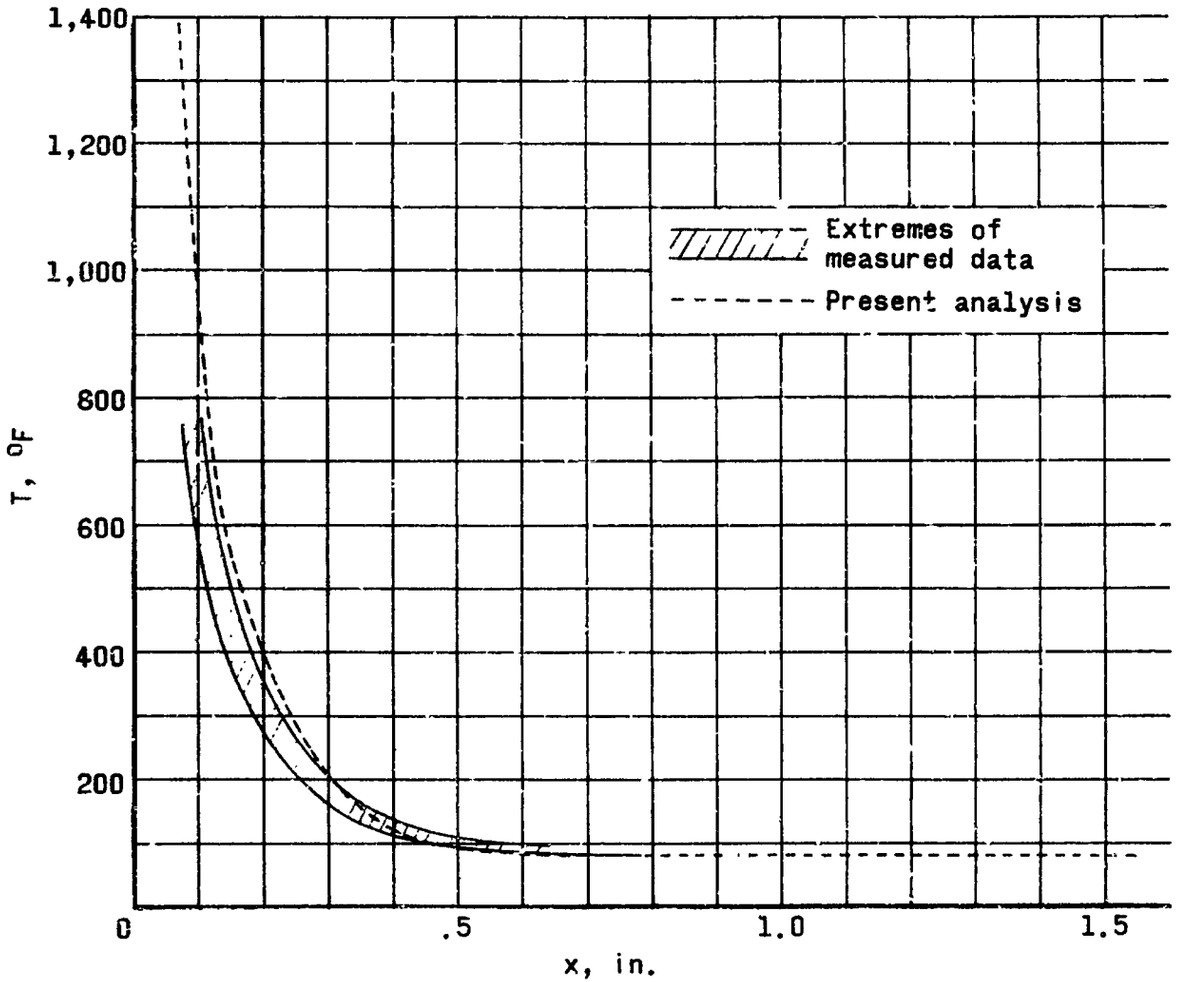

(a) Time = 540 seconds.

Figure 19.- Comparison of measured and calculated temperature distributions at several times during the Big Joe flight.

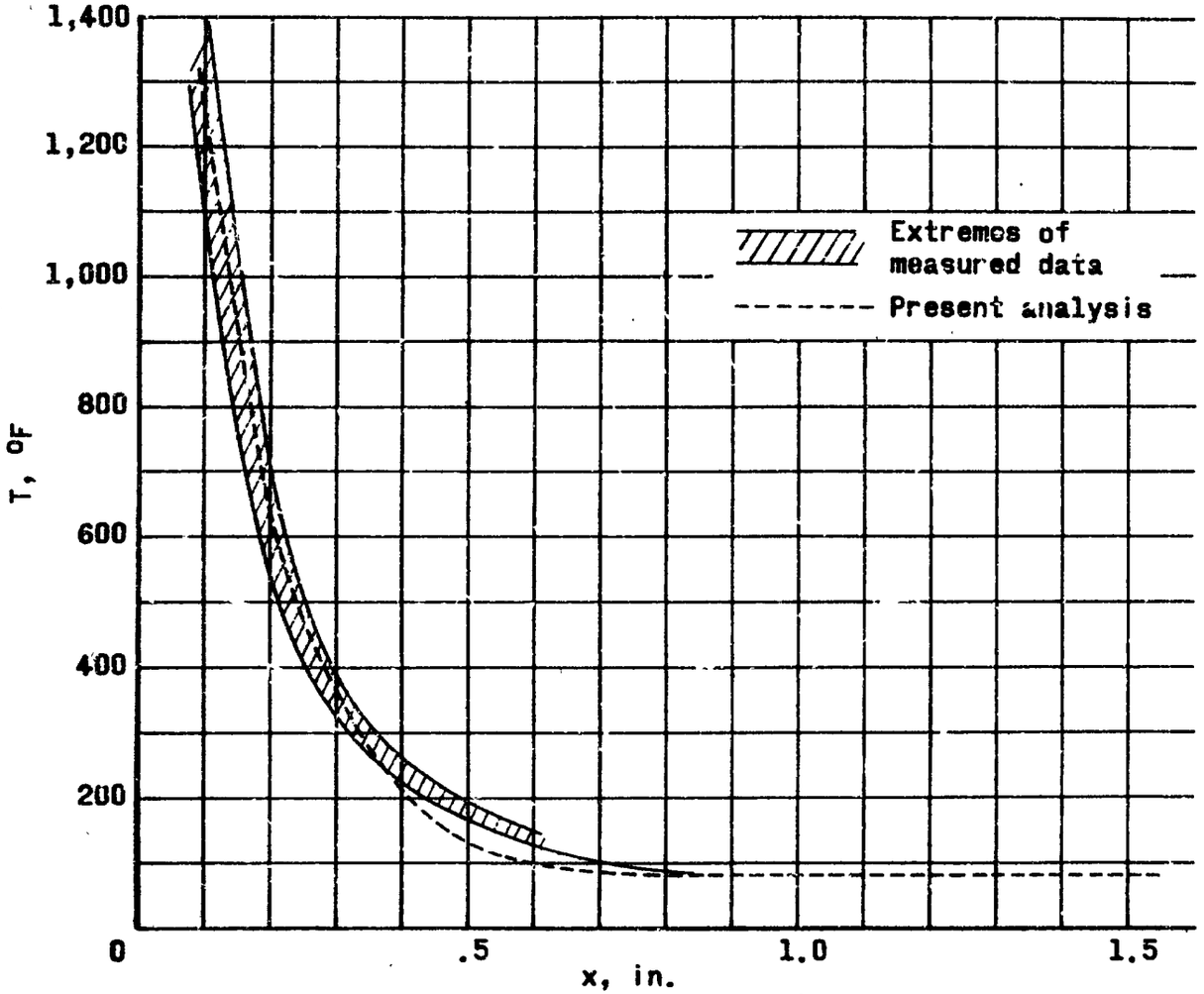

(b) Time = 580 seconds.

Figure 19.- Continued.

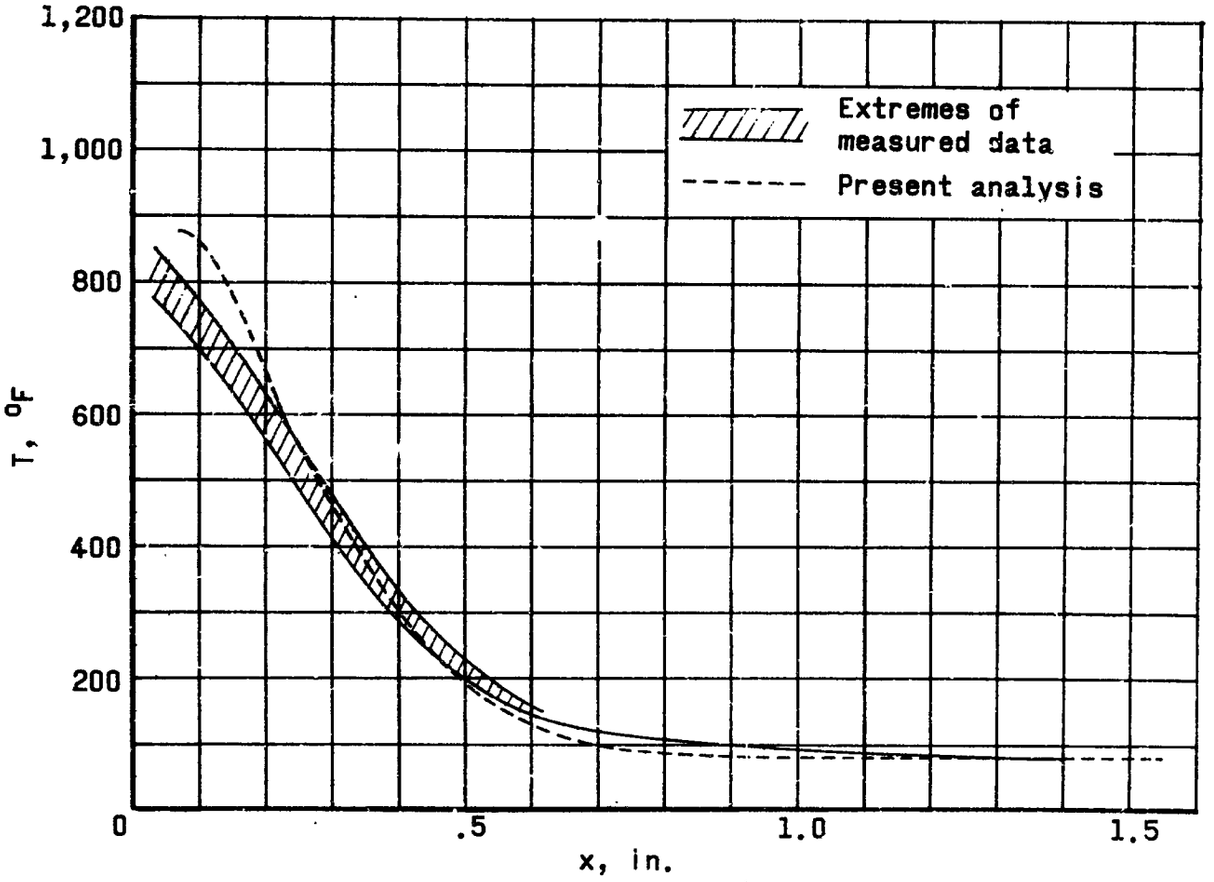

(c) Time = 620 seconds.

Figure 19.- Concluded.

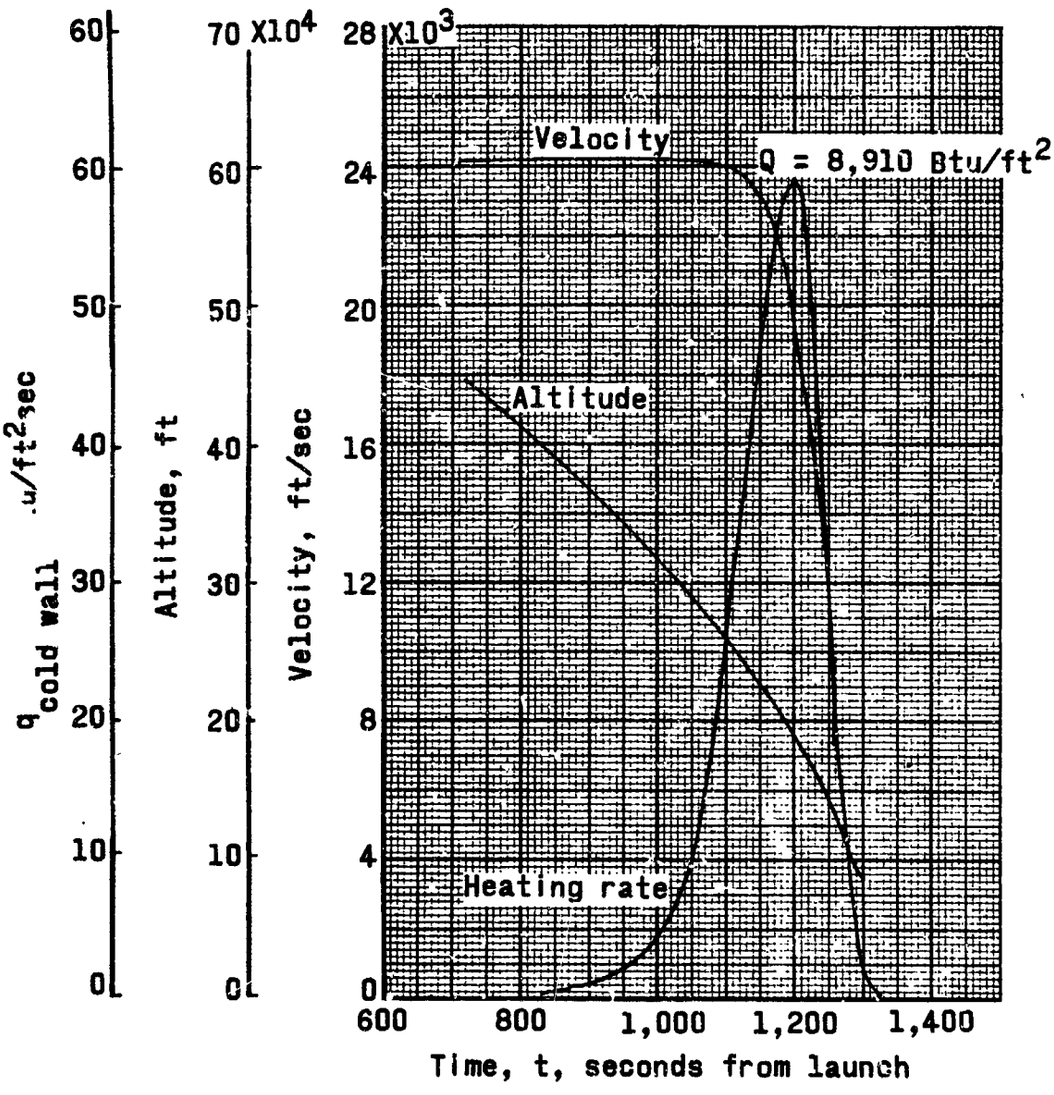

Figure 20.- Mercury nominal design entry trajectory (two retrorockets firing).

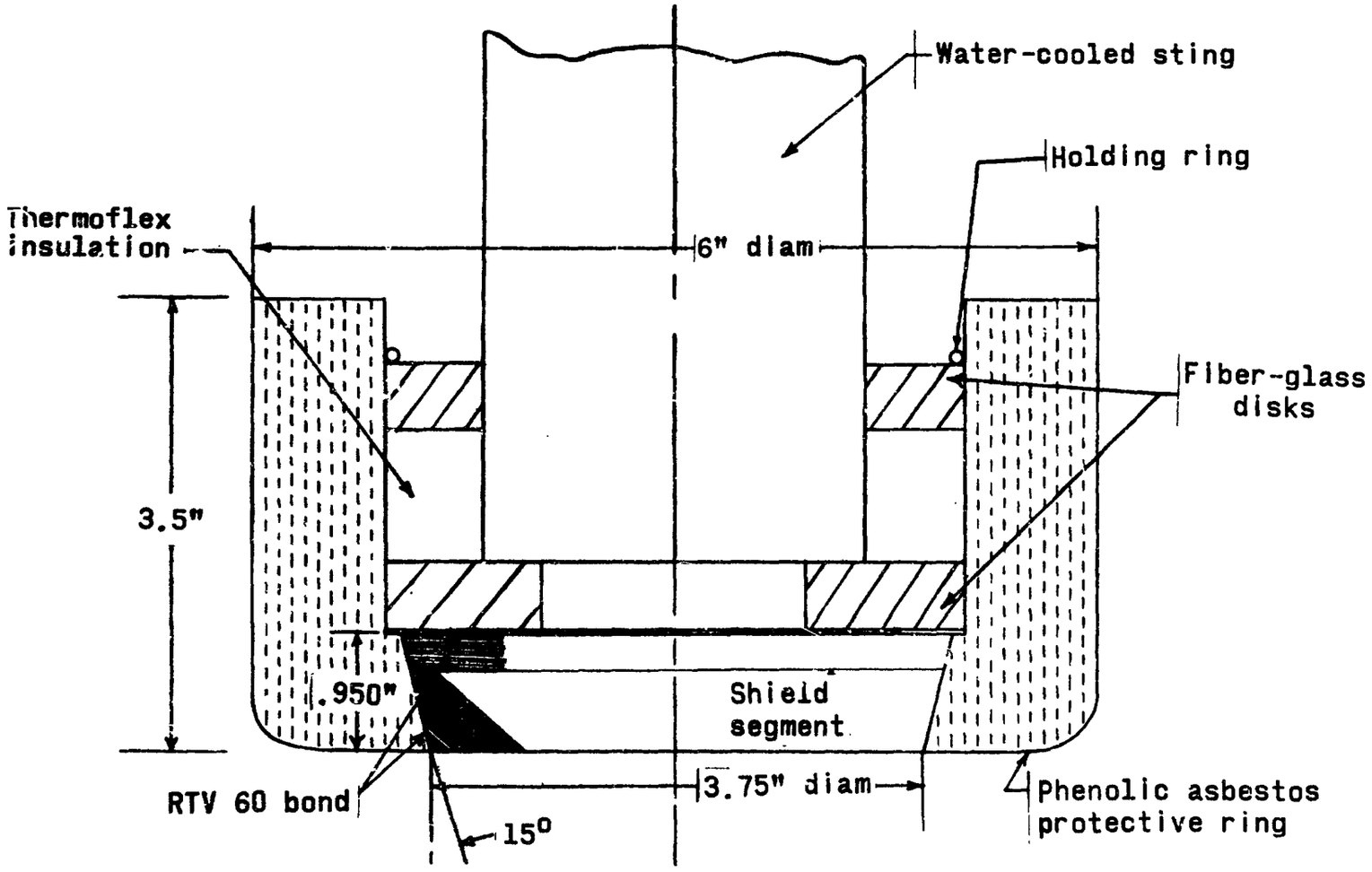

Figure 21.- Cross-section of arc-jet test-model design.

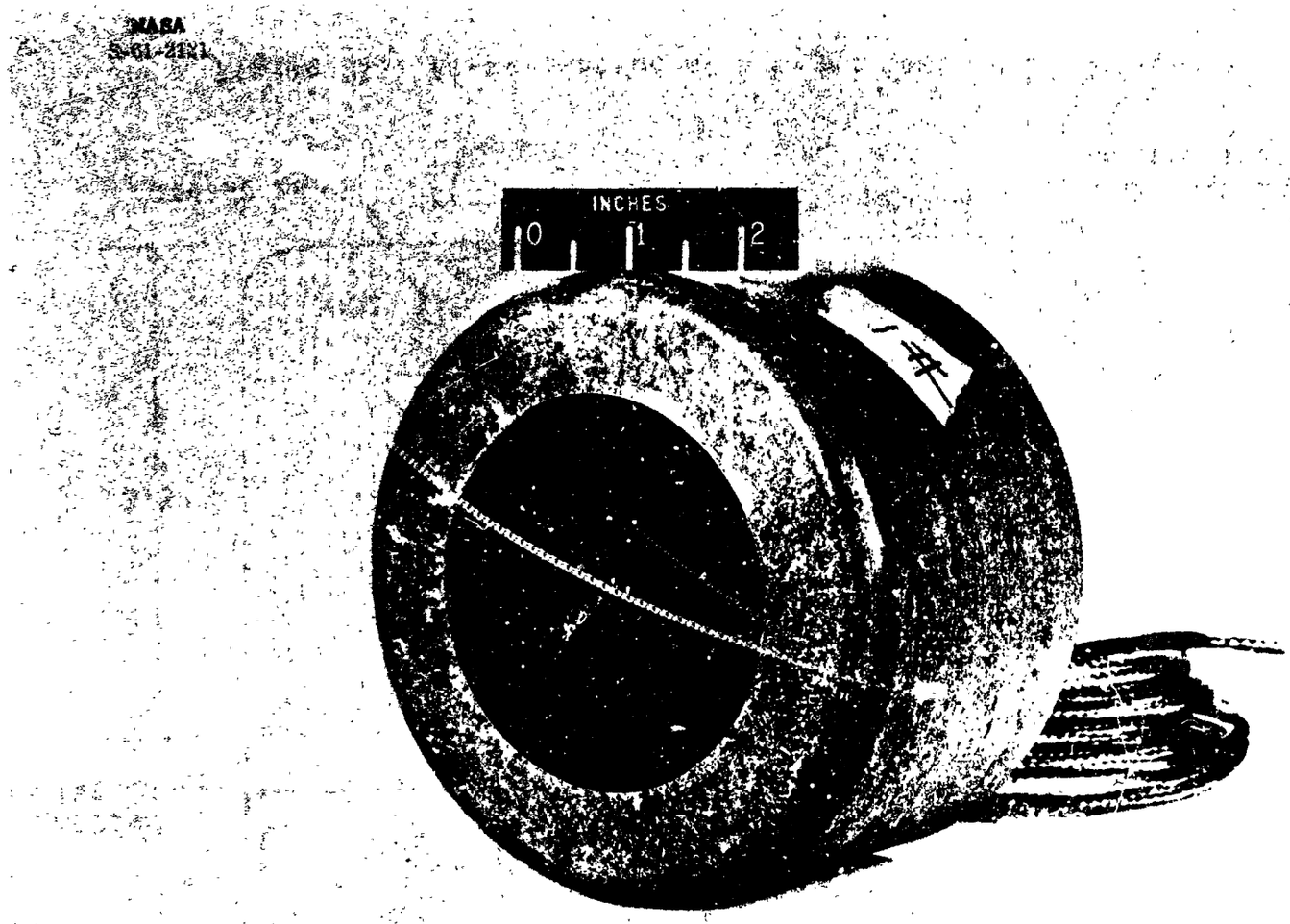

Figure 22.- Photograph of typical arc-jet test model before testing.

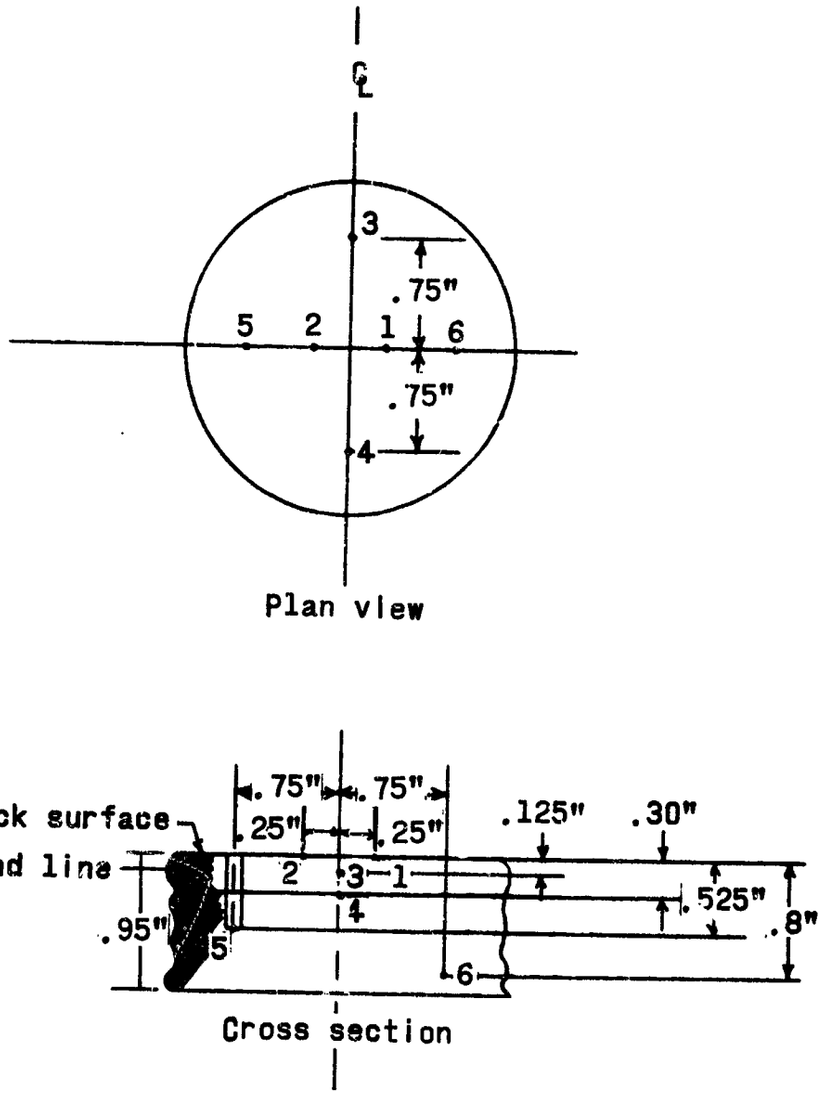

Figure 23.- Thermocouple instrumentation on arc-jet test model.

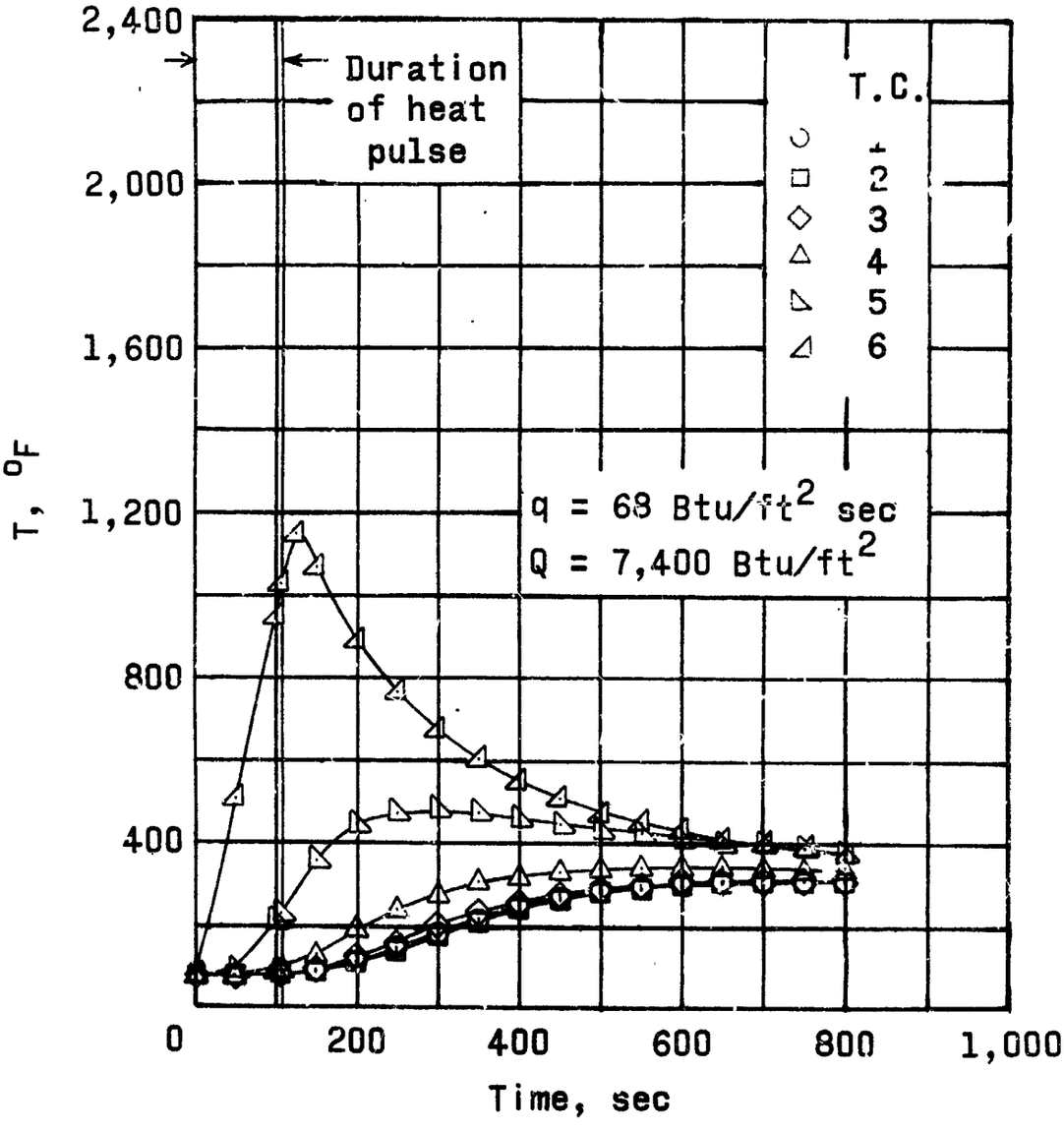

Figure 24.- Measured temperature-time history from a typical arc-jet specimen, test 1.

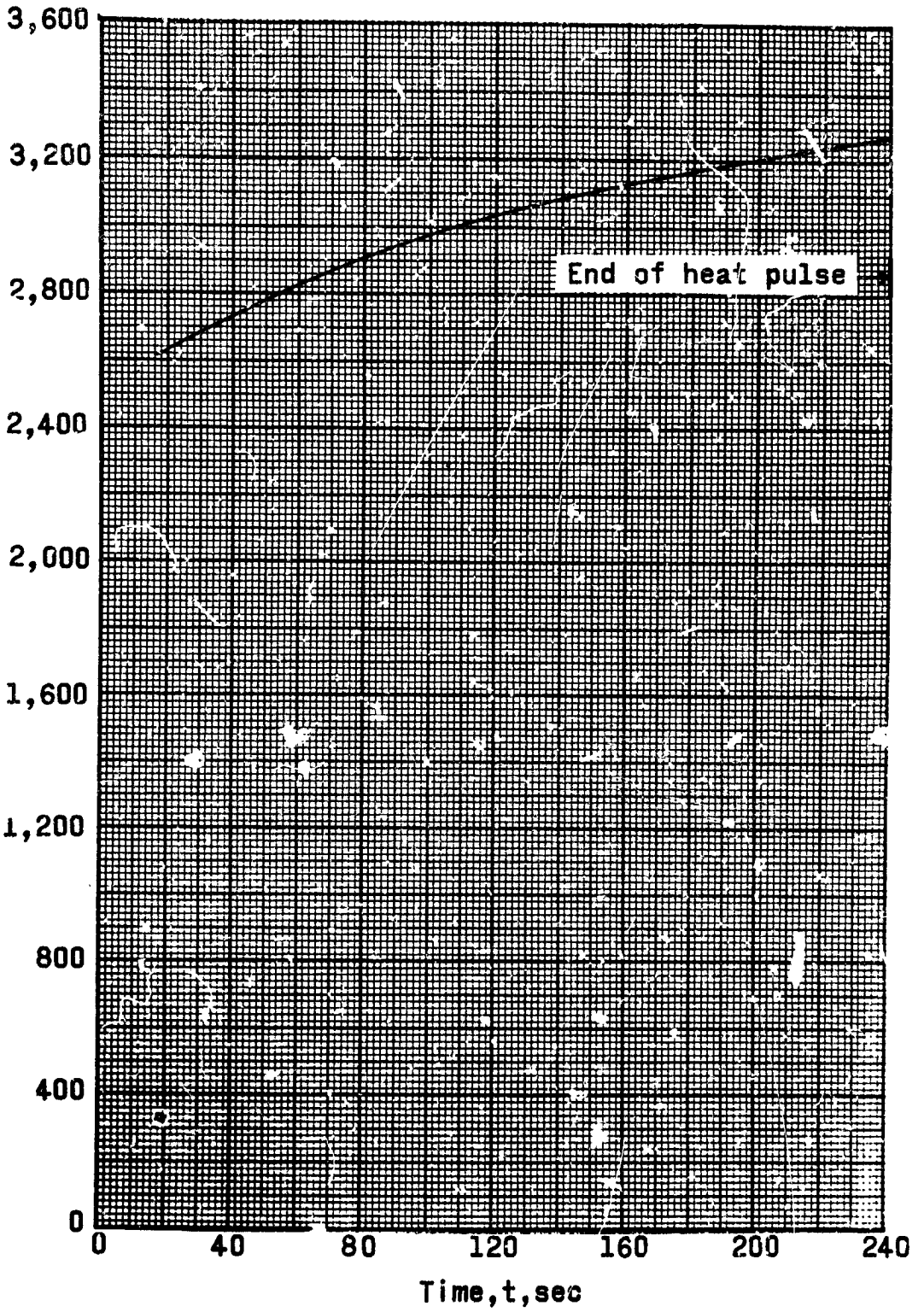

Figure 25.- Measured surface temperature-time history from a typical arc-jet specimen, test 5.

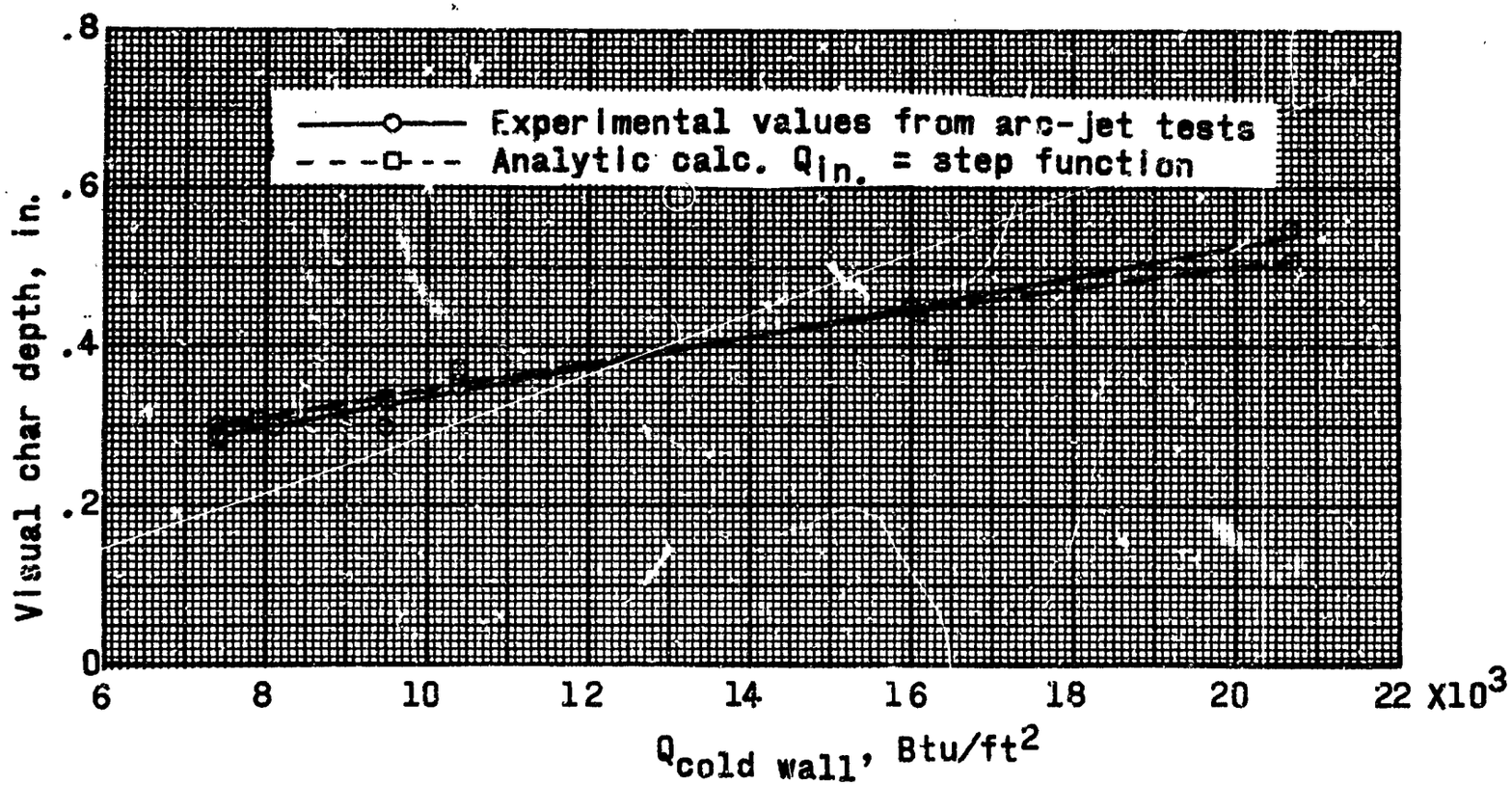

(a) Visual char depth.

Figure 26.- Comparison of experimental and analytical estimates on the basis of total cold wall heat pulse.

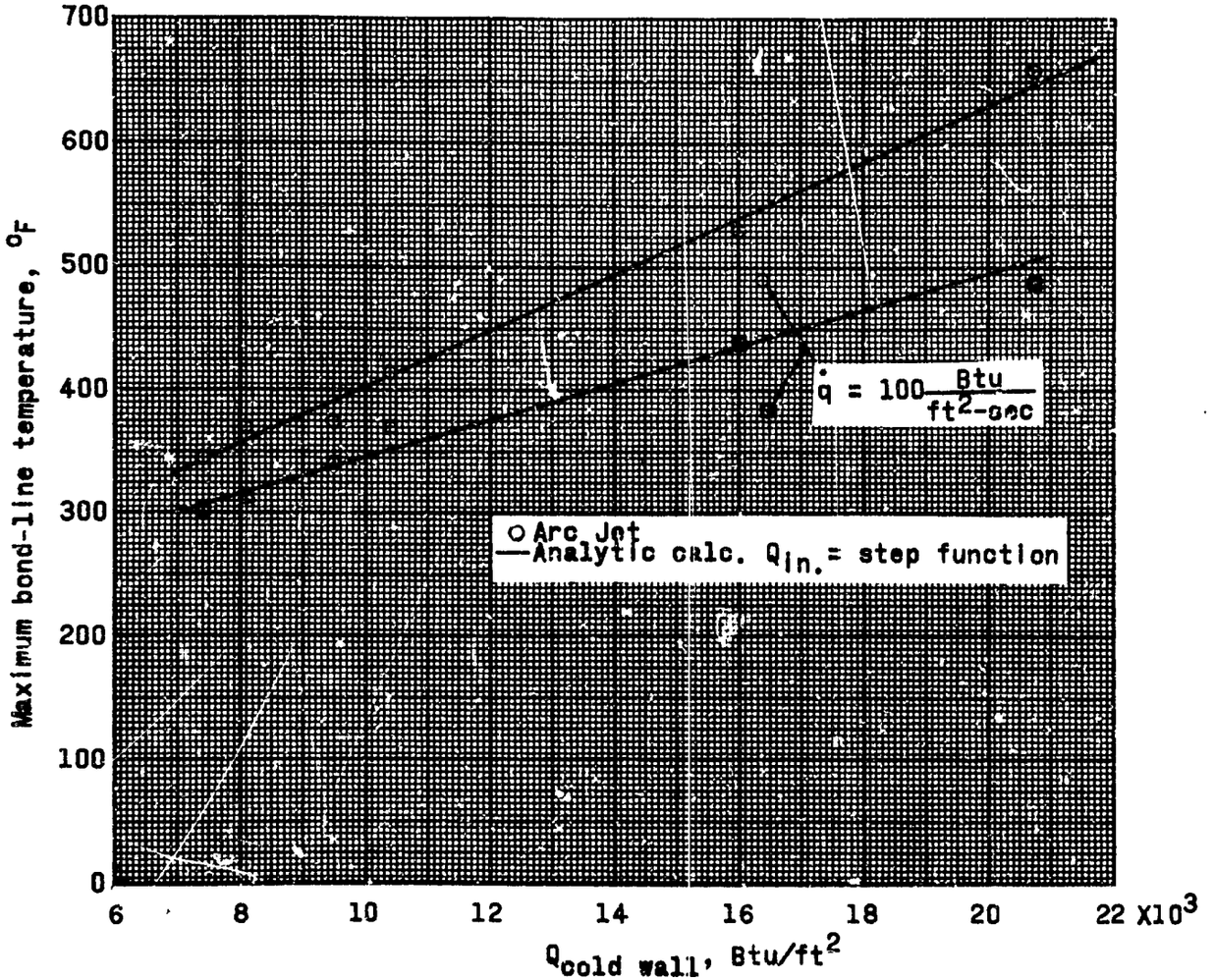

(b) Maximum bond-line temperature.

Figure 26.- Concluded.

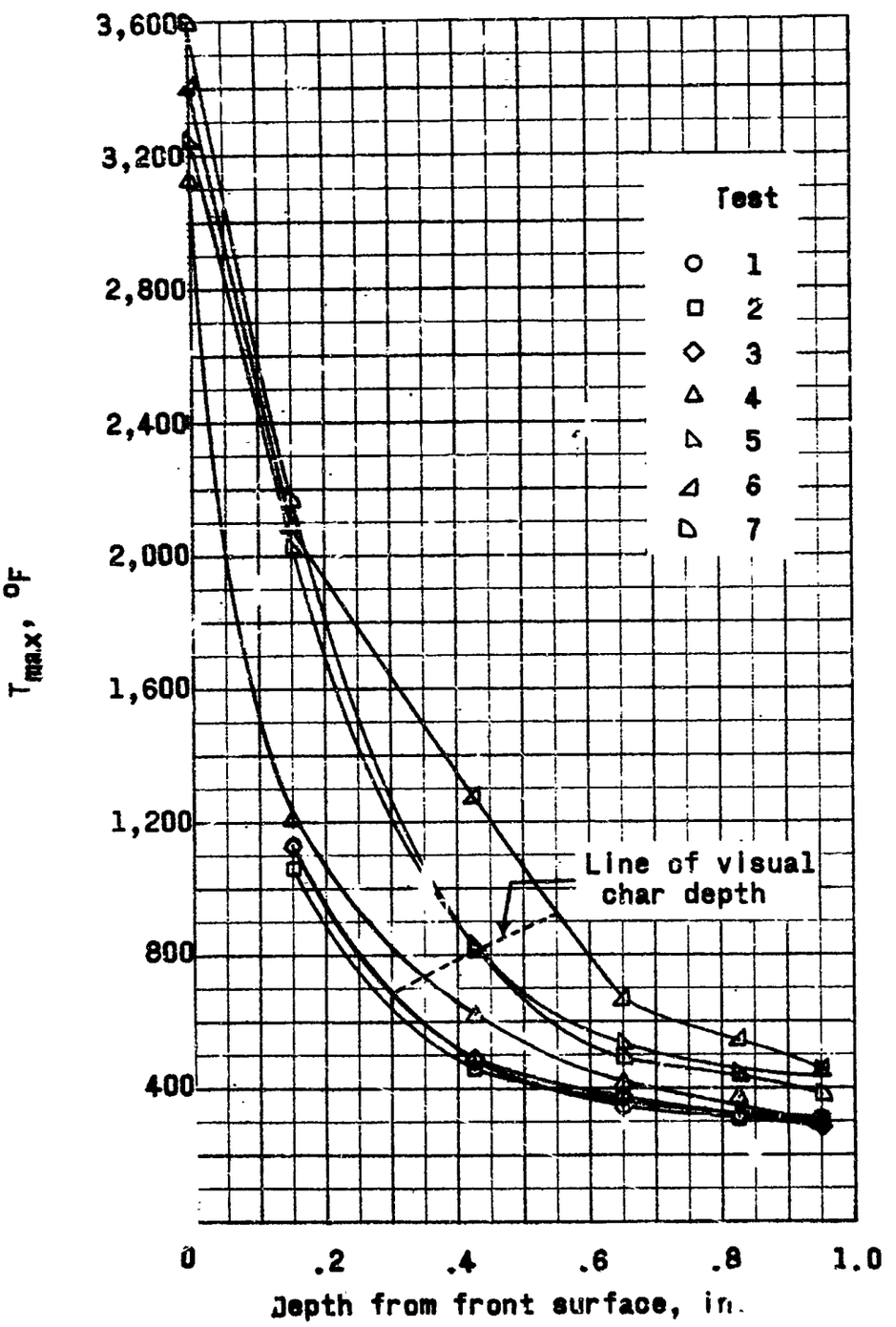

Figure 27.- Maximum temperatures experienced at various depths in the arc-jet tested specimens.

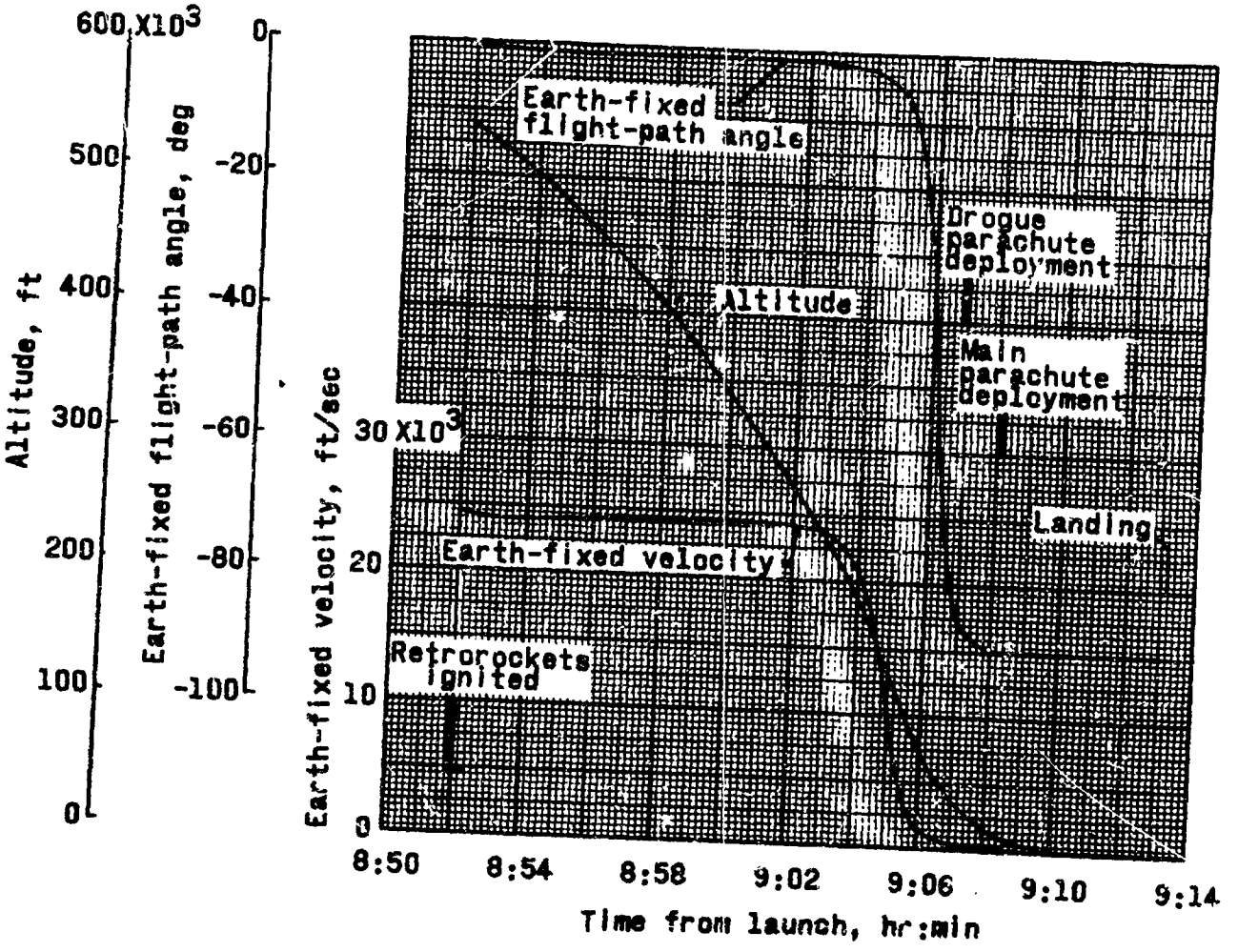

(a) Earth-fixed velocity, flight-path angle, and altitude.

Figure 28.- Flight reentry trajectory parameters for a typical Mercury mission (MA-8).

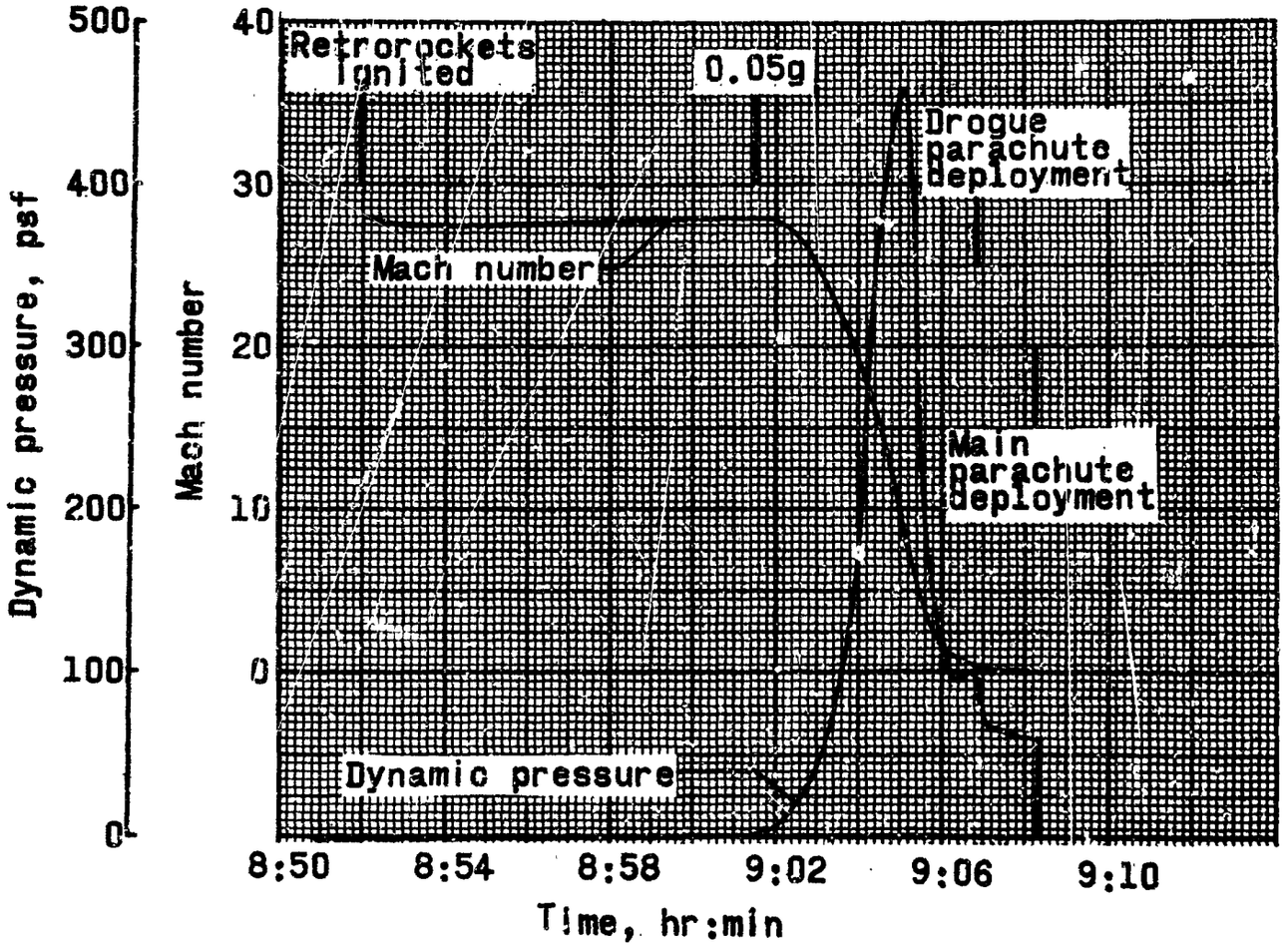

(b) Dynamic pressure and Mach number.

Figure 28.- Continued.

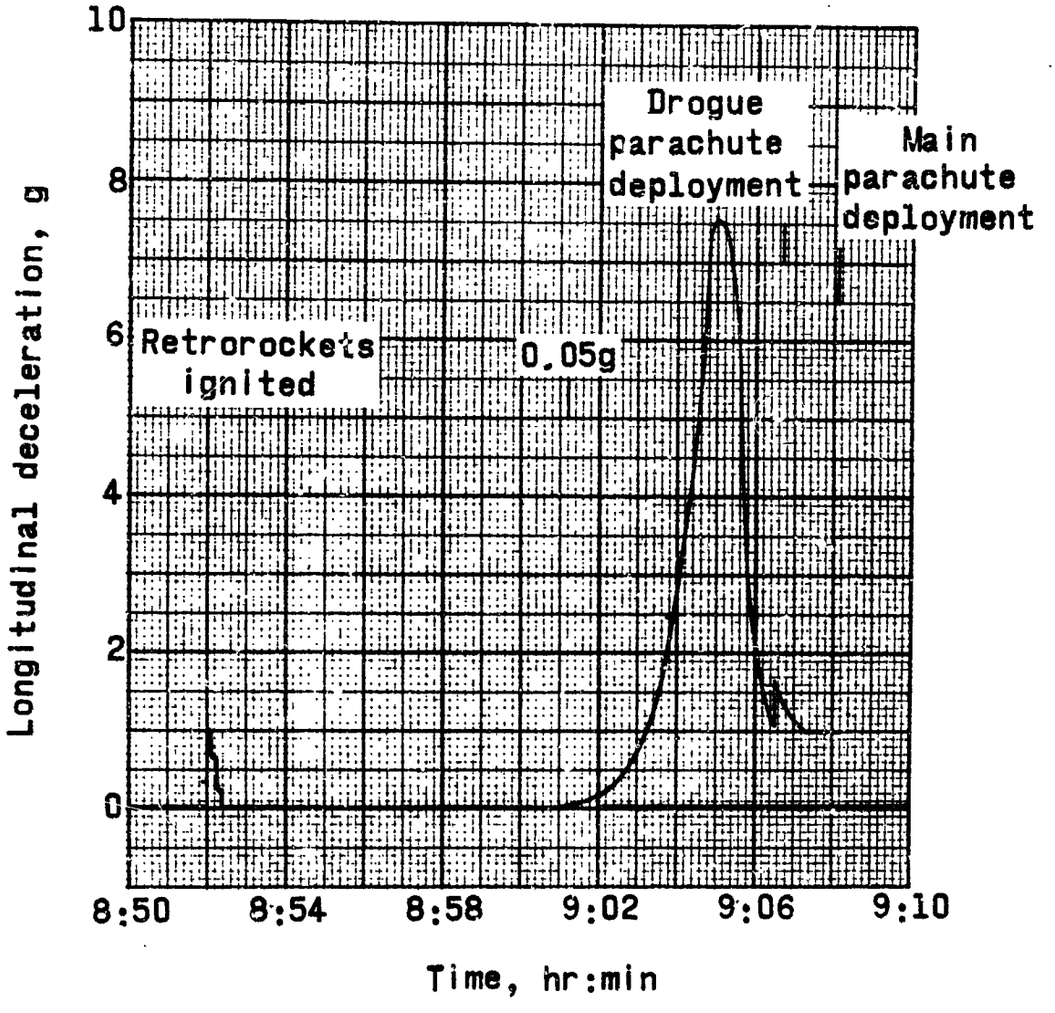

(c) Longitudinal deceleration along spacecraft Z-axis.

Figure 28.- Concluded.

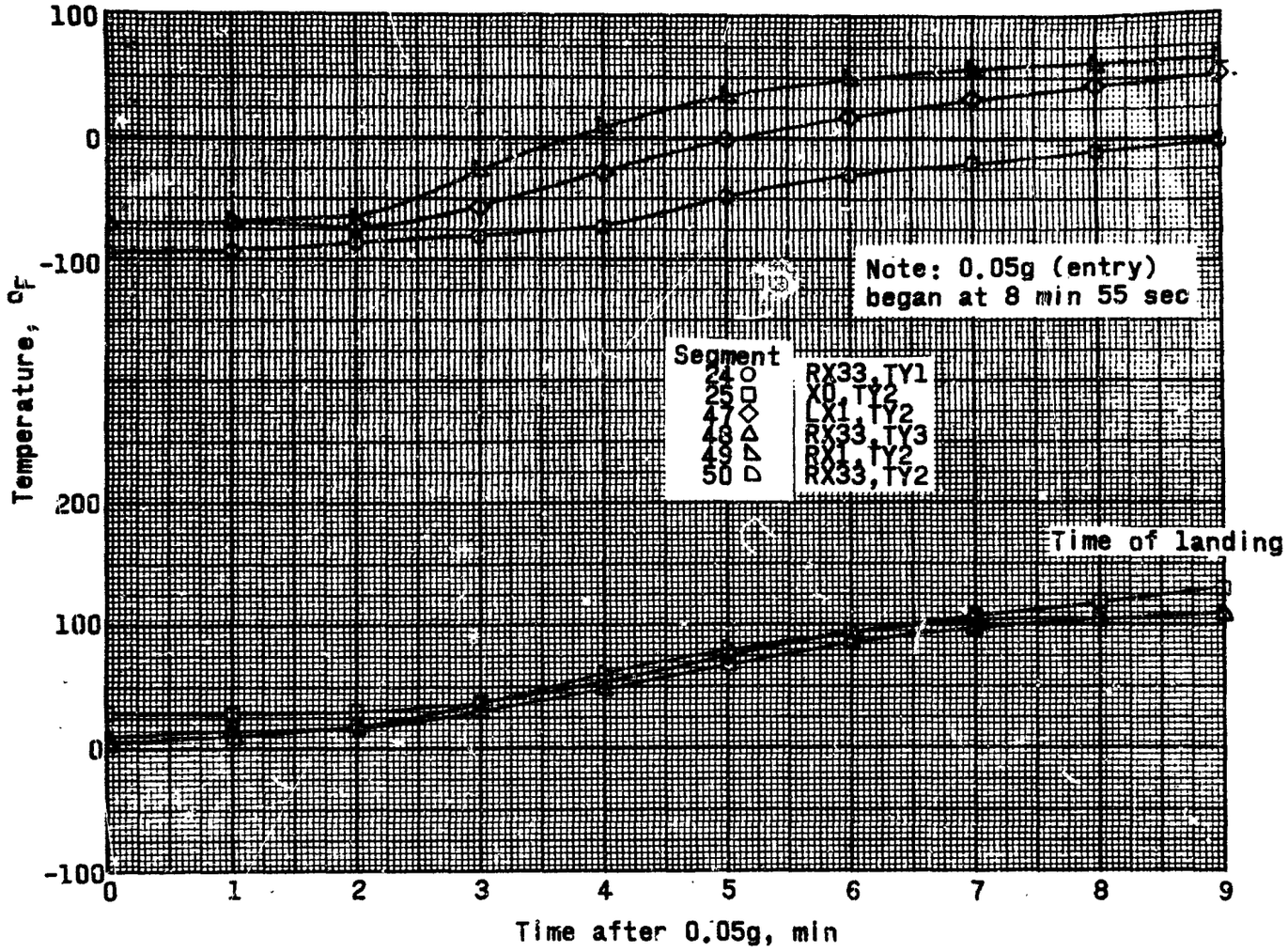

(a) MA-2.

Figure 29.- Mercury-Atlas heat shield temperatures.

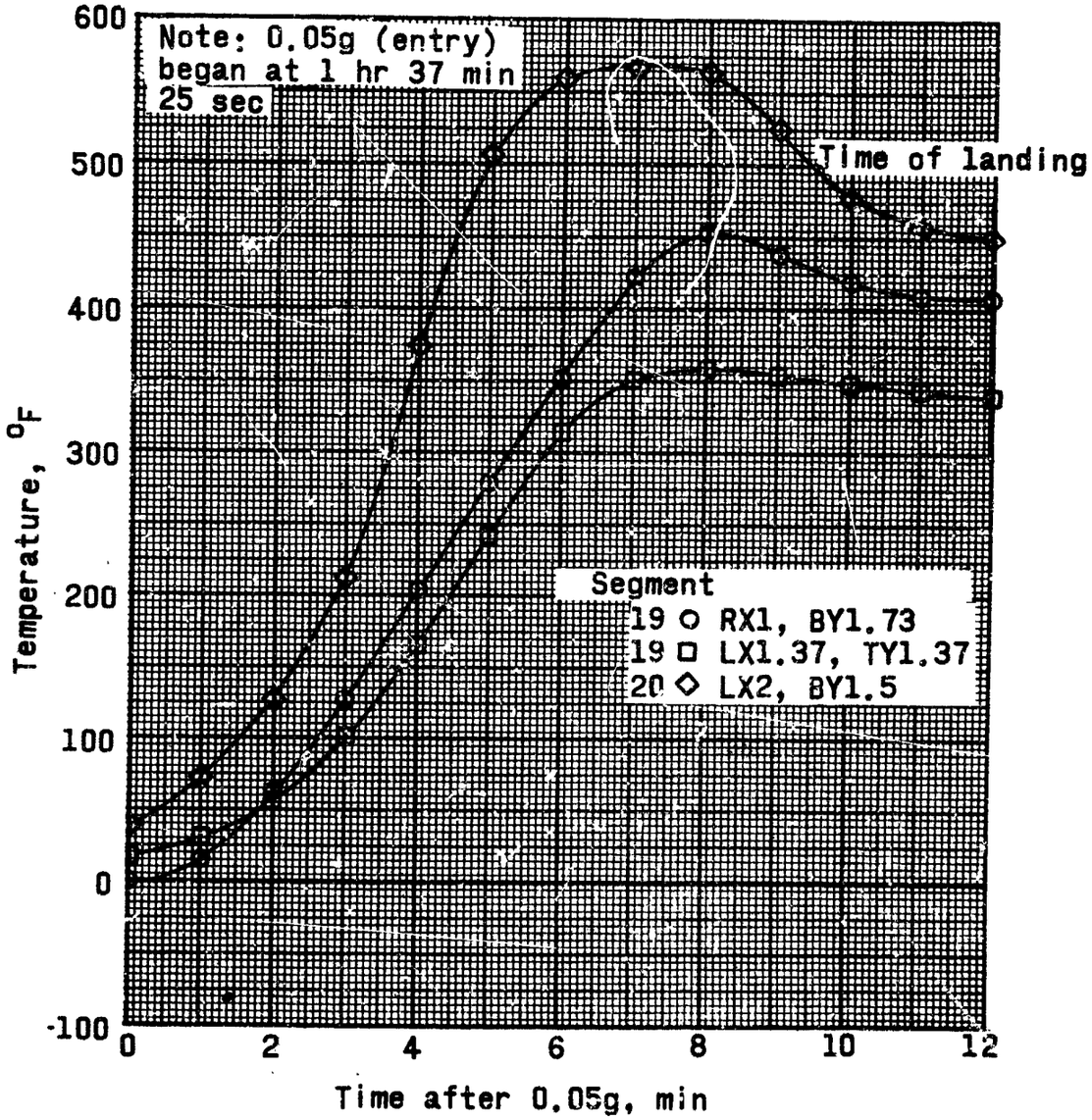

(b) MA-4.

Figure 29.- Continued.

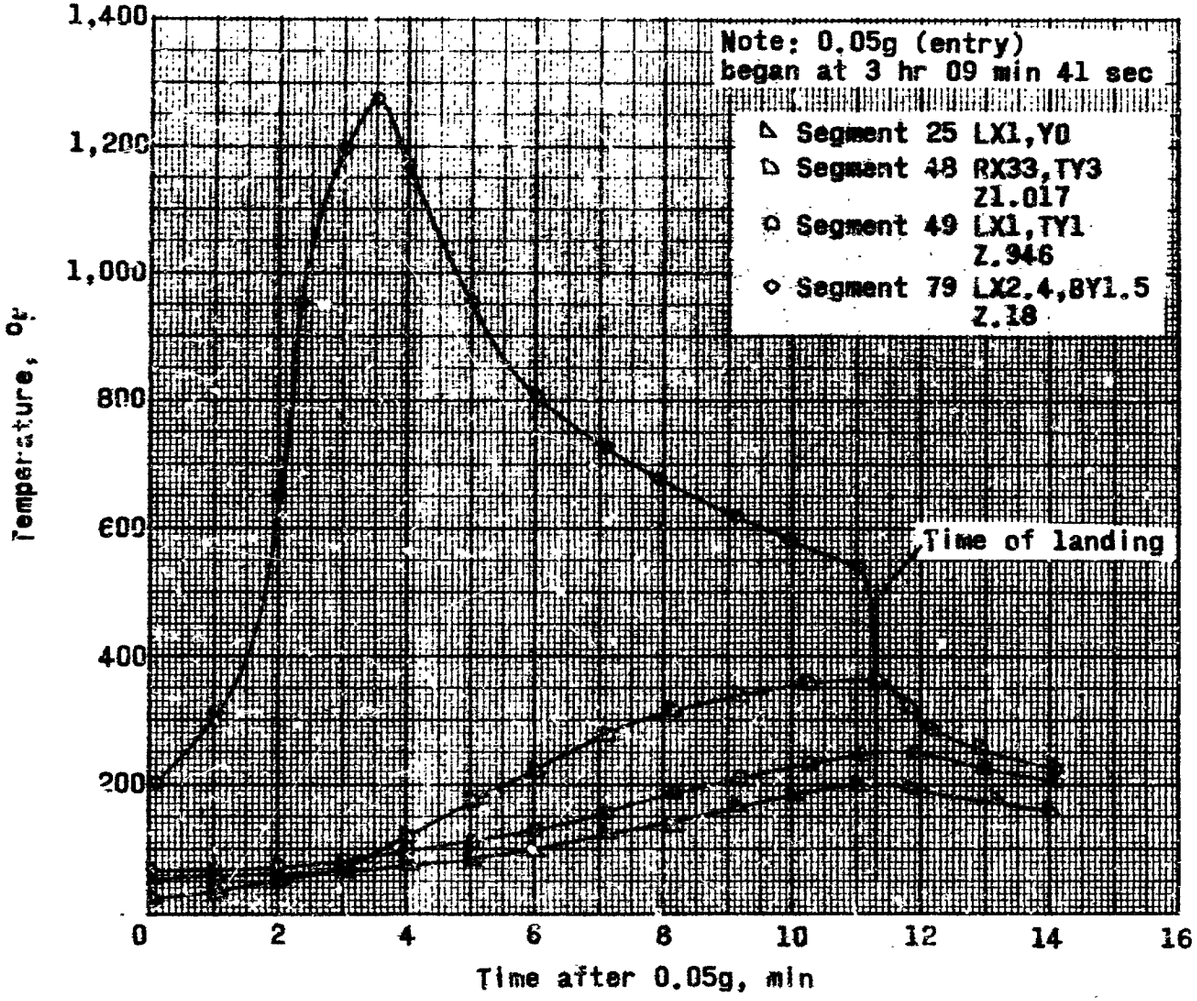

(c) MA-5.

Figure 29.- Continued.

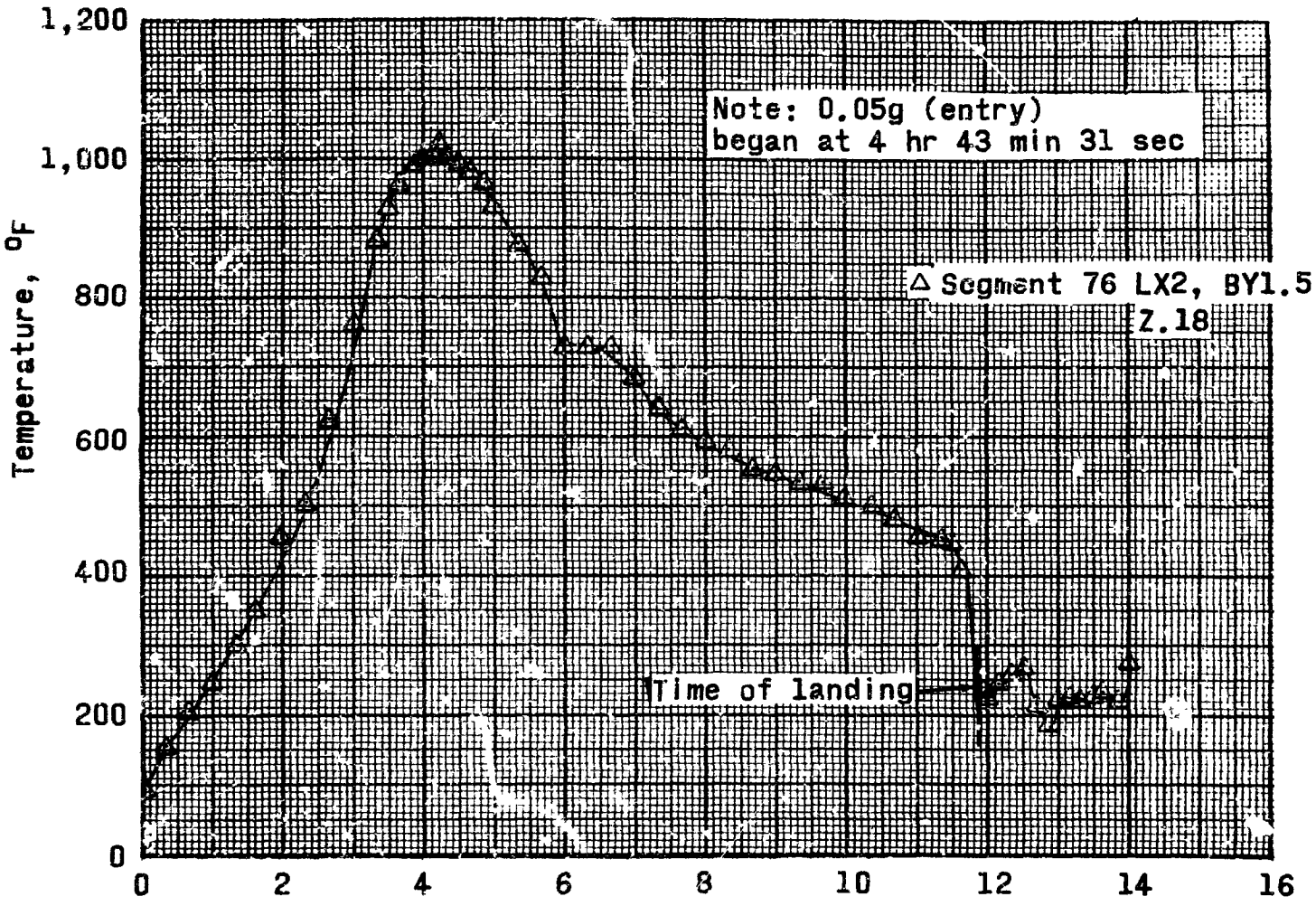

(d) MA-6.

Figure 29.- Continued.

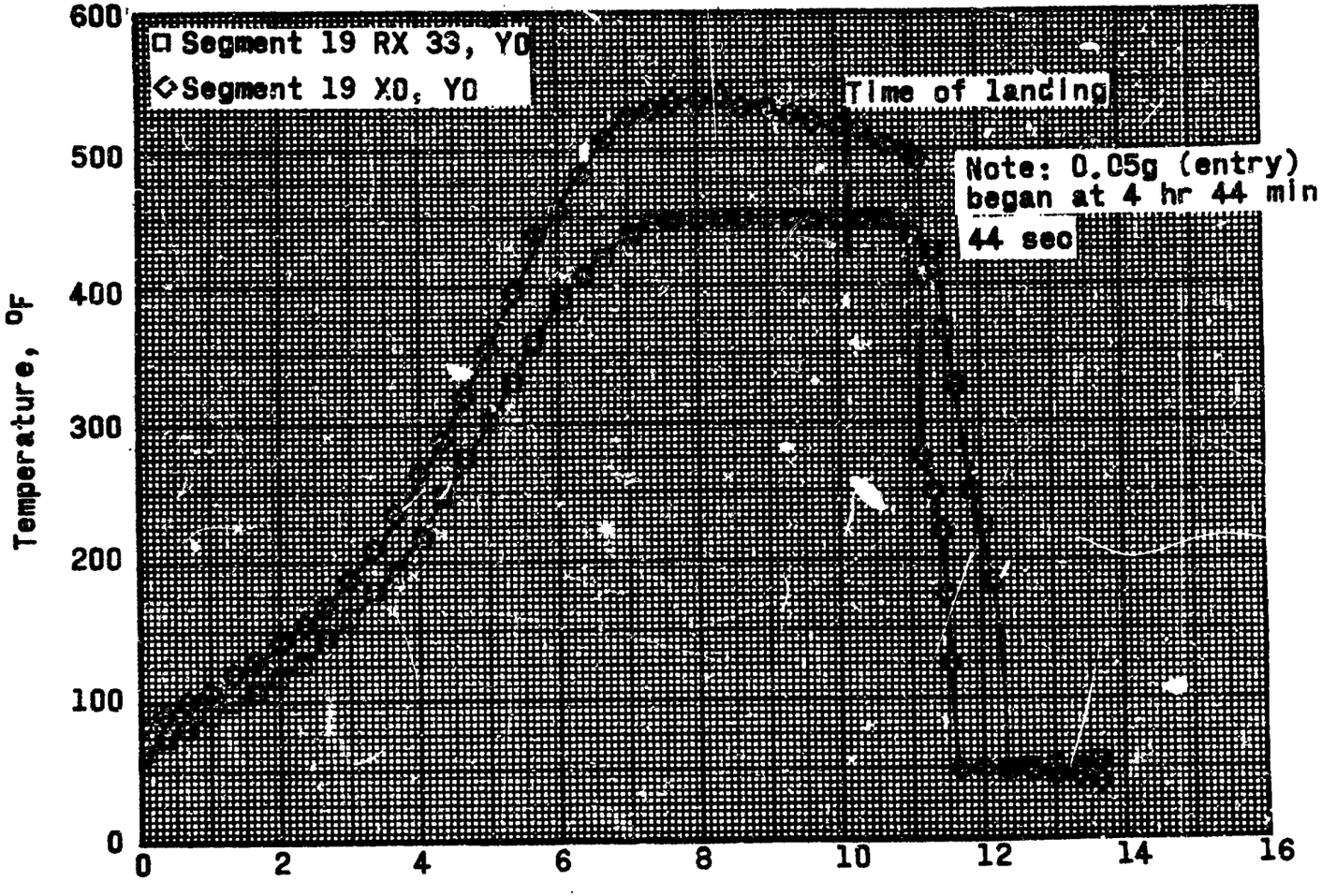

(e) MA-7.

Figure 29.- Continued.

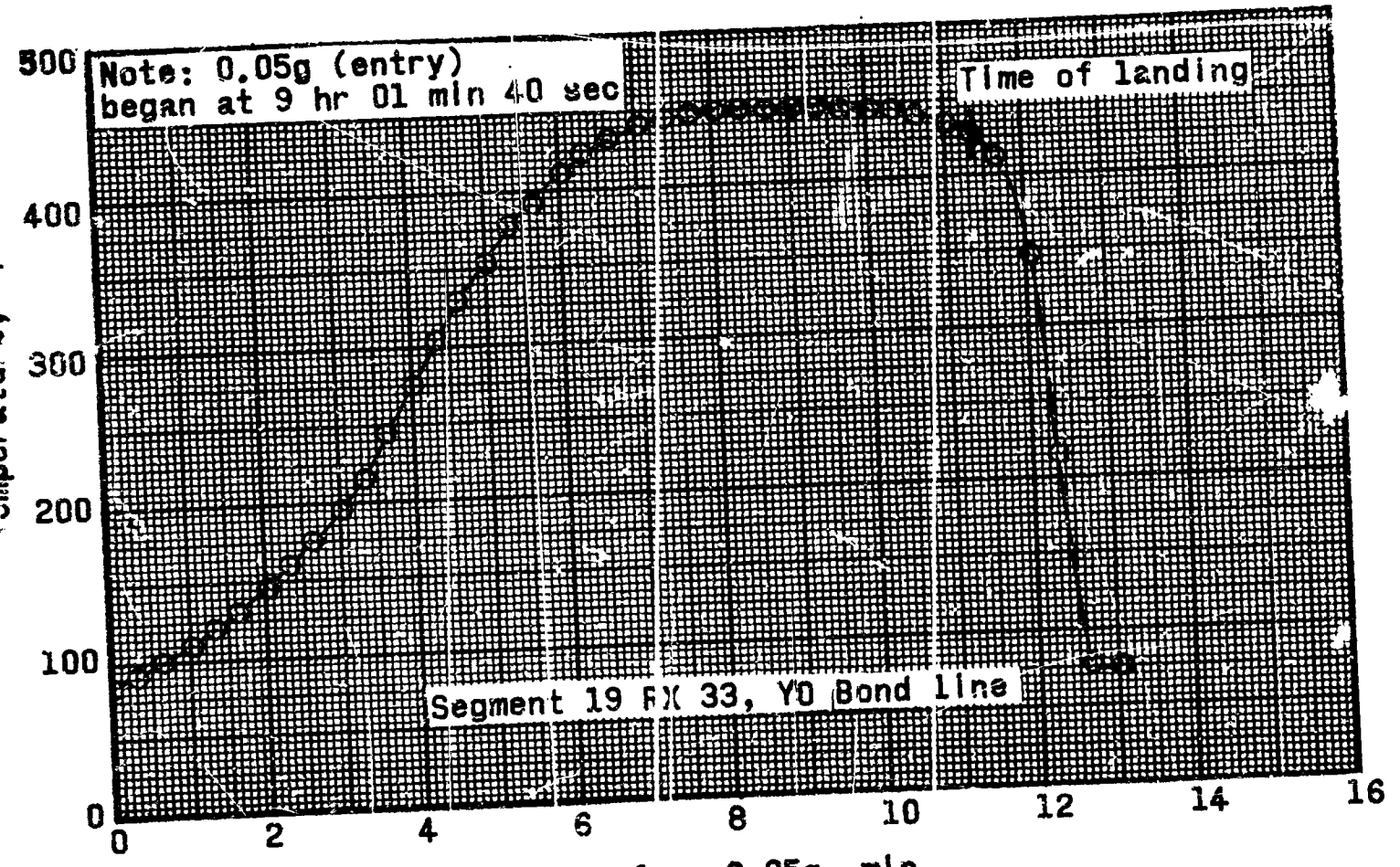

(f) MA-8.

Figure 29.- Continued.

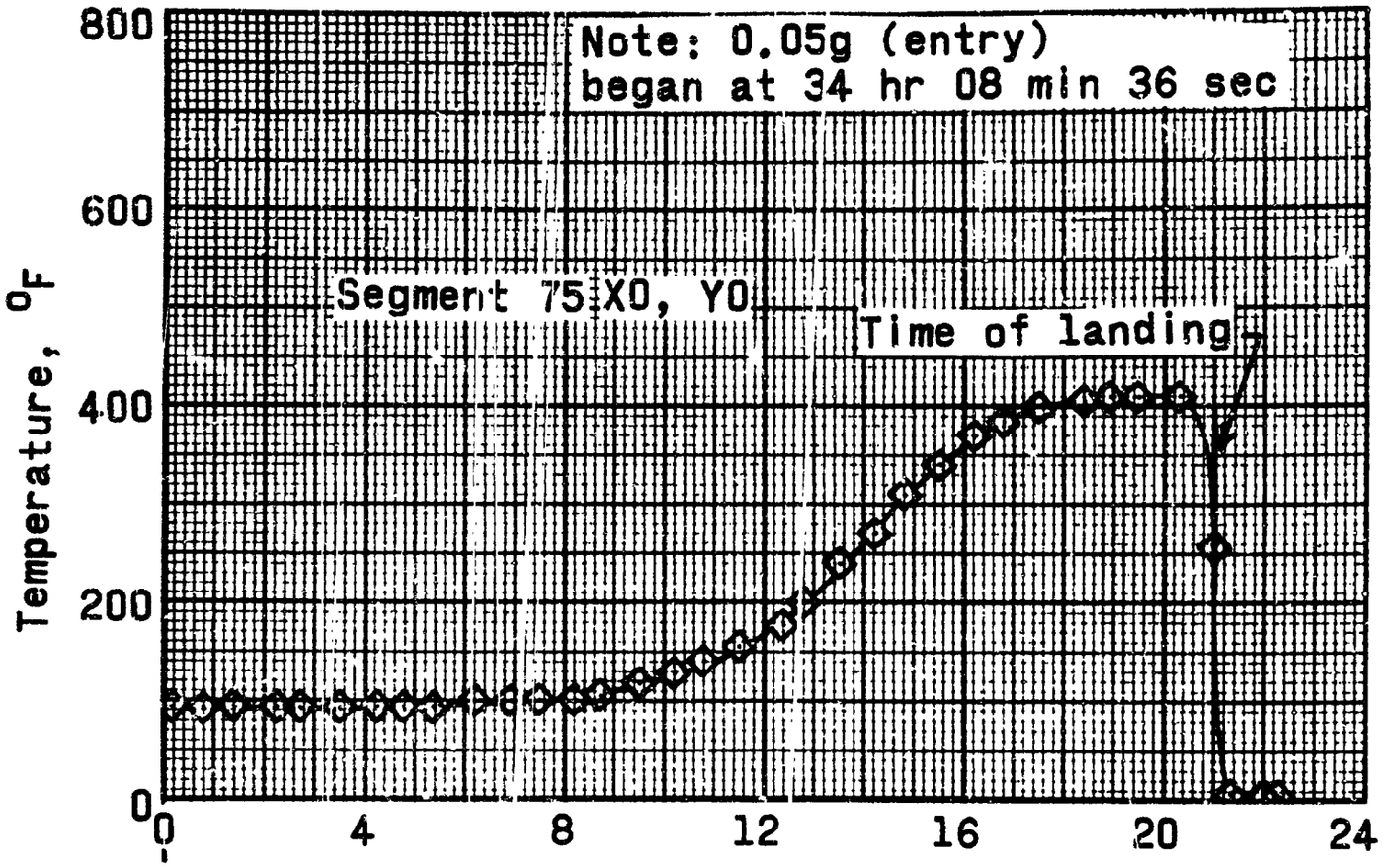

(g) MA-9.

Figure 29.- Concluded.

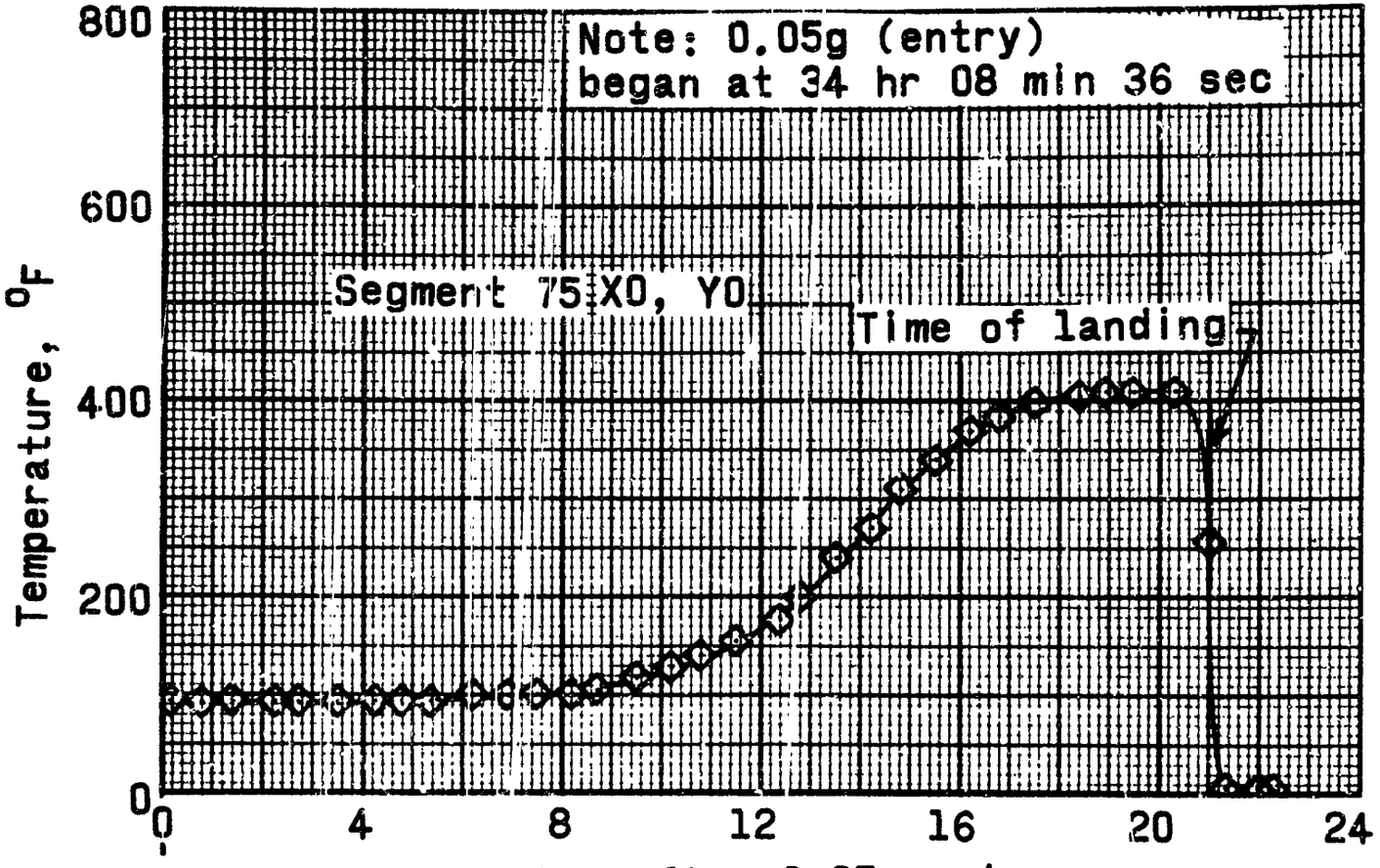

(g) MA-9.

Figure 29.- Concluded.

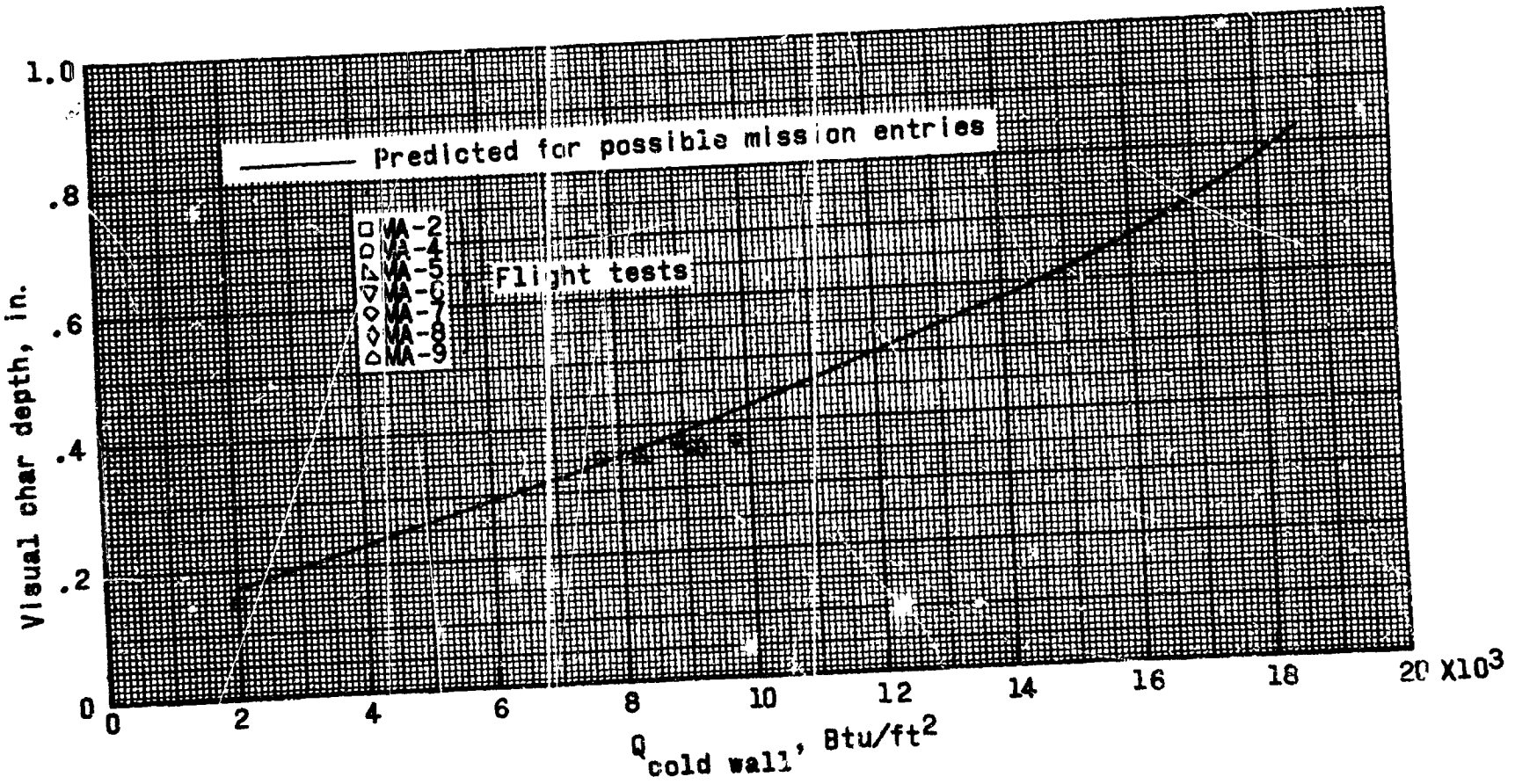

(a) Visual char depth.

Figure 30.- Comparison of flight results and predicted estimates on the basis of total cold-wall heat pulse.

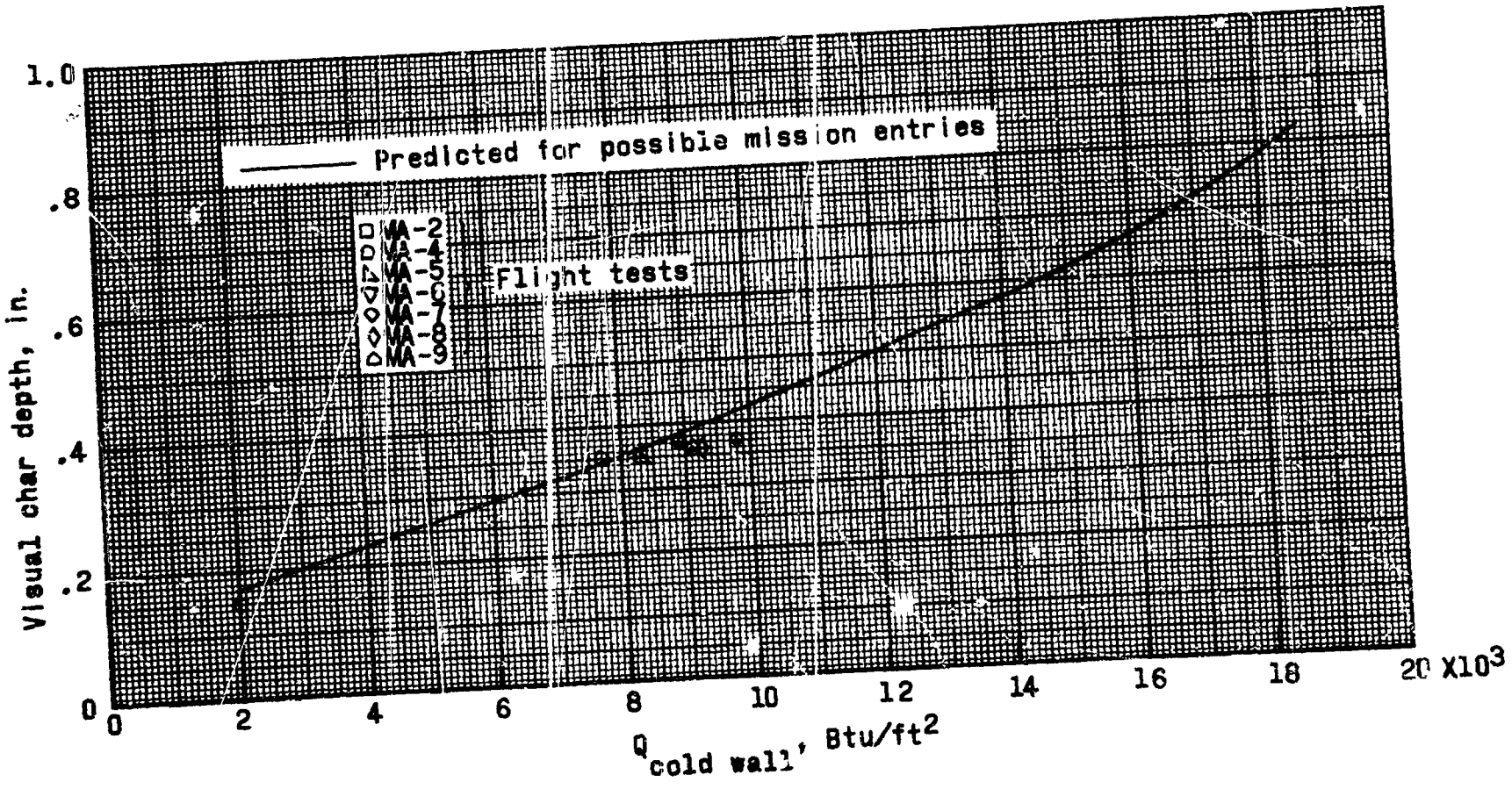

(a) Visual char depth.

Figure 30.- Comparison of flight results and predicted estimates on the basis of total cold-wall heat pulse.

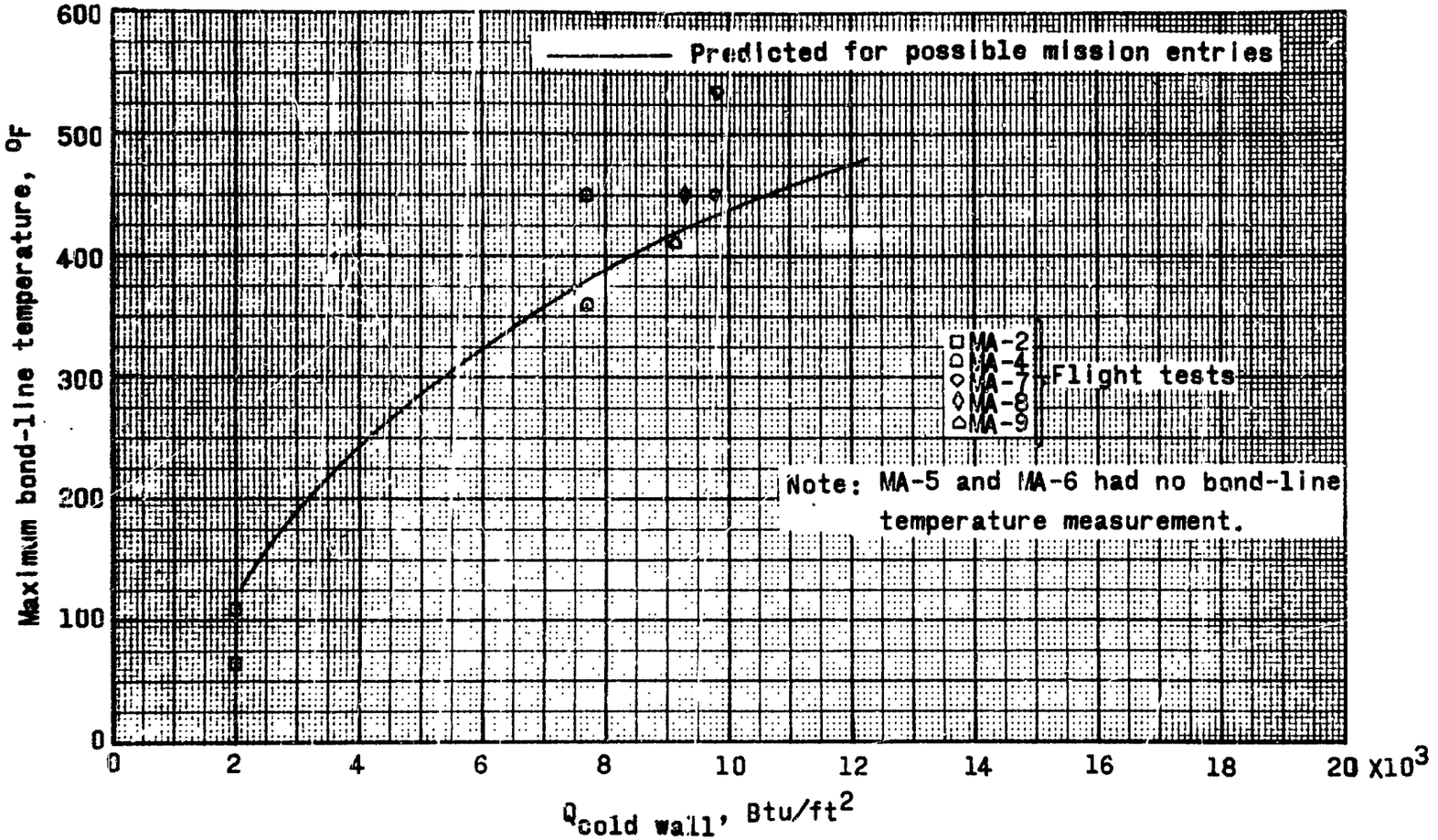

(b) Maximum bond-line temperature.

Figure 30.- Concluded.

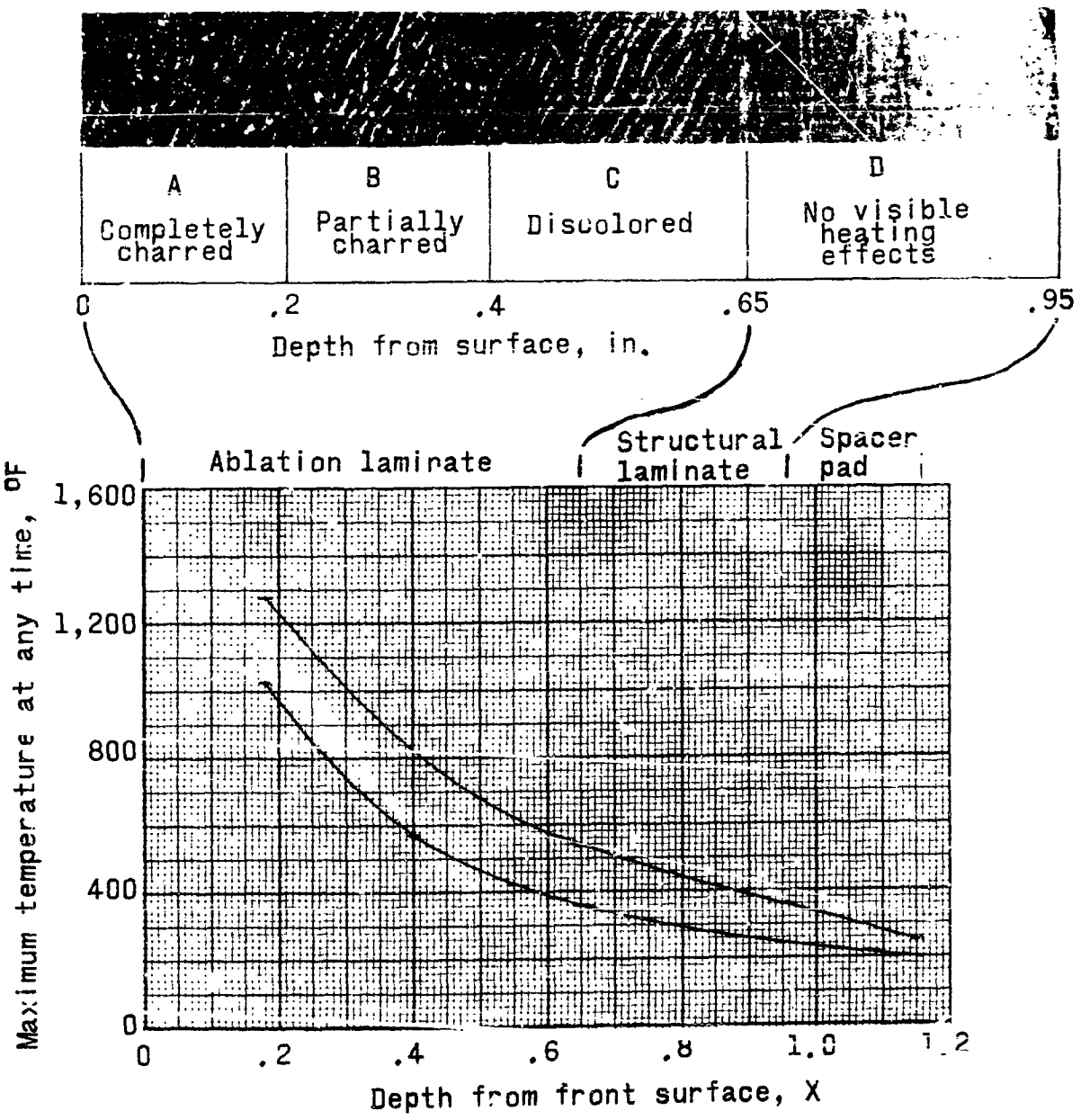

Figure 31.- Variation of maximum Mercury-Atlas heat-shield temperatures with depth from front surface for all orbital missions.

6246-64

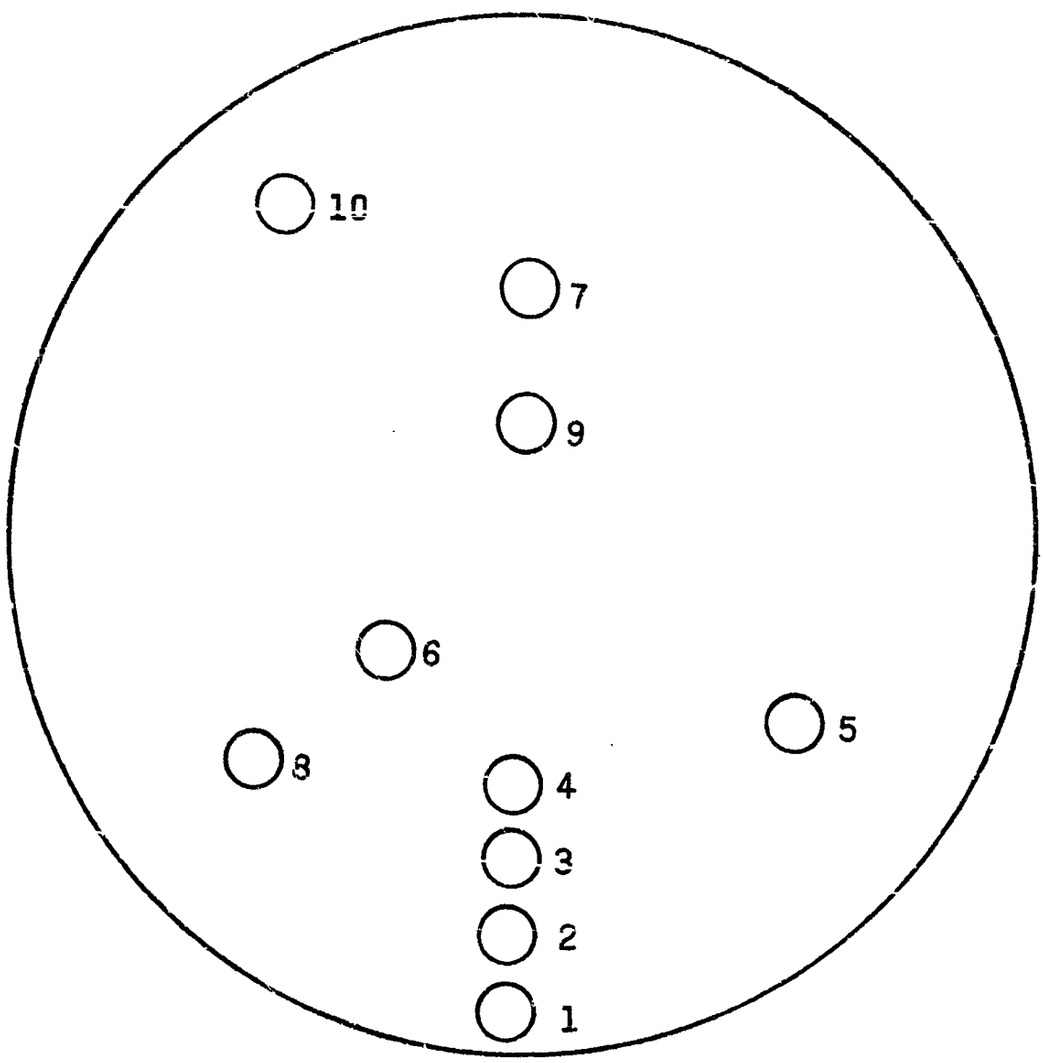

Figure 32.- Core locations for typical specimens for postflight analysis, MA-7.

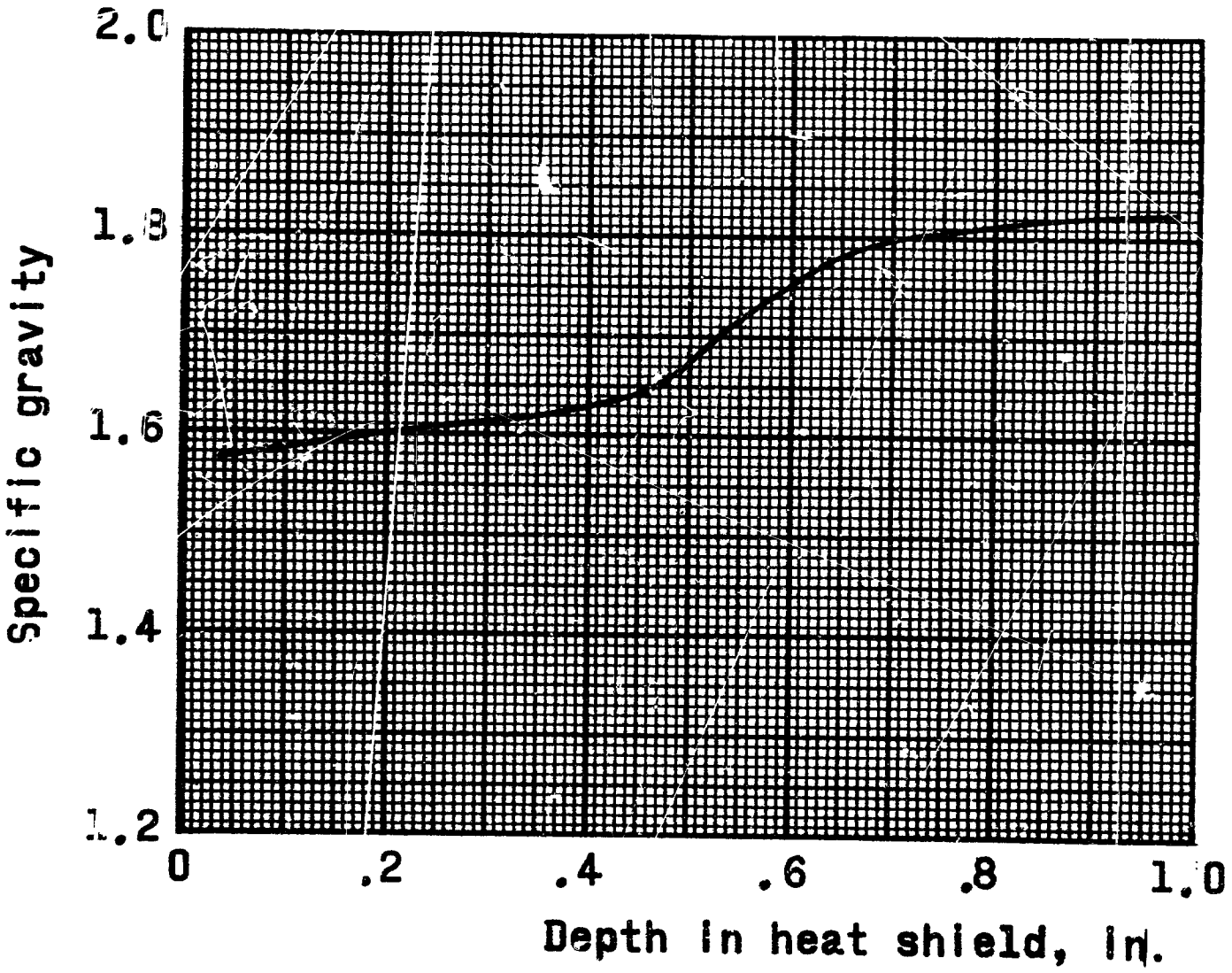

Figure 33.- Variation of specific gravity through a typical heat-shield specimen, MA-7.

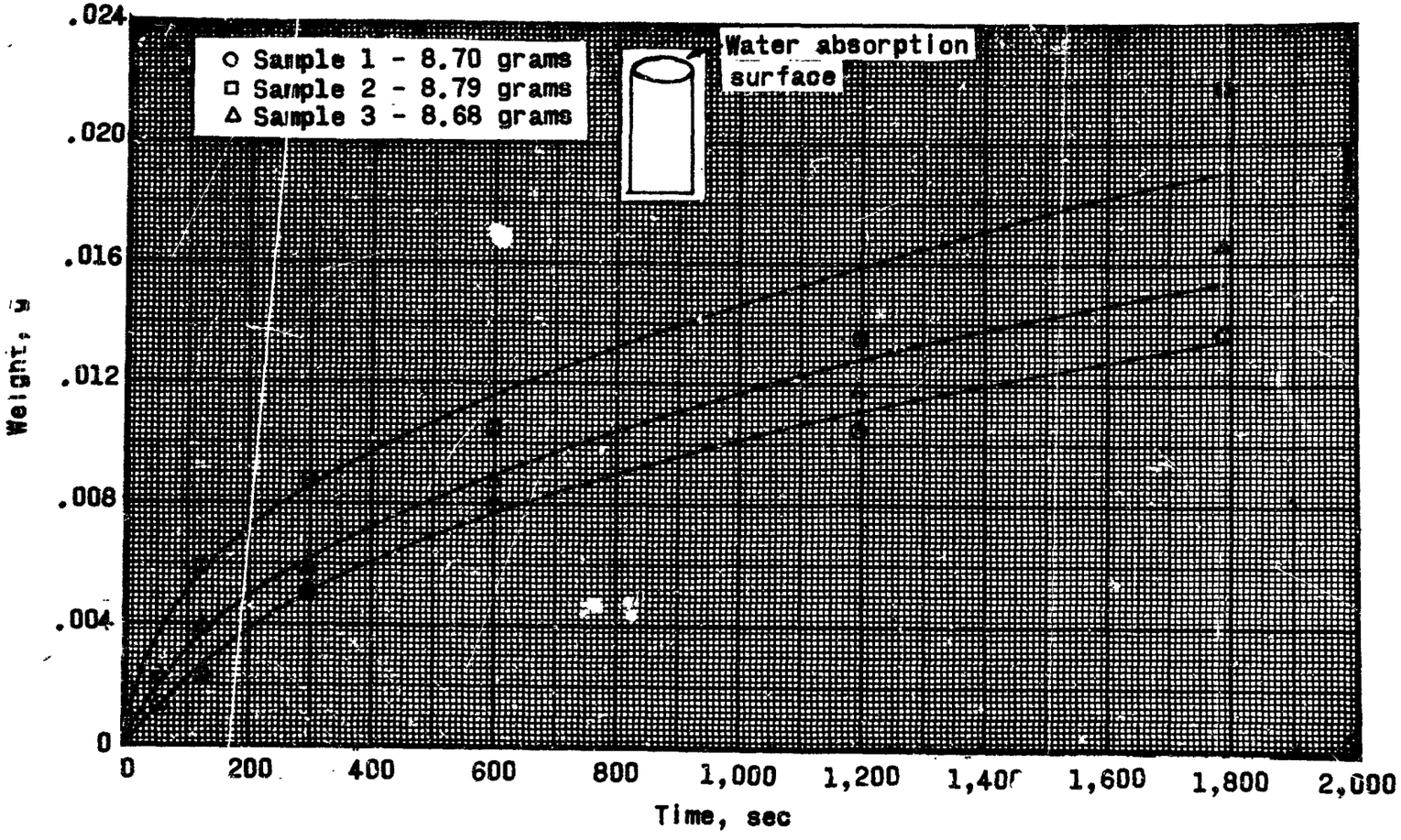

Figure 34.- Water-absorption history for virgin Mercury heat-shield material.

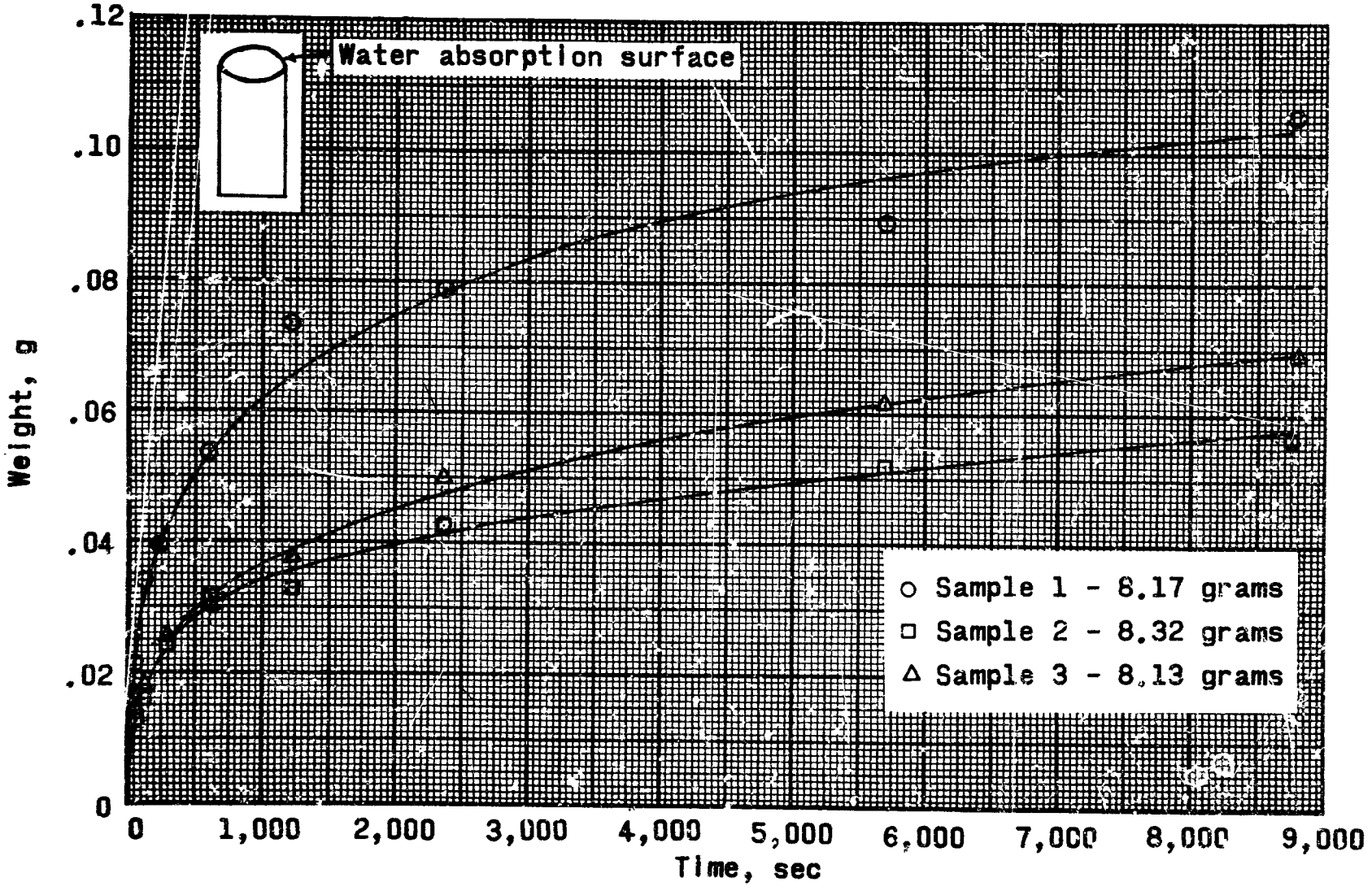

Figure 35.- Water-absorption history for charred MA-9 heat-shield material.

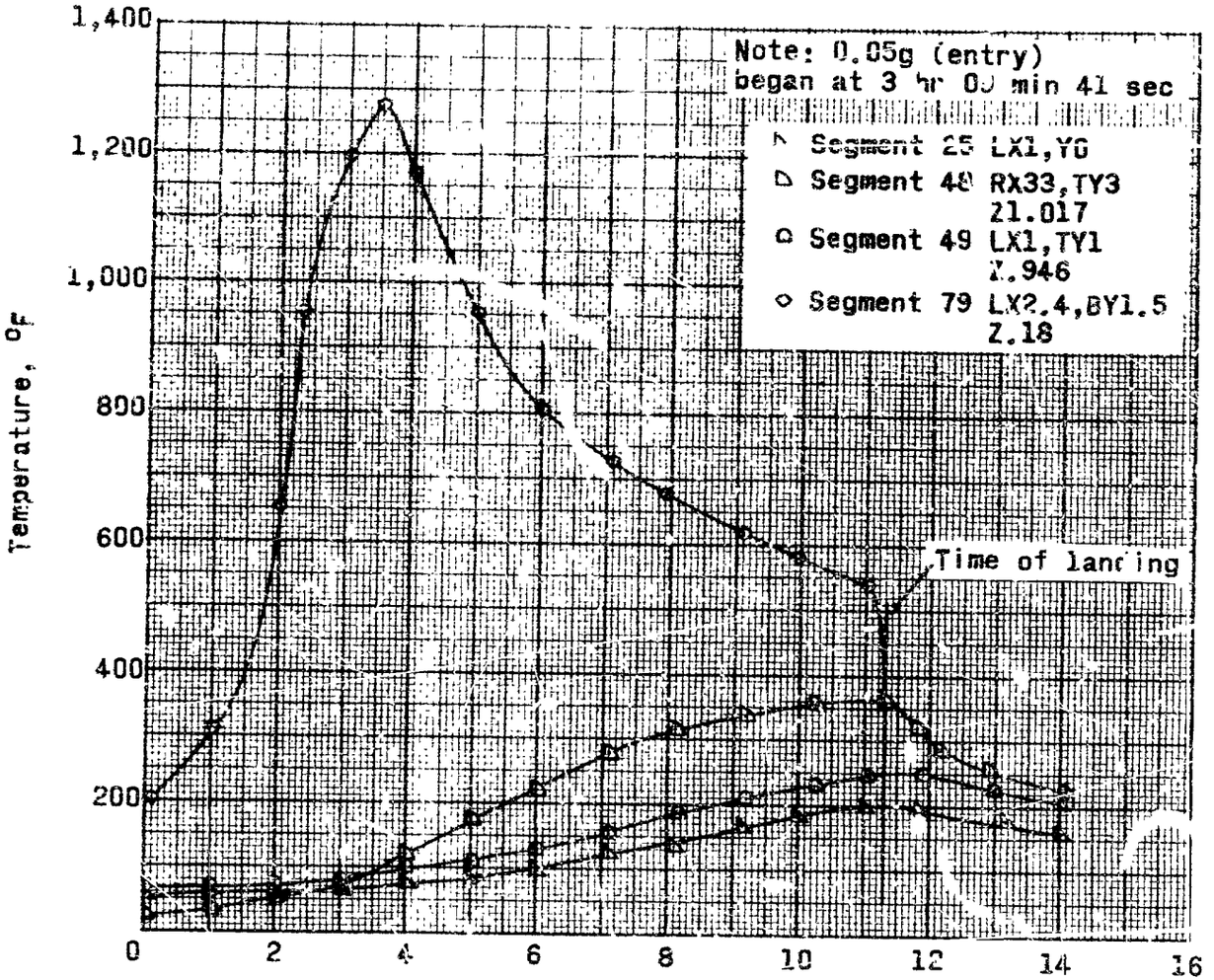

(c) MA-5.

Figure 29.- Continued.